Novel Design of Nano-Silica Network in Polypropylene Using Sol-Gel Method with Supercritical Carbon Dioxide

KENGO TAKEUCHI

Japan Advanced Institute of Science and Technology

Doctoral Dissertation

Novel Design of Nano-Silica Network in Polypropylene Using Sol-Gel Method with Supercritical Carbon Dioxide

by

Kengo Takeuchi

***Supervisor*: Professor Dr. Minoru Terano**

School of Materials Science
Japan Advanced Institute of Science and Technology

March 2015

Referee-in-chief: **Professor Dr. Minoru Terano**
Japan Advanced Institute of Science and Technology

Referees: **Professor Dr. Masayuki Yamaguchi**
Japan Advanced Institute of Science and Technology

Professor Dr. Noriyoshi Matsumi
Japan Advanced Institute of Science and Technology

Associate Professor Dr. Toshiaki Taniike
Japan Advanced Institute of Science and Technology

Professor Dr. Katsuhisa Tokumitsu
The University of Shiga Prefecture

Preface

The present dissertation is the result of the studies under the direction of Professor Dr. Minoru Terano during 2012-2015. The purpose of this dissertation is developing knowledge for high performance polypropylene (PP)-based materials based on the novel design of nanosilica network structure.

First of all, PP-based nanocomposite materials have been attracted due to achieve further reinforcement, which is expected to expand the using area of PP. The first chapter is a general introduction according to the object of this research. Chapter 2 describes sol-gel synthesis of nano-sized silica in confined amorphous space of polypropylene and relationship between nano-level structures of silica and physical properties of resultant nanocomposites. Chapter 3 describes morphological control of silica in polypropylene using confined amorphous space as template. Chapter 4 describes development of bio-inspired polypropylene-based materials through sol-gel reaction in laminated biaxially oriented polypropylene. Chapter 5 describes the conclusion of this dissertation.

Kengo Takeuchi

Terano Laboratory,

School of Materials Science,

Japan Advanced Institute of Technology

March 2015

Contents

Chapter 1.

General Introduction

1.1. Polypropylene

Concept of polymer was pronounced in 1920s by Staudinger, who insisted that polymer is composed of long molecules connected by covalent bond. Thermoset resins such as urea resin and/or phenol resin were initially produced from coal, and then the new polymer materials had been rapidly developed after Staudinger's contribution. The linear polymers prepared from oil such as polyester, polyamide and polyolefin were newly appeared and the production amount had rapidly enlarged to replace the traditional materials like metal because of their excellent properties.

Polymer materials are mainly classified into commodity plastics, engineering plastics and super engineering plastics. The commodity plastics represented by polyethylene (PE), polypropylene (PP), polyvinyl chloride and polystyrene are widely used due to some advantages such as the low production costs, balanced mechanical properties good processability and so on. On the other hand, polymers with high strength and heat resistance are called as engineering plastics including polyamide, polycarbonate, polyacetal, polybutylene terephthalate and denaturated polyphenylene ether. In addition, super engineering plastics were also produced for the usage in high temperature. While engineering plastics and super engineering plastics have excellent properties, the demerits coming from poor processability, high production cost and poor chemical resistance lead to the limitation of the using area. Therefore, reinforced commodity plastics are highly desired.

The production amount of PP is the highest in all polymers in the world. Crystalline PP with high molecular weight was firstly synthesized by Natta in 1955 using catalyst based on titanium and aluminum [1,2]. The commercial production of PP started in 1957 in USA and in 1958 in Europe. Due to its comprehensive advantages in cost,

thermal properties, mechanical and rheological properties, environmental load and so on, the production amount have been increased. The properties of PP are complicatedly dominated by various factors such as primary structure, high order structure and additives. The structure and resulting properties of PP is firstly written in this chapter.

1.2. Primary structure of PP

1.2.1. Tacticity

Higher order structure of PP is determined not only by crystallization conditions but also primary structure of PP. One of important factors on the primary structure is stereoregularity. Vinyl polymer with a side chain possesses asymmetric carbon in main chain, where the structures with different substituent direction were defined as *d* and *l*, respectively. On the other hand, the properties of PP are dominated by the repeating units of the carbons in terms of the same and zig-zag direction, so-called meso (*m*) and racemo (*r*). The structures with only *m*, *r* and random sequences are defined as isotactic, syndiotactic and atactic polypropylene, respectively (Figure 1).

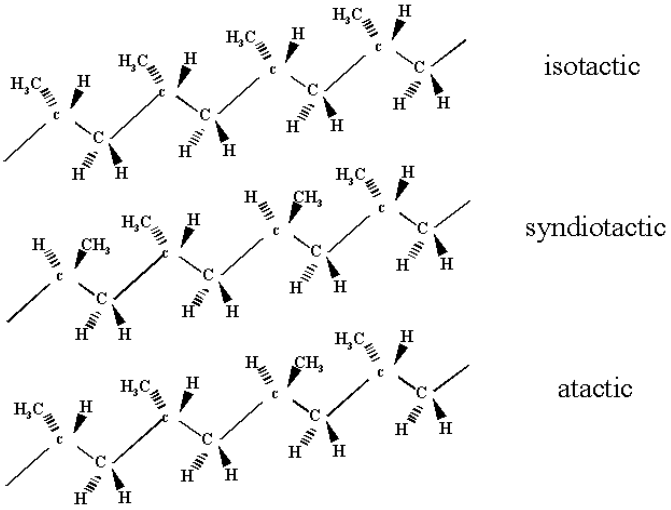

Figure 1. Stereo configuration of polypropylene.

The higher order structure and physical properties both in solid and in molten-state are dramatically affected by the stereoregularity. For example, PP with long isotactic and syndiotactic sequence respectively induce 3/1 herix [3] and 2/1 herix structure [4], resulting in semi-crystalline polymer, whereas crystal structures are not formed in atactic PP. The crystallinity of usual isotactic polypropylene is from 40 to 70% and the length of isotactic or syndiotactic sequences play a key role to increase the crystallinity of PP [5]. While sPP has high toughness compared to iPP [6], iPP is commercially employed due to some advantages such as stiffness, price, heat distortion temperature and so on. The stereoregularity is usually evaluated by ^{13}C nuclear magnetic resonance (NMR).

1.2.2. Polypropylene copolymer

Copolymerization, which is the procedure to incorporate other monomer into polymer chain, is performed to modify the properties of PP. In case of propylene

copolymerization, random copolymer incorporating ethylene 1-butene or 1-hexene is often prepared. The defect region is induced by comonomer in polymer chain and interrupts the crystallization, resulting in low melting temperature and crystallinity. Therefore, the resulting polymer usually obtains high impact strength and transparency. Decrease of the crystallinity and melting temperature on propylene random copolymer largely depends on the kinds of comonomer (Figure 2).

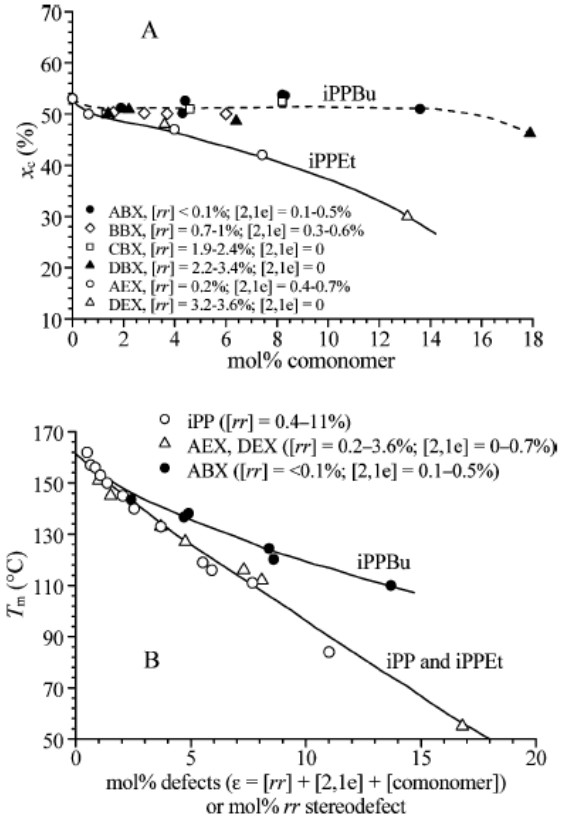

Figure 2. Effects of comonomer types and content on crystallinity and melting temperature [7].

The crystallinity and melting temperature of propylene/1-butene copolymer are generally higher than that of propylene/ethylene or 1-hexene copolymer because a 1/3 helix is fabricated by side chain of butene group, permitting incorporation of

comonomer unit in lamellar [7,8]. Amorphous ethylene propylene rubber (EPR) is prepared above 30% of ethylene content [9]. EPR regarded as rubber is vulcanized using peroxide, but vulcanization using surfer is impossible due to absence of double bond in the main chain.

1.3. Higher Order Structure of Polypropylene

Higher order structure of PP is composed by hierarchical architecture. The architecture is defined in order of size as unit cell, lamellar, spherulite, skin-core (Figure 3). The properties of PP are affected by higher order structure intricately, so precise control of the higher order structure is important to control the properties of PP.

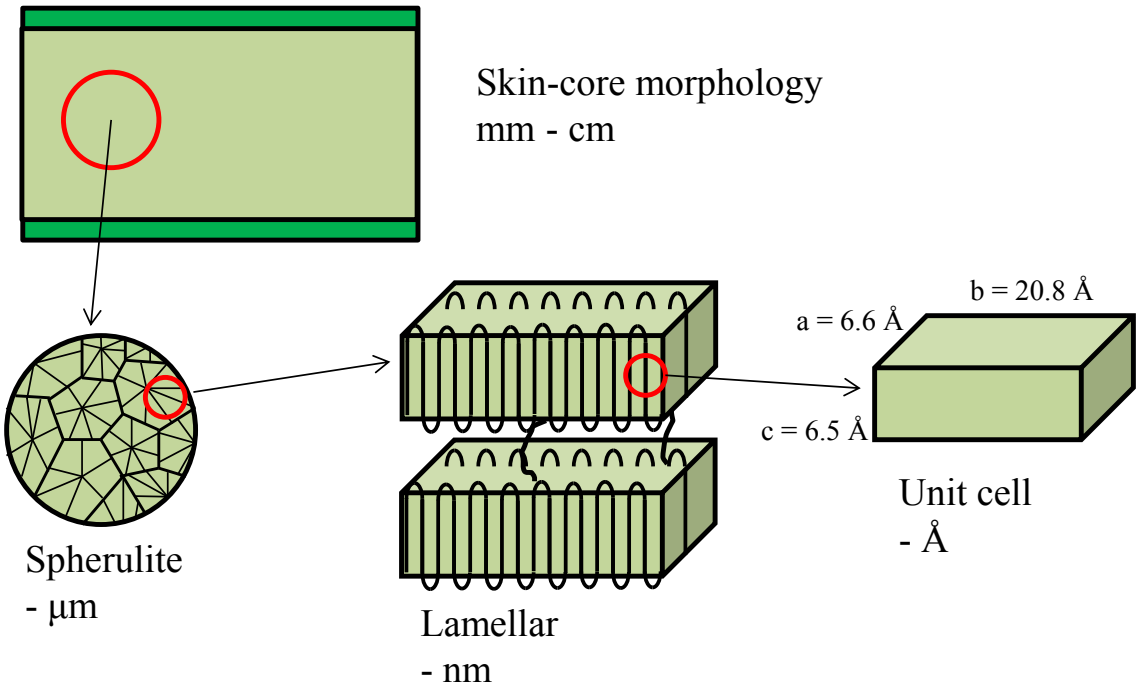

Figure 3. Higher order structure of PP.

1.3.1. Crystalline structure

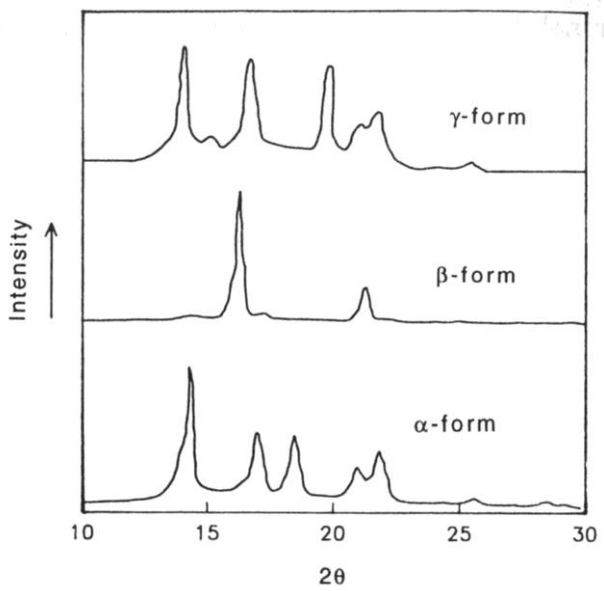

Figure 4. Wide angle X-ray diffraction patterns of PP with different crystalline structures.

The conformation of iPP with methyl group in side chain is 1/3 helix structure connected by trans and gauche alternately [10]. There are up and down types of helices owing to the differences in the direction of methyl groups in side chain. In addition, the difference of the rotating direction also causes right-handed and left-handed helices. Various crystalline structures are constructed by crystal asymmetry and arrangement of isotactic chain in iPP, and these are called as α, β and γ, which are evaluated by wide angle X-ray diffraction. In this session, structure, formation and properties of each crystalline are described.

α crystal is the most dominant crystal formed by usual crystallization procedure of iPP. There are two kinds of α crystal with different crystallographic symmetry, which are classified as $C2/c$ for α_1 [10] and $P2_1/c$ for α_2 [11]. These structures of

crystallographic symmetry are shown in Figure 5 [13]. The unit cells are a = 0.665 nm, b = 2.096 nm, c = 0.650 nm, β = 99.62° and $\alpha = \gamma$ = 90° for α_1 and a = 0.666 nm, b = 2.078 nm, c = 0.6495 nm, β = 99.62° and $\alpha = \gamma$ = 90° for α_2 [12].

The transition from α_1 to α_2 is induced by heat treatment above 150°C [14,15].

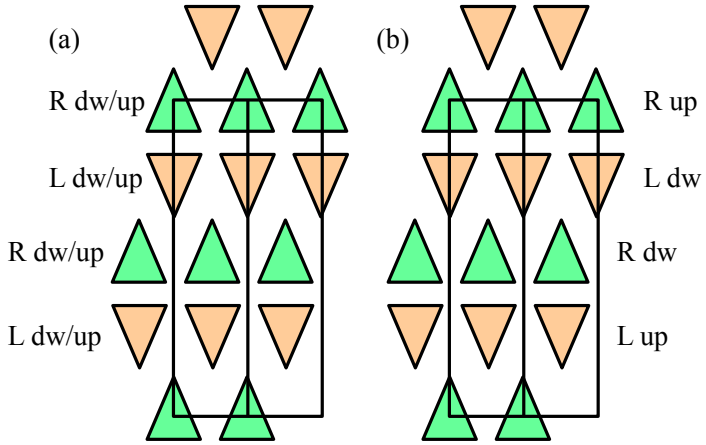

Figure 5. Two monoclinic space groups of (a) α_1 and (b) α_2 forms in iPP [13].

The lamellar with α crystal exhibits cross-hatching morphology showing highly characteristic lamellar branching [15]. The morphology is directly observed by electron microscopy [16,17]. The structure is composed by mother lamellar formed to the direction of radial in spherulite and daughter lamellar tangentially grown on the mother lamellar. The angle between mother lamellar and daughter lamellar is 80° [18].

β crystal with hexagonal lattice was discovered in 1959 [4]. The formation of β crystal results in high impact strength, better toughness and less tensile strength compared to that of α crystal. The crystallographic symmetry is shown in Figure 6. The lattice is $a = b$ = 19 Å and c = 6.5 Å [20-23]. The preparation of iPP with rich β crystal has been achieved by crystallization in a temperature gradient [24,25] or in a flow gradient [26-28] and the addition of a nucleating agent [29-32]. The β crystal

fraction (k) in iPP is evaluated by wide angle X-ray diffraction from following equation,

$$k = \frac{H_{\beta 1}}{H_{\beta 1} + (H_{\alpha 1} + H_{\alpha 2} + H_{\alpha 3})}$$

where $H_{\alpha 1}$, $H_{\alpha 2}$ and $H_{\alpha 3}$ corresponds to the intensity of θ = 7.1, 8.5 and 9.4 ° coming from α crystal respectively and $H_{\beta 1}$ corresponds to intensity of θ = 8.1 ° coming from β crystal [3].

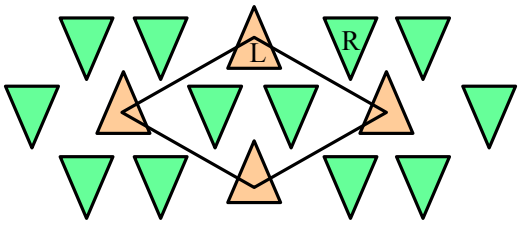

Figure 6. Hexagonal lattice of β crystal [19].

γ crystal with triclinic lattice was discovered in 1960s [3]. The formation of γ crystal was epitaxially occurred on α crystal. The angle between α and γ crystal is 40°, which is different from cross hatching structure observed in α crystal [18,33]. Figure 7 indicates crystallographic symmetry of γ crystal. The crystal lattice is a = 8.54 Å, b = 9.93 Å and c = 24.41 Å [34].

γ crystal is observed not under general crystallization of PP homopolymer but crystallization of low molecular weight PP [35,36] or crystallization of PP at high pressure above 200 MPa [37,38]. Another important factor is the length of isotactic sequences. The formation of γ crystal is attributed from short isotactic sequence, which is often observed in PP copolymer and PP synthesized by metallocene catalyst [5,39-41]. In addition, γ crystal fraction between α and γ crystal tends to be increased

by high isothermal crystallization temperature [42]. According to Turner-Jones [43], γ fraction (K_γ) in the crystalline phase of PP containing both α and γ phases can be calculated using the following equation from intensity measured by wide angle X-ray diffraction:

$$K_\gamma = \frac{I_\gamma(117)}{I_\gamma(117) + I_\alpha(130)}$$

where $I_\gamma(117)$ and $I_\alpha(130)$ denote integral intensities of the $(117)_\gamma$ and $(130)_\alpha$ diffraction peaks, respectively.

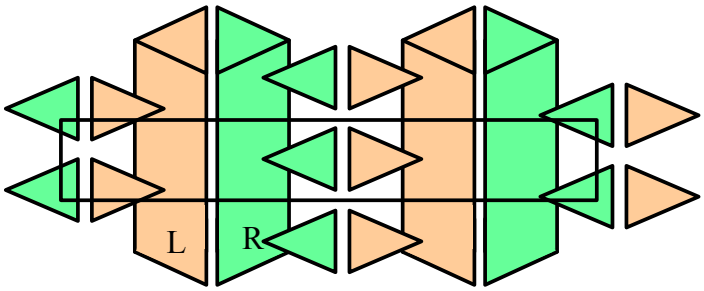

Figure 7. Triclinic lattice of γ crystal [44].

Molten iPP transforms into mesophase when it is quenched below 0°C at the cooling speed with at least 80 °C/s [45]. The structure is said to correspond to the smectic phase, which is intermediate structure between glass and crystal [46]. The chain conformation of mesophase is also 3/1 helix, but the crystallographic symmetry occupied by the chain is completely disordered. Since the helix is important to form mesophase, PP with short isotactic sequence does not exhibit mesophase [47].

It is known that these crystalline structures are converted into other by specific treatment. For example, mesophase is thermodynamically unstable crystal which easily transforms to α crystal by heat treatment [3,48,49]. The heat or elongation of

iPP with β crystal leads to the transformation to α crystal [50]. De Rosa et al. showed the crystalline conversion of PP largely depends on isotactic sequence and elongation ratio [51]. Since the properties and hierarchical structures of PP are dominated by crystalline structure, control of a crystalline structure is important for resulting PP materials.

1.3.2. Lamellar

Lamellar thickness is correlated with melting temperature and the relation is shown by following equation [52],

$$T_m = T_m^0\{1-(\frac{2\sigma_e}{\Delta h_l l})\}$$

where T_m, T_m^0, σ_e Δh_l and l are the melting temperature, the equilibrium melting temperature, the melting enthalpy of a perfect crystal and free surface energy of the end face at which chains fold and lamellar thickness. The value of T_m^0, σ_e and Δh_l are 464 K [53], 102.9 J/cm^2 [53] and 209 J/g [54], respectively. The melting temperature of general PP is 160-165 °C, affected by crystallization conditions. Large lamellar is observed not in folded chain crystal but extended chain crystal.

1.3.3. Spherulite

After cooling molten polymer below melting temperature, spherical texture growing from center part is observed using polarized optical microscopy (POM). The texture is called as spherulite. The spherulite is grown with spherical shape, then heterogeneously grown to fill all region after reaching the boundary between spherulites.

Black crossed lines, so called, maltese cross are observed in spherulite using POM. The lines correspond to the direction of cross nicol, and the structure observed by POM is attributed from the difference of refraction index.

Since polymer is connected by covalent bond, the difference of refraction index between the direction among connecting chain and the vertical direction leads to anisotropy of light transmittance. It is called as birefringence (Δn) and expressed by following equation:

$\Delta n = n_c - n_{ab}$,

where n_c and n_{ab} are the refraction index among molecular axis and average refraction index of the vertical direction, respectively. Δn is expressed by positive and negative, which is determined by growth direction of lamellar. This phenomenon is explained by regime theory. Three different crystallization regimes are proposed by Hoffmann on nucleation and growth mechanism under supercooling (Figure 8) [55].

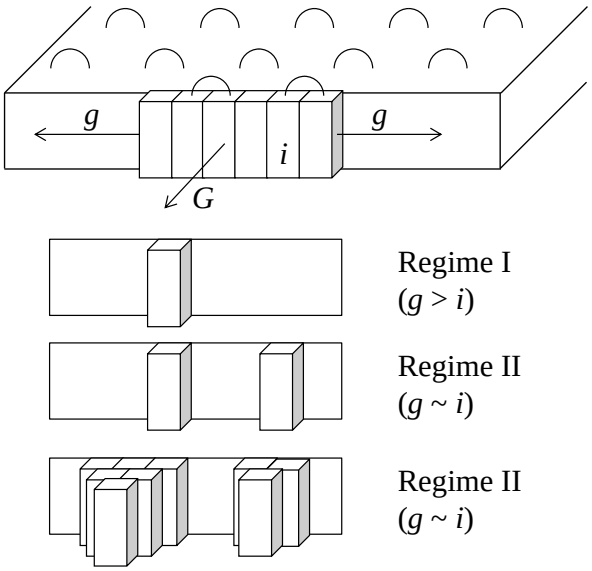

Figure 8. Illustration of regime on crystallization.

The regime is determined by the ratio of relative rate between substrate completion rate (g) and surface nucleation rate (i). Lamellar formed in Regime I ($g > i$) has flat growth surface. A lot of nucleation occurs before the flat surface is constructed in Regime II ($g \sim i$). Multilayer of stem is formed on growing surface before initial crystal layer is completed in Regime III ($g < i$). The growing mechanism is determined by isothermal crystallization temperature. Low crystallization temperature tends to induce the formation of lamellar in Regime III, and the transformation from Regime II to Regime III is observed at 137 °C on isothermal crystallization [56,57]. Regime II is also converted to Regime I at 148 °C [56]. The above mentioned temperature is affected by molecular weight of PP and insertion of comonomer. For example, comonomer insertion leads to the transformation from Regime II to Regime III at lower temperature [58]. Concerning birefringence, the lamellar formed in Regime I and II shows negative birefringence and positive birefringence is attributed from that in Regime III [59].

Impact resistance and transparency of PP are affected by spherulite size. Large spherulite size usually results in low impact resistance and unclearness of resulting PP. In order to reduce the spherulite size, addition of a nucleating agent is effective way [60,61]. Another approach is to control crystallization behavior, especially rapid cooling through mesophase leads to no spherulite structure, resulting in transparent PP [62-64].

1.3.5. Skin-core morphology

Skin-core morphology is frequently observed in products manufactured by injection molding. The formation of skin-core morphology is generally originated from

heterogeneity of chain conformation on crystallization. Since molecular chains of PP are oriented by strong shear flow during injection molding, a skin layer with strong orientation is formed near surface. However, the slow cooling coming from heat transfer to inside is sufficient to relax polymer chain before crystallization, resulting in a formation of a core layer with well-grown spherulite. It is well known that the morphology largely affects the resulting properties of PP. For example, mechanical properties like tensile strength, Young's modulus and impact strength were improved with increasing skin thickness [65,66]. The formation of skin-core morphology also induces transfer failure on injection molding. Therefore, several researchers have focused on the suppression of skin-core morphology by adding nucleating agent [67] or microfibrillar network [68].

1.3.5. Crystallization of Polypropylene

Polymer melted above non-equilibrium temperature and begins to be crystallized by supercooling from molten state. Crystallization behavior of PP is dramatically affected by the entanglement. Extended chain crystal (ECC) with a few ten micro meter and folded chain crystal (FCC) with a few ten nano meter are proposed as types of lamellar. FCC composed by quite thin two dimensional lamellar is unstable crystal due to large loss of surface free energy, and the size of ECC is large enough to be thermodynamically stable. Though ECC is more stable than FCC in terms of thermodynamic kinetics, formation of ECC hardly occurs. This is why the entanglement of polymer plays a key role to form FCC preferentially. Polymer in molten state is in the state of fully entangled Gaussian melt [69]. After the polymer is

supercooled, the crystal is gradually grown through chain sliding diffusion [70] because the chain is disentangled by the reputation motion of polymer chain. Since the actual polymer is usually in between fully entangled and completely disentangled states, the general crystallization leads to formation of FCC. No or less entangled polymer is at least necessary to construct ECC. It is found that control of the entanglement is very important on the crystallization.

Several methods have been proposed to prepare ECC using polyolefin, which is mainly classified into two approaches; catalyst technology and control of crystallization behavior. The former uses mesoporous silica as a supported structure for a catalyst to synthesize polyolefin with highly oriented chain, resulting in ECC [71,72]. The latter is achieved by crystallization under high pressure [73,74]. One of the novel crystals like ECC was developed by Hikosaka et al. who prepared nano oriented crystal (NOC) [75]. NOC with the lamellar thickness of about 20 nm was prepared through elongated crystallization by the compression of molten PP. About 100% of crystallinity was achieved by NOC and the tensile strength of resulting PP was seven times as high as that of general PP.

Disentanglement between polymer chains is gradually recovered by heat treatment under molten state [76]. Once ECC with less entanglement is melted, chain conformation is firstly changed from oriented to Gauss structures, and then the chains are gradually entangled. Therefore, fully entangled polymer is prepared by the heat treatment [77,78]. Formation of spherulite is also affected by polymer entanglement and center of spherulite is slightly moved by less entanglement moved during crystallization [79].

When molten PP is cooled to crystalize, the formed crystal is complicated by the

mode of crystallization like isothermal and non-isothermal crystallization. In case of non-isothermal crystallization with slow cooling rate, the polymer chains are largely disentangled by incorporating the chain into lamellar [80-82]. The phenomena, so called "reeling in", leads to high crystallinity and less entanglement, consequently resulting in high yield modulus and low strain hardening modulus [83,84]. On the other hand, less disentanglement of polymer chains is induced by isothermal crystallization. In case of isothermal crystallization, the most important parameter is supercooling temperature ($\Delta T = T_m^{\ 0} - T_c$ (T_c: isothermal crystallization temperature)) to define the higher order structure. It is known that nucleation rate (I) depends on degree of supercooling (ΔT), and Nishi et al. showed that the relationship was defined as

$$I = I_0 \exp(\Delta C/\Delta T_2),$$

where I_0 and C are constants [85] according to chain sliding theory. It is found that the size of spherulite is affected by ΔT. In addition, lamellar thickness is also express using ΔT as followed

$$l_c = \frac{a}{\Delta T} + b,$$

where a and b are constant [86]. Considering chain slide diffusion model, the heat treatment plays quite important role to control higher order structure.

The crystallization is often controlled by additives like nucleating agents. The roles of nucleating agents are described as followed: acceleration of crystallization rate, reducing spherulite size, formation of β crystal and so on. Another approach to control crystallization behavior is dimensional control of growth direction of lamellar. The confined crystallization is observed in thin film [87,88], porous structures [89-91] and micro-phase separation of block copolymer [92,93]. In addition, layer multiplying

extrusion was proposed as another approach to confine the growth direction of crystal. The method enables to fabricate films with tens of polymer nanolayer. Since polymer crystallization was confined in nanolayer, the formed lamellar is oriented parallel to film surface, leading to excellent gas barrier properties [94,95]. Thus, it is found that the crystallization of PP is affected not only by primary structure and crystallization conditions but also by additives.

1.3.6. Biaxially oriented polypropylene film

When polypropylene is extruded and stretched in both the machine direction and transverse direction, resulting film is called as BOPP. The strength and transparency are improved by biaxial orientation due to molecular and crystal orientation. BOPP is widely used as packaging materials [96]. In the processing, PP is firstly stretched in the machine direction (MD), and then subsequently drawn in the transverse direction (Figure 9). The mechanical properties are determined by draw ratio and molecular orientation [97,98].

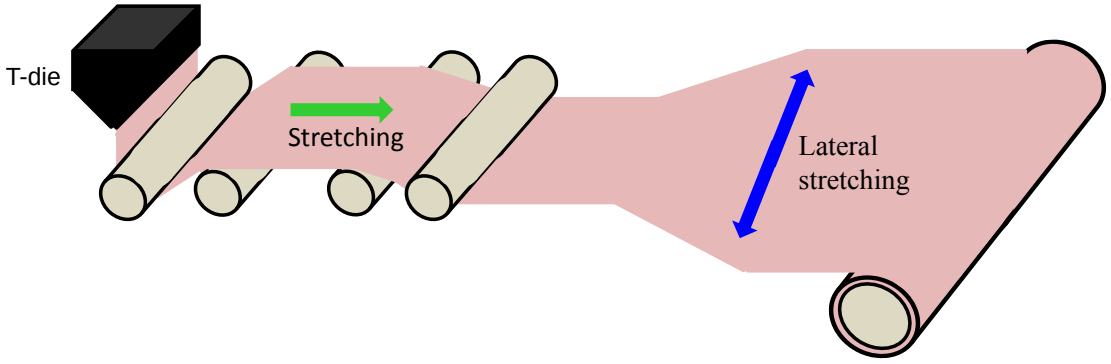

Figure 9. Preparation procedure of biaxially oriented polypropylene film.

1.4. PP compounds

1.4.1. Polypropylene composites

In the previous part, the importance of additives is described to control crystallization behavior. Introducing additive is a key factor not only to control crystallization behavior but also to add new functionality to polymer. There are several methods such as polymer alloy and polymer based composites to add new functionality. Especially, polymer-based nanocomposites are the most promising way to modify the mechanical properties. The addition of filler provides PP with comparative mechanical properties of other engineering plastics (Figure 10). Since PP has various merits compared to other plastics, further expansion of application of PP by replacing other plastics is highly desired.

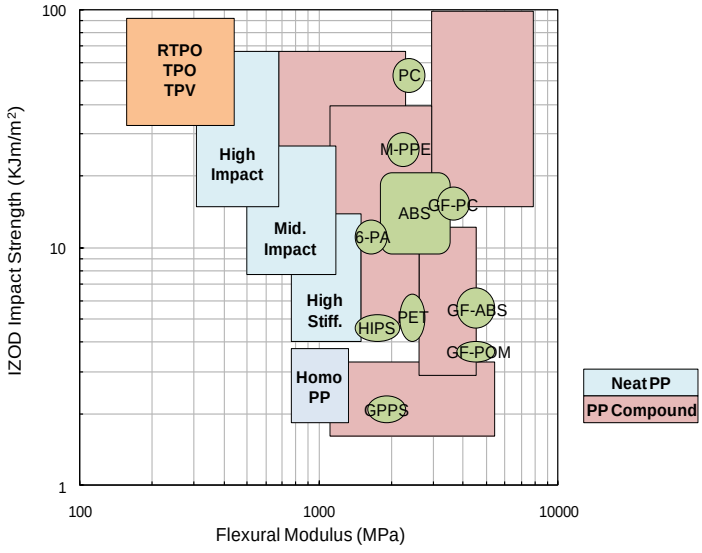

Figure 10. Mechanical properties of PP, PP compounds and other plastics.

The representative fillers are talc, calcium carbonate and glass fiber. Due to increasing needs of PP, the using amount of filler is gradually increased and talc is most

employed filler in PP compounds (Figure 11). These fillers also lead not only to further reinforcement of PP but also to decreasing the price.

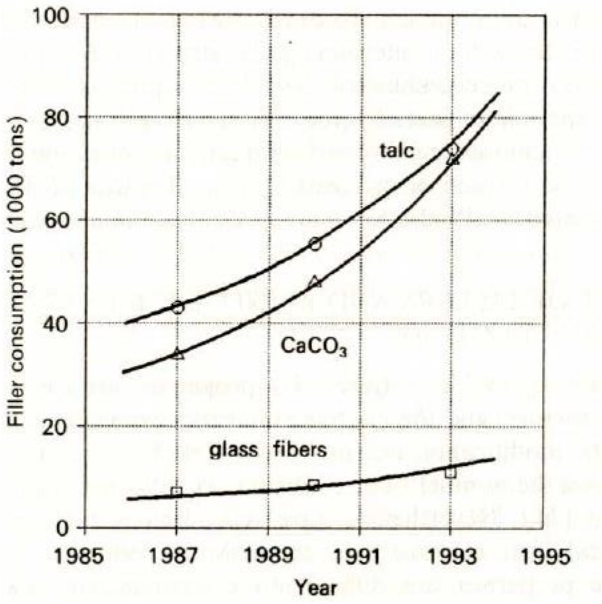

Figure 11. Amount of filler consumption in Western Europe for fillers (talc, $CaCO_3$ and glass fibers) as reinforcing agents for PP [99].

For example, talc is introduced in PP in order to improve the modulus, heat distortion temperature and shrinkage rate. Since talc does not enable to enhance the impact strength, rubber is also added to PP compounds. The representative materials are Toyota super olefin polymer, which mainly consists of PP homopolymer, EPR and talc. The special PP is widely used in the field of automobile production.

The surface of talc has usually hydrophilic nature, resulting in weak connectivity between PP and talc. The surface treatment using a silane coupling agent is frequently performed in order to solve the weak connectivity and reinforce dramatically [100]. Another important factor is the size of filler. The smaller the particle size is, the higher the reinforcement is (Figure 12) because specific surface area is increased with

decreasing particle size (Table 1).

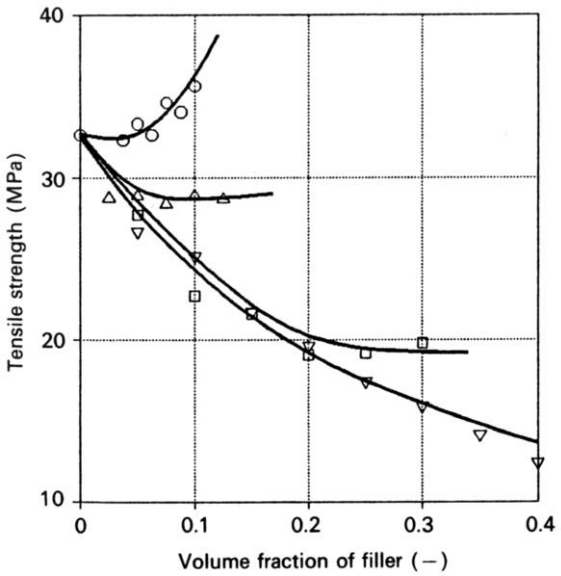

Figure 12. Effects of particle size on tensile strength of PP/$CaCO_3$ composites (particle diameter of (○) 0.01 μm, (Δ) 0.08 μm, (□) 3,3 μm, and (▽) 58.0 μm) [101,102].

Table 1. Relationship between particle size of $CaCO_3$ and the characteristic in PP.

Particle size (μm)	*Specific surface area* (m^2/g)	*Maximum packing* fraction (φ_f^{max})
58.0	0.5	0.82
3.5	1.9	0.66
3.6	2.2	0.49
3.6	3.3	0.40
1.3	5.0	0.31

Glass fibers are employed to obtain further reinforcement because glass fibers have large aspect ratio (Figure 13). On the other hand, optimization of melt mixing conditions is essential to obtain high reinforcement because of breakage of fibers during mixing.

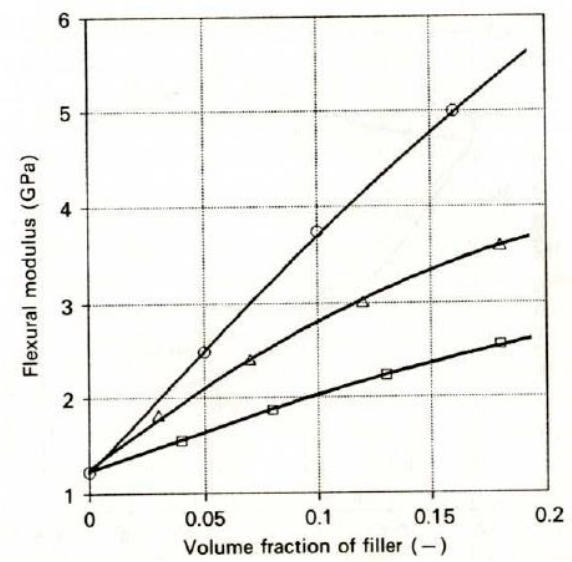

Figure 13. Effect of filler anisotropy on the flexural modulus of PP composites : (○) glass fiber, (Δ) talc, and (□) $CaCO_3$ [103].

1.4.2. Polymer-based nanocomposites

In the previous part, polymer-based composites using talc and glass fiber were described. In particular, fiber reinforced plastics (FRP) have been expected to highly improve the mechanical properties of polymer. However, the mismatch of size between polymer chain and fiber and/or defect structure in fiber prevent polymer from getting high reinforcement.

Polymer-based nanocomposites have been focused since Usuki et al. prepared

nylon6/clay nanocomposites in 1990s, which achieved dramatic reinforcement in modulus, heat and distortion temperature [104]. The reason why addition of nanoparticles leads to high reinforcement is that interactions between polymer and filler and/or between filler-filler is strengthened compared to that of micro-sized particle. The former is related to drastic increase of the specific surface area (Figure 14), which leads to effective load transfer from polymer to stiff nanoparticles [106-108].

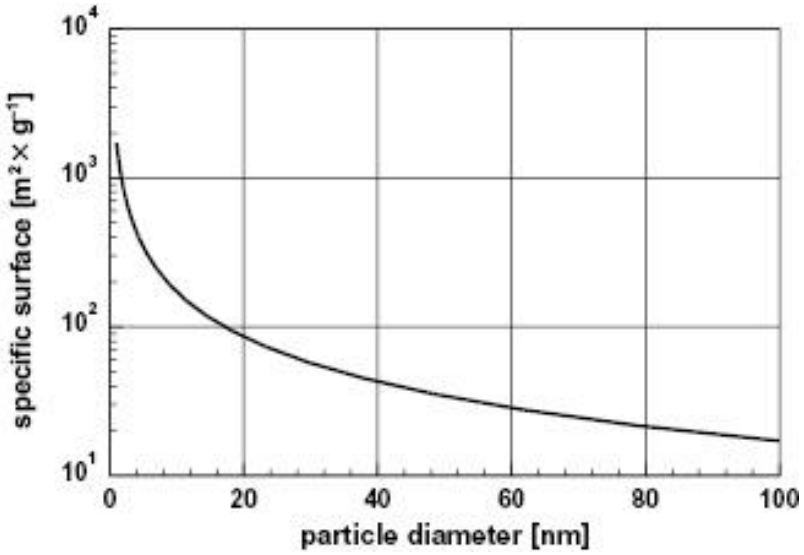

Figure 14. Relationship between particle diameter and specific surface area [105].

The latter is correlated with the confinement of polymer [109-111]. The formation of a network structure is also attributed from interaction and/or bridge through polymer chain between particles [112-114]. These factors result in drastic reinforcement at low filler loading (1 – 5 wt%). The nanocomposites are also expected not only as to improve the mechanical properties but also add functionalities such as electro conductivity, thermal conductivity, heat resistance, gas barrier properties and transparency. Many kinds of fillers including clay, carbon black, graphene, carbon nanotube, silica and so on have been employed to add required functionality into PP.

Since nanoparticles tend to aggregate in polymer due to strong interaction between nanoparticles, the control of the dispersion is quite important to achieve drastic reinforcement.

1.4.3. Network formation

Enhanced filler-filler and polymer-filler interactions in nanocomposites lead to the formation of network structures at a practical filler content, a key for constructing a pathway of load transfer [115-117] and exploitting the electro- and thermo-conducting properties of filler [118-121]. The percolation threshold which is minimum silica content to construct a network structure should be lower in terms of cost, embrittleness and density. The formation of a network structure is affected by the aspect ratio and dispersibility of filler particles as well as the polymer chemical structure and molecular weight [113,115,122-127]. Especially the control of filler dispersion is important to achieve a network formation. Akcora et al. used self-assembly approach in polystyrene to control aggregated structure of nano-silica [117]. Whereas 15 wt% of nano-silica is required on the homogeneous dispersion to construct network structure (Figure 15), the string or sheet-like aggregated structure lead to the disappearance of terminal flow in viscoelastic measurements at only a few loading (Figure 15).

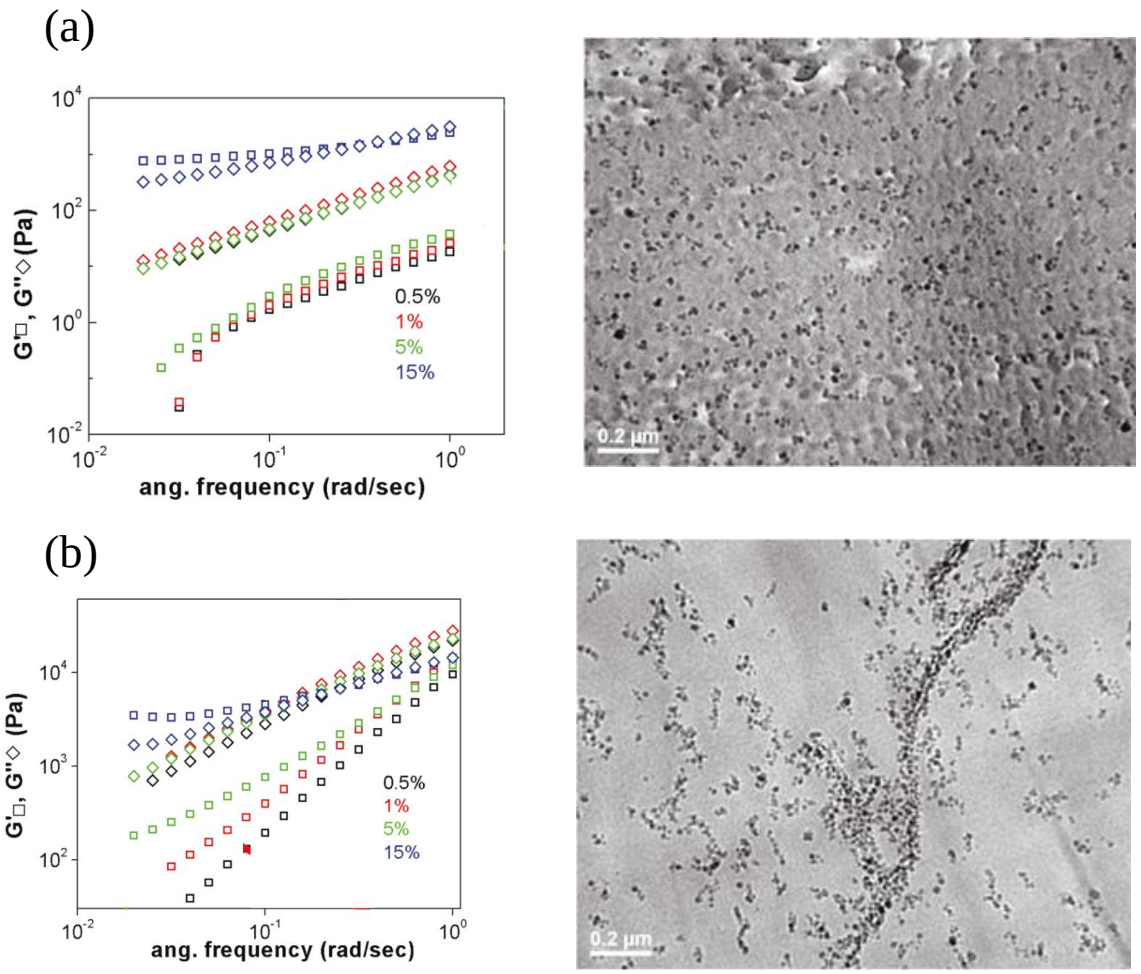

Figure 15. Dynamic viscoelastic measurement (left) and TEM picture (right) of PS/SiO_2 nanocomposites ((a) homogeneous dispersion and (b) formation of the sheet like aggregates).

Other promising methods to form low dimensional aggregates of nano-silica are to use template. When a filler is mixed in polymer blend, the filler is dispersed in one component or boundary between two different polymers because of the difference of polymer viscosity (Figure 16 (a)), resulting in diminished percolation threshold. The low dimensional aggregates were also produced in voids between polymer particles, which are prepared through latex technology (Figure 16 (b). The formation of low

dimensional aggregates is key role to reduce the percolation threshold.

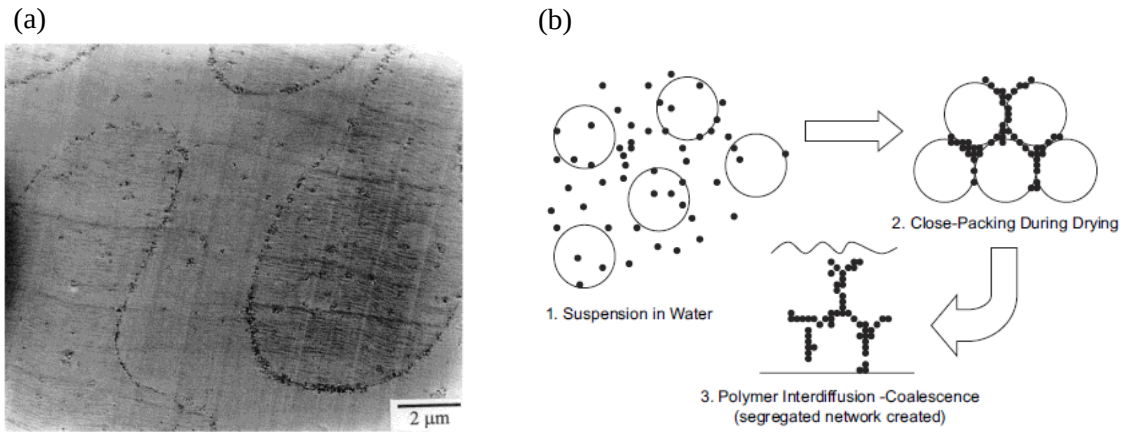

Figure 16. Template method for making low dimensional aggregates of silica (a) dispersed in boundary between two polymer components [128] and (b) dispersed in voids between polymer particles [129].

1.4.4. Biomaterials

One of the most ideal structures is represented by nature materials. Natural composites like tooth, bone, nacre exhibit far excellent mechanical properties in contrast to artificial mixture of their component (Figure 17).

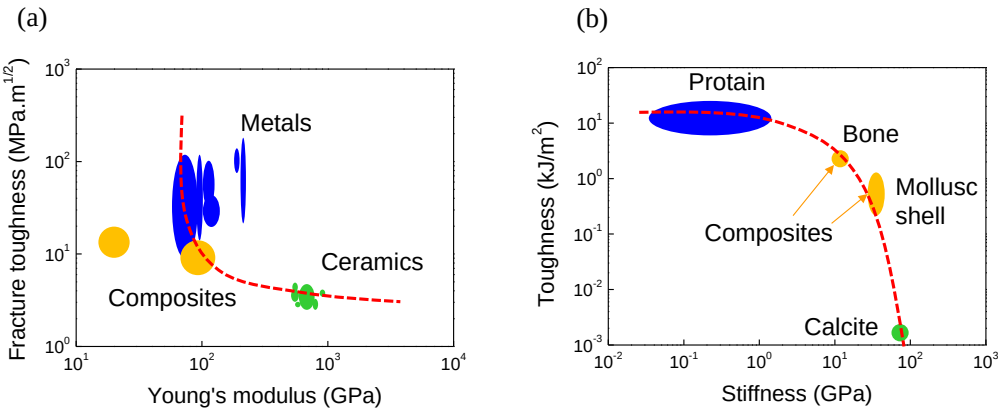

Figure 17. Mechanical properties of composite materials ((a) artificially prepared composites and (b) nature composites) [130].

In this session, nacre is used to explain the importance of the hierarchical structure. Nacre, which is composed by brittle $CaCO_3$ with a few percent addition of biopolymer exhibits a toughness about 3000 times higher than $CaCO_3$ [131], and the resulting properties are originated from architecture of nacre constructing the densely packed brick structure of layered $CaCO_3$ crystal (Figure 18). The formation of compact brick structures leads to the several mechanisms including crack deflection at the platelet/matrix interface [133], viscoelastic energy dissipation in the polymer matrix [134], interfacial strain hardening [135] and so on, resulting in strong and ductile hybrid materials. As shown below, nature materials are regarded as ideal composites structure.

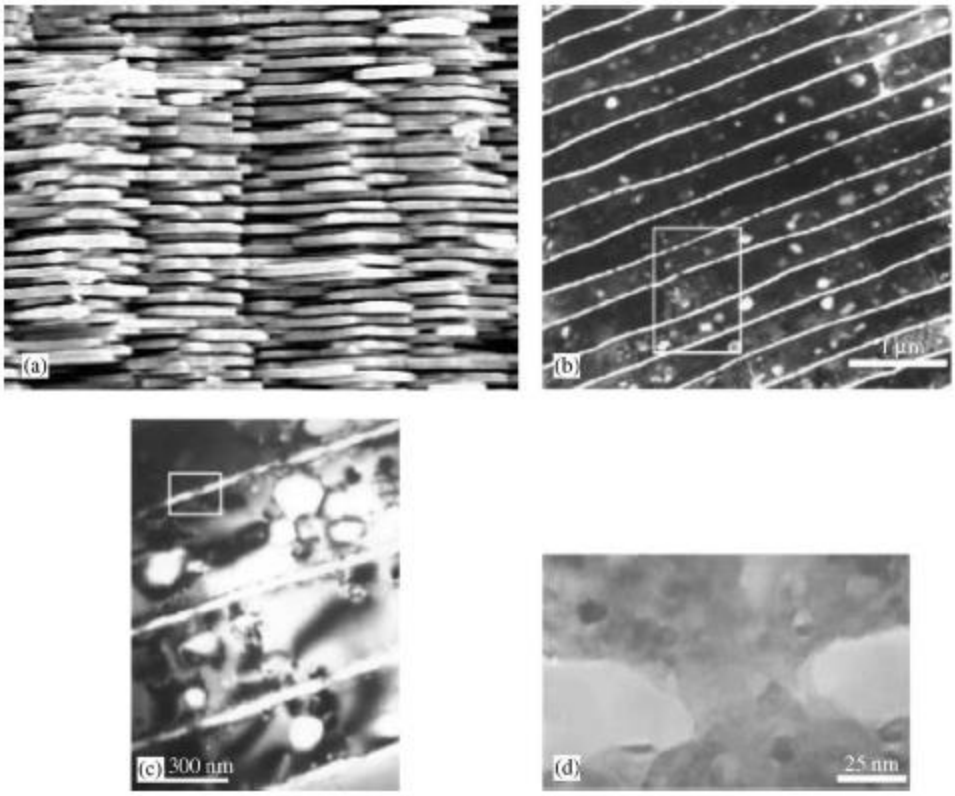

Figure 18　Hierarchical structures of nacre (a) SEM image, (b) TEM image, (c) and (d) TEM images of mineral bridges [132].

1.4.5. PP-based nanocomposites

It is essential for the drastic reinforcement to disperse highly in polymer matrix. However, apolar nature of PP makes it impossible to highly disperse polar nano-filler in PP. In order to remedy the poor compatibility between PP and filler, several approaches have been already proposed. The most frequently employed methods are adding compatibilizer [136-138] and/or the modification of filler surface [139-142]. Though these methods enable to disperse filler in PP, it is required for further reinforcement to acquire new knowledge like the establishment of structure property relationship on nanocomposites and/or the formation of special structure like nature

materials. We focused the preparation of PP/silica through sol-gel synthesis for these targets.

Sol-gel method is used to prepare metal oxide particle from metal alkoxide. The method consists of the hydrolysis of metal alkoxide and subsequent condensation. Sol-gel synthesis of metal oxide particle has many advantages compared to other synthesis methods. Firstly, metal oxide particles are synthesized at low temperature. The calcination temperature which is necessary to make crystal structure of metal oxide is also reduced by sol-gel synthesis. Secondary, the shape of formed silica is controlled by sol-gel method combined with other technique such as template method [143-145], dipping method [146] and so on. Thirdly, the structures like size and/or pore are controlled by conditions of sol-gel reaction including ratio of solvent, water and metal alkoxide, reaction time, catalyst. Especially, employed catalyst plays an important role to control the morphology of formed silica. In case of acid catalyst, since the hydrolysis reaction preferentially occurs, silica tends to form linear structure [147]. In contrast, sol-gel synthesis catalyzed by base leads to three dimensional network of silica (Figure 19).

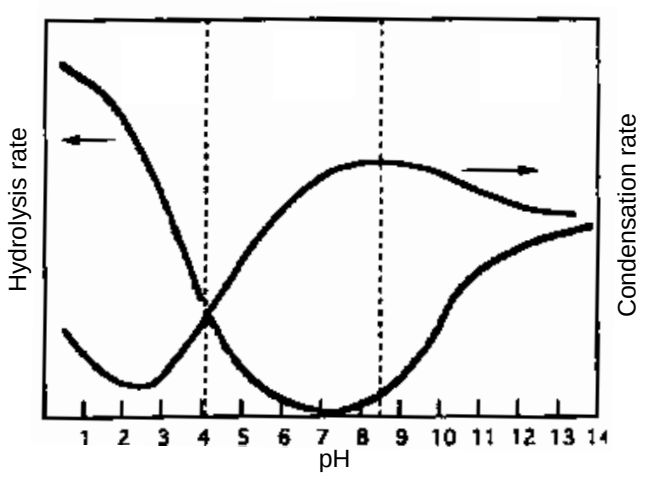

Figure 19. Effects of pH on hydrolysis rate and condensation rate.

Preparation of polymer-based nanocomposites based on sol-gel method is usually achieved by solvent mixing with polymer and metal alkoxide [148-150] and swell of polymer to impregnate metal alkoxide [151-154]. However, poor solubility and swelling properties of PP restrict the usage of these usual methods. Special combination is essentially required to employ sol-gel method for PP-based nanocomposites preparation, and impregnation [155], solid-state modification [156], elongation [157] and melt mixing [158-161] have been proposed.

1.5. Objective

The purpose of this study is getting knowledge to produce high performance PP materials. To achieve this purpose, the impregnation of PP amorphous region with silicon alkoxide with the aid of supercritical CO_2 ($scCO_2$) and subsequent sol-gel reaction were employed. $ScCO_2$ is frequently employed in the field of both academic and industrial application due to low critical point (Figure 20).

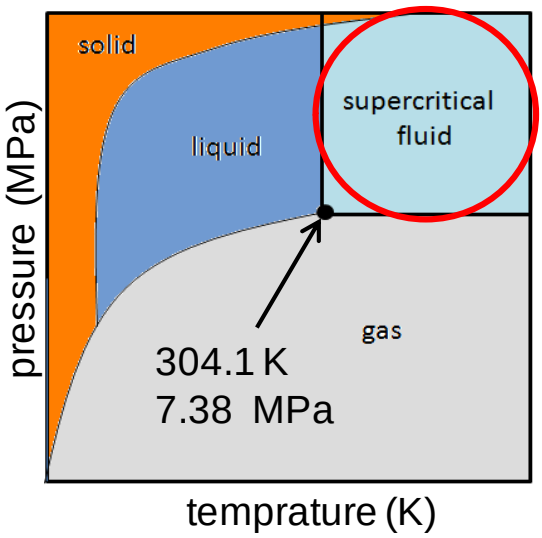

Figure 20. Schematic phase diagram for a pure CO_2.

Since $scCO_2$ has features including diffusivity like gas and solubility like solution, $scCO_2$ can disperse silicon alkoxide into the swollen amorphous region without dissolving the crystal part. The feature possesses many merits to get knowledge for high performance PP materials.

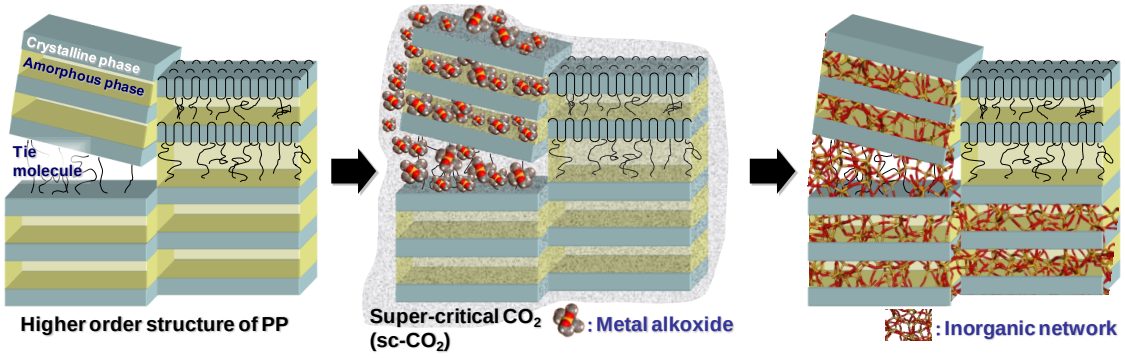

Figure 21. Synthetic images

Firstly, the higher order structure is not changed after incorporating silica. Since a filler is usually introduced before higher order structure of PP is defined, resulting higher order structure is affected by the filler through nucleating effects and/or confined crystallization [162-164], which causes the difficulty to establish the relationship between introduced filler structure and resultant properties. Because this method enables individual control between the higher order structure and silica structure formed by sol-gel method, it was expected to establish the structure property relationship.

Secondary, the sol-gel synthesis is performed in confined amorphous space in PP. Spherical silica is synthesized by usual sol-gel method. Therefore, template is frequently employed to control the morphology of silica [143-145]. Sol-gel synthesis in amorphous region of PP is also regarded as template synthesis because confinement of silica formation is induced by nano-space of the amorphous region, resulting in morphological control of silica.

Thirdly, top down synthesis of bio-inspired PP-based nanocomposites is expected using BOPP. Since the structures formed by combination of oriented crystal and oriented silica formed in oriented amorphous region is similar with that of nacre, drastic reinforcement was expected.

The contents are classified into five chapters. In this chapter, importance of PP and PP compounds on structure and properties were described. In the chapter 2, sol-gel synthesis of nano-sized silica in confined amorphous space of polypropylene and relationship between nano-level structures of silica and physical properties of resultant nanocomposites was discussed. In the chapter 3, morphological control of silica in polypropylene using confined amorphous space as template was discussed. In the chapter 4, development of bio-inspired polypropylene-based materials through sol-gel reaction in laminated biaxially oriented polypropylene was discussed. In chapter 5, the general conclusion was described.

It was believed that the obtained results must be contributed for the knowledge to produce high performance PP materials.

References

[1] Natta G, Pino P, Corradini P, Danusso F, Mantica E, Mazzanti G, Moraglio G. J Am Chem Soc 1955;77:1708.

[2] Ziegler K. Angew Chem 1952;64:323.

[3] Turner-Jones A, Aizlewood JM, Beckett DR. Makrom Chem 1964;75:134.かぶり

[4] Keith HD, Padden Jr FJ, Walker NM, Wyckoff HW. J Appl Phys 1959;30:1485.

[5] De Rosa C, Auriemma F, Capua AD, Resconi L, Guidotti S, Camurati I, Nifant'ev IE, Laishevtsev IP. J Am Chem Soc 2004;126:17040.

[6] Stricker F, Bruch M, Mülhaupt R. Polymer 1997;38:5347.

[7] De Rosa C, Auriemma F, De Ballesteros OR, Resconi L, Camurati I. Macromolecules 2007;40:6600.

[8] Hosoda S, Hori H, Yoda K, Nakahara S, Tsuji M. Polymer 2002;43:7451.

[9] Deanin RD. Polymers, Structure, Properties and Applications. Cahners Pub.Co.; 1972.

[10] Natta G, Corradini P. del Nuovo Cimento 1960;15:40.

[11] Mencik Z. Chem Prum 1960;10:377. Hikosaka M, Seto T. Polym J 1973;5:111.

[12] Hikosaka, M, Sato T. Polym J 1973;5:111.

[13] Auriemma F, De Ballesteros OR, De Rosa C, Corradini P. Macromolecules 2000;33:8764.

[13] Naiki M, Kikkawa T, Endo Y, Nozaki K, Yamamoto T, T Hara Polymer 2000;42:5471.

[14] De Rosa C, Guerra G, Napolitano R, Petraccone V, Pirozzi B. Eur Polym J 1984;20:937.

[15] Khoury FJ. Res Nat Bur St 1966;70A:29.

[16] Lot B, Wittmann JC. J polym Sci Phys Ed 1987;25:1079.

[17] Padden FJ, Keith HD. J Appl Phys 1996;37:4013.

[18] Lotz B, Graff S, Straupe S, Wittman JC. Polymer 1991;32:2902.

[19] Samuels RJ, Yee RY. J Polym Sci 1972;20:385.

[20] Leugering HJ. Makromol Chem 1967;109:204.

[21] Lotz B, Kopp S, Dorset DCR. Acad Sci Paris IIb 1994;319:187.

[22] An B. Acta Polym Sin 1993;3:330.

[23] Lotz B, Wittmann JC, Lovinger AJ, Polymer 1996;37:4979.

[24] Fujiwara Y. Colloid Polym Sci 1975;253:273.

[25] Lovinger AJ, Chua JO, Gryte CC. J Polym Sci Polym Phys Ed 1977;15:641.

[26] Leugering HJ, Kirsch G. Angew Makromol Chem 1973;33:17.

[27] Devaux E, Chabert B. Polym Commun 1991;32:33.

[28] Somani RH, Hsaio BS, Nogales A, Fruitwala H, Srinivas S, Tsou AH. Macromolecules 2001;34:5902.

[29] Asano T, Fujiwara Y. Polymer 1978;19:99.

[30] Morrow DR. J Macro Sci Phys 1969;133:53.

[31] Ulmann W, Wendorff JH. Prog Colloid Polym Sci 1979;66:25.

[32] Moos KH, Tilger B. Angew Makromol Chem 1981;94:213.

[33] Brückner S, Meille SU, Petraccone U, Pirozzi B. Prog Polym Sci 1991;16:361.

[34]Campbell RA, Phillips PJ. Polymer 1997;21:97.

[35] Marrow DR, Newman BA. J Appl Polym Sci 1968;39:4944.

[36] Kojima H. J Polym Scie 1968;6:1255.

[37] Assouline E, Fulchiron R, Gerard JF, Wachtel E, Wagner HD, Marom G. J Polym Sci Part B: Polym Phys 1999;37:2534.

[38] Campbell RA, Philips PJ. Polymer 1997;38:5725.

[39] Lotz B. Dur Phys J E 2000;B39:109.

[40] Imai M, Mori K, Mizukami T, Kaji K, Kanaya T. Polymer 1992;33:4451.

[41] Thomann R, Wang C, Kressler J, Mülhaupt R. Macromolecules 1996;29:8425.

[42] Jeon K, Palza H, Quijada R, AlamoRG. Polymer 2009;50:832.

[43] Turner-Jones A. Polymer 1971;12:487.

[44] Lotz B, Graff S, Straupé C, Wittmann JC. Polymer 1994;32:2903.

[45] Coccorullo I, Pantani R, Titomanlio G. Polymer 2003;44:307.

[46] Hsu CC, Geil PH, Miyaji H, Asai K. J Polym Sci Polym Phys 1986;24:2379.

[47] Konishi T, Nishida K, Kanaya T, Kaji K. Macromolecules;38:8749.

[48] Wang ZG, Hsiao BS, Srinivas S, Brown GM, Tsou AH, Cheng SZD, Stein RS. Polymer 2001;42:7561.

[49] Martorana A, Piccarolo S, Sapoundjieva D. Macromol Chem Phys 1999;200:531.

[50] Varga J. Angew Makromol Chem 1982;104:79.

[51] De Rosa C, Auriemma F. J Am Chem Soc 2006;128:11024.

[52] Laurizen JI, Hoffman JD. J Res Nat Bur Std 1962;64A:73.

[53] Bershtein VA, Egorov VM. Differential Scanning Calorimetry of Polymers. Physics, Chemistry, Analysis, Ellis Horwood, London, 1994.

[54] Jose RI, Leo M, Maria JG, Rufina GA. J Polym Sci Part B Polym Phys 1998;37:323.

[55] Lauritzen JI, Hoffman JD. J Appl Phys 1973;44:4340. Hoffman JD. Polymer 1983;24:3.

[56] Cheng SZD, Janimak JJ, Zhang A, Cheng HN. Macromolecules 1990;23:298.

[57] Clark EJ, Hoffman JD. Macromolecules 1984;17:878.

[58] Monasse B, Haudin JM. Colloid Polym Sci 1988;266:679.

[59] Padden Jr FJ, Keith HD. J Appl Phys 1959;30:1479.

[60] Beck HN, J Appl Polym Sci 1965;9:2131.

[61] Morrow DR. J Macromol Sci Phys 1965;B3:53.

[62] Gezovich DM, Geil PH. Polym Eng Sci 1968;8:202.

[63] Nishida K, Konishi T, Kanaya T, Kaji K. Polymer 2004;45:1433.

[64] Nitta K, Odaka K. Polymer 2009;50:4080.

[65] Fujiyama M, Awaya H. J Polym Scie Polym Phys Ed 1977;21:3291.

[66] Kantz MR, Newman HD, Stigale FH. J Appl Polym Sci 1972;16:1249.

[67] Zhu PW, Edward G. Macromol Mater Eng 2003;288:301.

[68] Zhang GJ, Li L, Mendes E, Byelov D. Fu Q, Li ZM. Macromolecules 2006;39:6771.

[69] Yamazaki S, Hikosaka M, Toda A, Wataoka I, Gu F. Polymer 2002;43:6585.

[70] Hikosaka M. Polymer 1990;31:458.

[71] Kageyama K, Tamazawa J, Aida T. Science 1999;285:2113.

[72] Millera CJ, O'Hare D. Chem Commun 2004;15:1710.

[73] Wunderlich B, Melillo L. J Polym Sci 1969;A27:2091.

[74] Bassett DC, Turner B. Phil Mag 1974;29:925.

[75] Okada K, Washiyama J, Watanabe K, Sasaki S, Masunaga H, Hikosaka M. Polym J 2010;42:464.

[76] Pandey A, Champouret Y, Rastogi S. Macromolecules 2011;44: 4952.

[77] Mezghani K, Anderson-Campbell R. Phillips PJ. Macromolecules 1990;23:298.

[78] Martuscelli E, Pracella M, Crispino L. Polymer 1983;24:693.

[79] Wang X, Wang Z, Luo K, Huang Y. Macromolecules 2011;44:2844.

[80] DiMarzio EA, Guttman CM, Hoffman JD, Faraday Discuss 1979;68:210.

[81] Hoffman JD. Polymer 1982;23:656.

[82] Peterlin A. Macromolecules 1980;13:777.

[83] van Melick HGH, Govaert LE, Meijer HEH Polymer 2003;44:2493.

[84] Schrauwen BAG, Janssen RPM, Govaert LE, Meijer HEH. Macromolecules 2004;37:6069.

[85] Nishi M, Hikosaka M, Ghosh SK, Toda A, Yamada K. Polym J 1999;31:749.

[86] Gedde UW. Polymer physics. London: Kluwer; 1999.

[87] Frank CW, Rao V, Despotopoulou MM, Pease RFW, Hinsberg WD, Miller RD, Rabolt JF. Science 1996;306:76.

[88] Despotopoulou MM, Miller RD, Rabolt JF, Frank CW J Polym Sci Part B Polym Phys 1996;34:2335.

[89] Shin K, Woo E, Jeong YG, Kim C, Huh J, Kim KW. Macromolecules 2007;40:6617.

[90] Woo E, Huh J, Jeong YG, Shin K. Phys Rev Lett 2007;98:136103.

[91] Duran H, Steinhart M, Butt HJ, Floudas G. Nano Lett 2011;11:1671.

[92]Shin K, Xiang HQ, Moon SI, Kim T, McCarthy TJ, Russel TP. Science 2004;306:76.

[93] Chen HL, Wu JC, Lin TL, Lin JS. Macromolecules 2001;34:6936.

[94] Wang H, Keum JK, Hiltner A, Baer E, Freeman B, Rozanski A, Galeski A. Science 2009;323:6.

[95] Chung TM, Ho RM, Kuo JC, Tsai JC, Hsiao BS, Sics I. Macromolecules 2006;39:2739.

[96] Kissel KJ, Han JH, Meyer JA Handbook of Polypropylene and Polypropylene

Composites, Marcel Dekker, New York, 2003.

[97] Peterlin A. J Appl Phys 1977;48:4099.

[98] Strobel JM, Nam S. J Appl Polym Sci 1991;42:159.

[99] Schlumpf HP. Modern aspects of fillers in polypropylene, presented at the 10th International Macromolecule Symposium, 20-21 September, 1990, Interlaken, Switherland.

[100] Pluddeman EP. Silane Coupling Agents, Plenum Press, New York, 1982.

[101] Pukánszky B, Turscányi B, Tüdös F. Effect of interfacial interaction on the tensile yield stress of polymer composites, in Interfaces in Polymer, Ceramic, and Metal Matrix Composites, Elsevier, New York, 1988.

[102] Pukánszky B. Composites 1990;21:255.

[103] Schlumpf HP. Kunststoffe 1983;73:511.

[104] Usuki A, Kawasumi Y, Kojima Y, Okada A, Kurauchi T, Kamigaito O. J Mater Res 1993;8:1174.

[105] Vollath D. Nanoparticles-Nanocomposites Nanomaterials: An Introduction for Beginners. Wiley, 2013.

[106] Wang S, Liang R, Wang B, Zhang C. Chem Phys Lett 2008;457:371.

[107] Schadler LS, Giannaris SC, Ajayan PM. Appl Phys Lett 1998;73:3842.

[108] Srivastava I, Mehta RJ, Yu ZZ, Schadler L, Koratkar N. Appl Phys Lett 2011;98: 063102.

[109] Xu B, Zheng Q, Song Y, Shangguan Y. Polymer 2006;47:2904.

[110] Termonia Y. J Polym Sci Part B: Polym Phys 2010;48:687.

[111] Lu H, Nutt S. Macromolecules 2003;36:4010.

[112] Starr FW, Douglas JF, Glotzer SC. J Chem Phys 2003;119:1777.

[113] Jouault N, Vallat P, Dalmas F, Said S, Jestin J, Boué F. Macromolecules 2009;42:2031.

[114] Otsubo Y. Langmuir 1990;6:114.

[115] Chabert E, Bornert M, Bourgeat-Lami E, Cavaillé JY, Dendievel R, Gauthier C, Putaux JL, Zaoui A. Mat Sci Eng A 2004;381:320.

[116] Moll JF, Akcora P, Rungta A, Gong S, Colby RH, Benicewicz BC, Kumar SK. Macromolecules 2011;44:7473.

[117] Akcora P, Kumar SK, Moll J, Lewis S, Schadler LS, Li Y, Benicewicz BC, Sandy A, Narayanan S, Ilavsky J, Thiyagarajan P, Colby RH, Douglas, JF. Macromolecules 2010;43:1003.

[118] Foygel M, Morris RD, Anez D, French S, Sobolev VL. Phys Rev B 2005;71:104201.

[119] Bonnet P, Sireude D, Garnier B, Chauvet O. Appl Phys Lett 2007;91:201910.

[120] Moniruzzaman M, Winey KI. Macromolecules 2006;39:5194.

[121] Gojny FH, Wichmann MHG, Fiedler B, Kinloch IA, Bauhofer W, Windle AH, Schulte K. Polymer 2006;47:2036.

[122] Lu C, Mai YW. Phys Rev Lett 2005;95:088303.

[123] Li J, Kim JK. Compos Sci Technol 2007;67:2114.

[124] Li J, Ma PC, Chow WS, To CK, Tang BZ, Kim JK. Adv Funct Mater 2007;17:3207.

[125] Barnes HA. Rheology Reviews 2003. British Society of Rheology; 2003. p. 1-36.

[126] Zhu Z, Thompson T, Wang SQ, von Meerwall ED, Halasa A. Macromolecules 2005;38:8816.

[127] Zhang Q, Archer LA. Langmuir 2002;18:10435.

[128] Cheah K, Forsyth M, Simon GP. J Polym Sci Part B: Polym Phys 2000;38:3106.

[129] Kim YS, Wright JB, Grunlan JC. Polymer 2008;49:570.

[130] Espinosa HD, Rim JE, Barthelat F, Buehler MJ. Prog Mater Sci 2009;54:1059.

[131] Fratzl P, Gupta HS, Paschalis EP, Roschger P. J Mater Chem 2004;14:2115.

[132] Songa F, Sohb AK, Bai YL. Biomaterials 2003;24:3623.

[133] Fratzl P, Gupta HC, Fischer FD, Kolednik O. Adv Mater 2007;19:2657.

[134] Bouchbinder E, Brener EA. J Mech Phys Solid 2011;59:2279.

[135] Espinosa HD, Juster AL, Felix J. Latourte, Loh OY, Gregoire D, Zavattieri PD. Nature Commun 2011;2:173.

[136] Hasegawa N, Kawasumi M, Kato M, Usuki A, Okada A. J Appl Polym Sci 1998;67:87.

[137] Hasegawa N, Okamoto H, Kato M, Usuki A. J Appl Polym Sci 2000;78:1918.

[138] Pavlidou E, Bikiaris D, Vassiliou A, Chiotelli M, Karayannidis G. J Phys 2005;10:190.

[139] Wu CL, Zhang MQ, Rong MZ, Friedrich K. Compos Sci Technol 2002;62:1327.

[140] Cai LF, Huang XB, Rong MZ, Ruan WH, Zhang MQ. Polymer 2006;47:7043.

[141] Zhou HJ, Rong MZ, Zhang MQ, Ruan WH, Friedrich K. Polym Eng Sci 2007;47:499.

[142] Umemori M, Taniike T, Terano M. Polym Bull 2012;68:1093.

[143] Yang P, Zhao D, Chmelka BF, Stucky GD. Chem Mater 1998;10:2033.

[144] Niesz K, Yang P, Somorjai GA, Chem Commun 2005;15:1986.

[145] Lakshimi BB, Patrissi CJ, Martin CR. Chem Mater 1997;9:2544.

[146] Matsuda A, Matoda T, Kogure T, Tadanaga K, Minami T, Tatsumisago M. Chem Mater 2005;17:749.

[147] Sakka S, Kamiya K, Makita K, Yamamoto Y. J Non-Cryst Solids 1984;63:223.

[148] Hsu YG, Tu LC, Lin KH. J Polym Res 2001;8:37.

[149] Tang H, Wan Z, Pan M, Jiang AP. Electrochem Commun 2007;9:2003.

[150] Bounour-Legaré V, Angelloz C, Blanc P, Cassagnau P, Michel A. Polymer 2004;45:1485.

[151] Mark JE, Ning YP, Jiang CY, Tang MY, Roth WC. Polymer 1985;26:2069.

[152] Chaichua B, Prasassarakich P, Poompradub S. J Sol-Gel Sci Technol 2009;52;219.

[153] Yuan QW, Mark JE. Macromol Chem Phys 1999;200:206.

[154] Tangpasuthadol V, Intasiri A, Nunticanich D, Niyompanich N, Kiatkamjournwong S. J Appl Polym Sci 2008;109:424.

[155] Sun D, Zhang R, Liu Z, Huang Y, Wang Y, He J, Han B, Yang G. Macromolecules 2005;38:5617.

[156] Jain S, Goossens H, Picchioni F, Magusin P, Mezari B, van Duin M. Polymer 2005;46:6666.

[157] Adachi K, Hirano T, Kasai PH, Nakamae K, Iwabuki H, Murakami K. Polym. Int. 2010;59:510.

[158] Mizutani Y, Nago S J Appl Polym Sci 1999;72:1489.

[159] Dou Q, Zhu X, Peter K, Demco DE, Möller M, Melian C, J Sol-Gel Sci Technol 2008;48:51.

[160] Bahloul W, Legare VB, David L, Cassagnau P. J Polym Sci Part B Polym Phys 2010;48:1213.

[161] Kaneko K, Yadav N, Takeuchi K, Maira B, Terano M, Taniike T. Compos Sci Tech 2014;102:120.

[162] Nam PH, Maiti P, Okamoto M, Kotaka T, Hasegawa N, Usuki A. Polymer

2001;42:9633.

[163] Ma J, Zhang S, Qi Z, Li G, Hu Y, J Appl Polym Sci 2002;83:1978.

[164] Fukuyama Y, Kawai T, Kuroda S, Toyonaga M, Taniike T, Terano M. J Therm Anal Calorim 2013;113:1511.

Chapter 2.

Sol-gel Synthesis of Nano-sized Silica in Confined Amorphous Space of Polypropylene and Relationship Between Nano-level Structures of Silica and Physical Properties of Resultant Nanocomposites

2.1. Introduction

Polymer nanocomposites have attracted great attention in these two decades as an attractive way to attain drastic improvements in various properties (such as mechanical strength, gas barrier, heat resistance, etc.) at a small content of nano-sized filler. In comparison with micron-sized filler, the nano-sized filler offers much shorter particle-particle distance and much greater interfacial area with polymer. Thus enlarged filler-filler and polymer-filler interaction in nanocomposites facilitate the formation of network structures at a practical filler content, a key for constructing a pathway of load transfer [1-4] and exploitting the electro- and thermo-conducting properties of filler [5-8].

The term “percolation threshold” express the minimum content of filler required to form a network structure. While the increase of the filler content necessarily leads to the network formation, the percolation at a small filler content is practically important in terms of cost, density, and embrittlement all adversely affected by excess loading. The percolation threshold is affected by various factors, for example, the aspect ratio and dispersibility of filler particles as well as the polymer chemical structure and molecular weight [3,4,9-22]. However, the most fundamental parameter is the nano-level dispersion of filler particles in polymer. In this light, several groups attempted to precisely control the dispersion of filler for establishing relationships between the filler dispersion and physical properties of resultant nanocomposites (structure-property relationship) [23-27].

Akcora et al. successfully controlled the dispersion of spherical filler in amorphous polystyrene by utilizing self-assembly of the filler particles, and concluded that low-dimensional aggregates with the morphology of one-dimensional string or

two-dimensional sheet morphology result in much higher reinforcement and lower percolation thresholds, compared with zero-dimensional uniform dispersion and three-dimensional compact aggregates [3]. Jouault et al. also presented a self-assembly-based novel methodology to form small aggregates with fractal-like morphology in polystyrene over a wide range of filler contents [4]. They observed the appearance of a solid-like behavior in melt linear viscoelastic measurements at the silica content as small as 3 vol%, while the percolation threshold was determined as 7 vol%. The template method is an alternative strategy to provide such low-dimensional aggregates in polymer through aggregation of filler particles within confined spaces (templates) [16-22]. Significant reductions in the percolation threshold were reported by localizing filler particles at boundaries in co-continuous morphology of immiscible polymer blends with co-continuous morphology [16-18], and by concentrating filler particles in interparticle voids of polymer particulates [19-22]. The template approach has an advantage to shape the dispersion structures of nanoparticles by utilizing predefined spaces, but it has been rarely employed for studying structure-property relationships.

Polypropylene (PP) is one of the most widely used plastics from commodity to specialty applications due to its comprehensive advantages in cost, thermal properties, mechanical and rheological properties, environmental load and so on. Motivated by its huge market, a lot of research has been done on PP-based nanocomposites. Especially, the largest efforts were devoted to alleviate poor dispersion of nanoparticles and weak interfacial connections between PP and nanoparticles. For example, the addition of a compatibilizer such as maleic anhydride-grafted PP is the most adopted approach to improve the dispersion of nanoparticles [28-30]. Grafting polymeric chains onto

nanoparticles is a promising approach to remedy both the poor dispersion and weak connection [31-34]. However, these solutions generally promote the homogeneous dispersion (i.e. zero-dimensional) of nanoparticles, and an attempt to manufacture dispersion structures having intermediate fractal dimensions other than three and zero is highly desired, which is essential not only to lower the percolation threshold but also to establish the said structure-property relationships.

The main difficulties are obviously attributed to the poor compatibility of PP with nanoparticles, easily falling into three-dimensional aggregates, and to the poor solubility of PP in polar solvents, making the controlled self-assembly strategy inapplicable. Another serious problem is related to phenomena that occur during the crystallization of polymer in the presence of nano-sized filler: The addition of nano-sized filler generally affects the crystallization behavior of polymer through nucleation effects and/or confined crystallization [35-40]. Therefore, physical properties of nanocomposites are not merely affected by the dispersion structure of filler, but also affected or even dominated by differences in polymer higher-order structures that originate from dependence of the polymer crystallization on the filler dispersion. It is also known that the growth of lamellar structures changes the placement of each nanoparticle nanoparticles and consequently perturbs the dispersion of filler which are once designed in melt [41].

In order to control the dispersion structures of filler and to establish structure-property relationships for PP-based nanocomposites, we sought an approach to introduce filler into predefined higher-order structures as a template without using usual melt- or solution-blending processes. Sun et al. presented a novel route to prepare PP-based nanocomposites, which consists of impregnation of metal alkoxide in a PP

film with the aid of supercritical CO_2 ($scCO_2$) and subsequent filler formation via sol-gel reaction [42]. Since $scCO_2$ can disperse metal alkoxide into the swollen amorphous region without dissolving the crystal part, this method is expected to enable individual control of polymer higher-order structures and filler dispersion structures. Furthermore, the sol-gel process in confined spaces such as mesopores is a scientifically attractive way to produce isolated nanoparticles [43-45]. In this light, metal oxide particles synthesized in low-dimensionally confined polymer amorphous nanospaces is an interesting and important target of study.

The purposes of the present study are twofold: i) To control the structure of silica nanoparticles in PP, based on the impregnation of silicon alkoxide with $scCO_2$ and subsequent sol-gel reaction, and ii) to establish relationships between the structure of the formed nanoparticles and physical properties of the nanocomposites. Silica particles formed in the amorphous region of PP were uniformly dispersed in the matrix with the sizes becoming less than 10 nm. The mass fractal dimension of the silica nanoparticles varied between two and three according to the kinds of employed silicon alkoxide and catalysts. It was found that the mass fractal dimension of the nanoparticles was well correlated with the Young's modulus in solid state and low-frequency storage modulus in molten state, where a lower dimension led to higher reinforcement.

2.2. Experimental

2.2.1. Materials

Random PP (M_w: 1.6 x 10^5, ethylene content: 2.5 wt%, donated by Japan

Polypropylene Co., Ltd.) was selected as a matrix to increase the volumetric ratio of the amorphous region, where silicon alkoxide is impregnated. Tetramethoxysilane (TMOS), tetraethoxysilane (TEOS), tetra-n-propoxysilane (TPOS) and tetra-n-buthoxysilane (TBOS) were used as silica precursors.

2.2.2. Sample preparation

The PP pellet was hot pressed at 230 °C under 20 MPa for 5 min, and then stepwisely quenched at 100 °C for 5 min and at 0 °C for 2 min to obtain a film with the dimension of 30 x 40 x 0.1 mm^3 and the crystallinity of 49 wt%. PP/silica samples were prepared by two steps: (1) impregnation of silicon alkoxide in the PP amorphous region using $scCO_2$, and (2) subsequent sol-gel reaction of the precursor in the matrix. In detail, a specified amount of liquid silicon alkoxide (1.5-30 mmol) was introduced in the bottom of a 50 ml stainless steel reactor, on which a PP film was placed. After sealing the reactor, CO_2 gas was forcibly introduced to produce a supercritical state at 80 °C under 165 kg/cm^2. $ScCO_2$ not only completely dissolves silicon alkoxide but also swells the amorphous region of PP. The impregnation of silicon alkoxide was continued for 12-36 h with the aid of $scCO_2$. After that, the film containing silicon alkoxide was immediately transferred in a glass reactor, where the sol-gel reaction was performed for 0.5-24 h in the presence of either HCl vapor at 80 °C or NH3 vapor at 60 °C. The film was hung in the glass reactor, while an aliquot volume of conc. HCl(aq) or conc. NH3(aq) was placed on the bottom of the glass reactor, thus preventing the direct contact between the film and liquid. It should be noted that when the film was soaked in acidic or alkaline aqueous solution, silicon alkoxide was completely transferred to the liquid phase and did not remain in the film.

2.2.3. Characterization

Fourier transform-infrared spectroscopy (FT-IR, JASCO FT/IR-6100) was employed to detect the formation of silica in PP film. The silica content in PP/silica was determined by thermogravimetric analysis (TGA, Mettler Toledo, TG50), where the inorganic residue was weighted after incinerating organic components at 600 °C under air.

Sample crystallinities were measured by wide-angle X-ray diffraction (WAXD, Rigaku, Rint2000). The measurements were performed in a reflection mode at room temperature with CuKα radiation operating at 40 kV and 30 mA with the step of 0.02° from 10° to 30°.

The dispersion and particle morphology of silica synthesized in PP were observed by a transmission electron microscope (TEM, Hitachi, H-7650). TEM specimens with the thickness of 100 nm were prepared by an ultramicrotome with a Leica ULTRACUT FCS. The morphology of silica that was prepared in aliphatic hydrocarbon solvent (tetradecane) was observed by a scanning electron microscope (SEM, Hitachi, S-4100) at an accelerating voltage of 20 kV. Small-angle X-ray scattering measurements (SAXS, Rigaku, Smartlab) were performed in the transmission mode using CuKα radiation at 40 kV and 30 mA with the step angle of 0.02° from 0.06° to 5°. The mass fractal dimension (D_m) of silica was determined from $I(q) \sim q^{-D_m}$ ($1 < D_m < 3$) in the range of $qR_g > 1$ [46, 47].

Tensile tests (Abecks Inc., DAT-100) were carried out at a crosshead speed of 1 mm/min at room temperature using a dumbbell-shaped specimen. The Young's modulus and tensile strength were determined as average values in ten measurements for two samples prepared at each same condition. The frequency dependence of linear

dynamic oscillatory shear properties in molten state was acquired by a cone-and-plate rheometer (TA, AR2000ex) at 180 °C with a frequency range from 100 to 0.01 rad/s under N_2 atmosphere. All the measurements were conducted in the linear regime confirmed by separate strain sweep experiments.

2.3. Results and discussion

In order to control the amount of synthesized silica, we firstly examined influences of the TEOS concentration during the $scCO_2$-aided impregnation (PPSN1-3, see Table 1 for the list of the prepared samples), where the sol-gel reaction was conducted at 80 °C for 24 h under HCl.

Table 1. Synthetic conditions and properties of PP/silica nanocomposites

Sample	TEOS concentration (mol/L)	Reaction time (h)	Catalyst	Silica content (wt%)[a]	Tensile strength (MPa)[b]	Young's modulus (MPa)[b]	log$G'_{plateau}$[c]	D_m[d]
PP	-	-	-	-	28.1±0.6	574±28	-	-
PPSN1	0.03	24	HCl	0.7	29.8±0.3	619±29	0.6	-
PPSN2	0.075	24	HCl	1.6	31.0±1.0	633±25	1.4	2.82
PPSN3	0.3	24	HCl	2.4	31.2±1.0	695±42	2.7	2.81
PPSN4	0.3	1	HCl	2.7	30.5±0.4	650±43	-	2.82
PPSN5	0.3	12	HCl	2.3	31.8±1.1	672±30	-	2.77
PPSN6	0.3	24	NH_3	1.1	31.2±0.9	687±29	2.6	2.32

[a] Determined by TGA.

[b] Determined by tensile test. Note that all of the samples could be elongated over the limitation of our tensile tester (500%).

[c] The value at the frequency of 0.01 rad/s in dynamic oscillatory shear measurements

[d] Determined by SAXS. The error range is ±0.1.

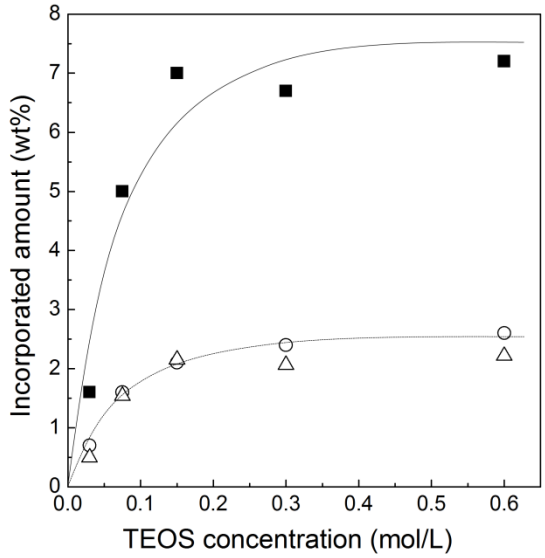

Figure 1. Effect of the TEOS concentration on incorporated amounts :(■) TEOS, (○) silica, and (Δ) the theoretical silica content.

Fig. 1 plots the mass uptake of TEOS against the TEOS concentration in $scCO_2$. The mass uptake increased linearly at a low concentration and then saturated over 0.3 mol/L. The mass uptake at the saturation, ca. 7 wt%, corresponded to 0.6 mol/L of TEOS in the amorphous region (calculated from the volume crystallinity). The fact that the saturated TEOS concentration in PP exceeded that in $scCO_2$ implied a kind of solvation for TEOS in the amorphous phase. Assuming 0.73 nm^3 per TEOS molecule, 1 nm^3 of the amorphous region contains 0.26 TEOS molecule, which corresponds to as large as 20 vol%. The amounts of formed silica measured by TGA coincided well with the theoretical values calculated from the TEOS mass uptakes under the assumption of the full conversion. Namely, the impregnated TEOS was almost completely fixed in the film as a result of the sol-gel reaction using HCl. It is notable that the impregnated

TEOS gradually volatilized from the film unless the sol-gel reaction was not immediately conducted.

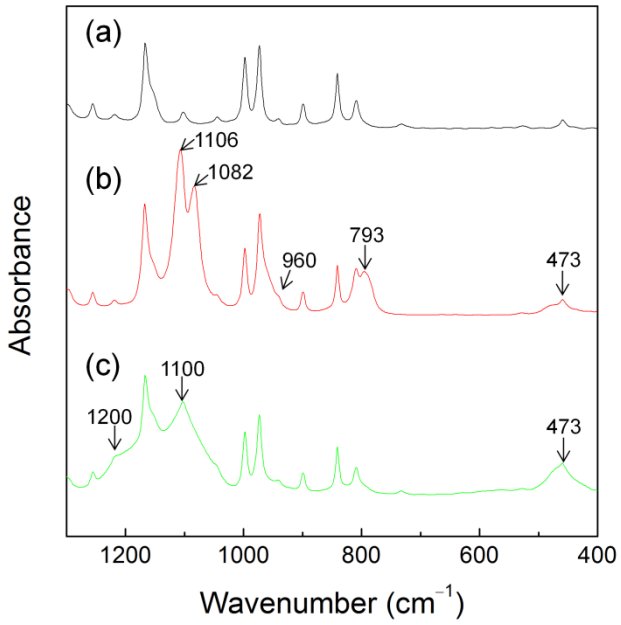

Figure 2. IR spectra of (a) PP, (b) PP/TEOS and (c) PP/ silica.

Fig. 2 shows the IR spectrum of PP/silica (PPSN3) compared with those of pristine PP and as-impregnated film. New absorption bands were observed around 473, 793, 960, 1082 and 1106 cm^{-1} after impregnation of TEOS, which is respectively assigned to the bending vibration of C-C-O, the stretching vibration of Si-O-C, the rocking vibration of CH2, the asymmetric stretching vibration of Si-O-C and the asymmetric stretching vibration of C-C-O (Fig. 2 (b)) of TEOS [48,49]. After the sol-gel reaction, two broad absorption bands were observed at 1000-1250 cm^{-1} and 400-500 cm^{-1} in addition to the PP-originated peaks (Fig. 2 (c)). They are respectively ascribed by the

asymmetric stretching vibration of Si-O-Si and the bending vibration of O-Si-O of silica. It is notable that a shoulder observed at around 1200 cm^{-1} is related to a cyclic framework of Si-O-Si in contrast to linear one at around 1100 cm^{-1}. The absence of the peak for Si-OH at around 950 cm^{-1} indicated successful completion of the condensation reaction.

Secondly, the conditions of the sol-gel reaction were varied (PPSN3-6, Table 1) to alter the structures of synthesized silica, while the impregnation conditions were fixed at 24 h and the TEOS concentration of 0.3 mol/L. The sol-gel reaction time did not affect the amount of formed silica, plausibly as a consequence of (partial) condensation of TEOS even for 1 h to prevent its volatilization. Though the degree of the condensation increases with the reaction time, it is not reflected in TGA, which completes the condensation by heating up to 600 °C. The sample prepared using NH3 had only 1.1 wt% of the silica content (PPSN6), in contrast to the full conversion of TEOS for HCl. This is because NH_3 is much less volatile than HCl, leading to much lower concentration of a catalyst in PP and thus allowing for TEOS to be evaporated prior to the condensation. When heavier formic acid or dilute HClaq (1 M) was used as a catalyst, the silica content became nearly zero. In this way, the catalyst concentration in PP was found to be critical for the efficient conversion of impregnated TEOS.

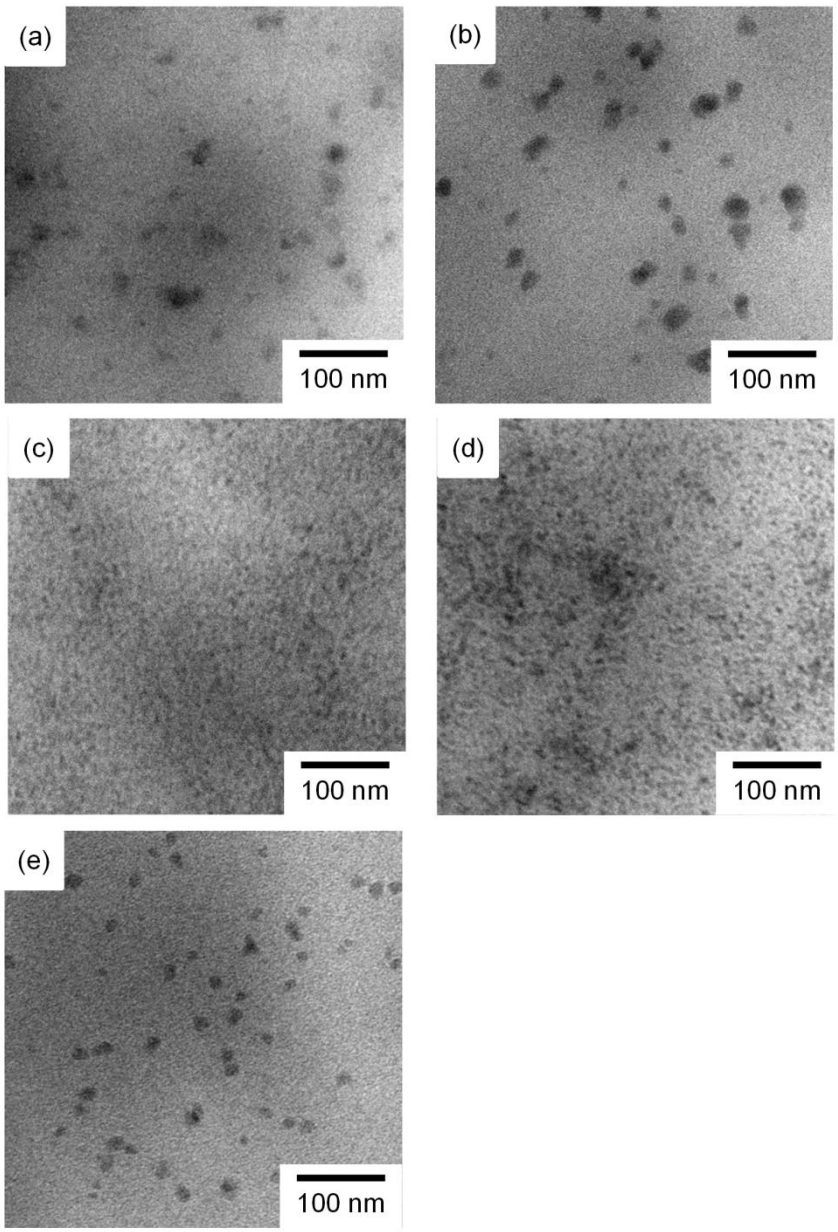

Figure 3. TEM images of (a) PPSN1, (b) PPSN2, (c) PPSN3, (d) PPSN4 and (e) PPSN6.

The dispersion and morphology of silica were observed with TEM (Fig. 3). In all of the cases, formed silica mainly had the morphology of highly dispersed nanoparticles with the sizes below 10 nm. However, larger nanoparticles around 20-30 nm were also observed when the silica content became lower than the full loading around 2.5 wt%

(PPSN1,2,6). The origin of the different dispersion could be as follows: TEOS is uniformly impregnated in the amorphous region with $scCO_2$, while it tends to form droplets after the removal of $scCO_2$ due to the incompatibility between PP and TEOS. Since the condensation accompanies bimolecular reaction between TEOS molecules, it is expected that a higher TEOS concentration leads to faster condensation, thus keeping the original dispersion created in the presence of $scCO_2$. Oppositely, it is expected that slower condensation at a lower TEOS concentration or a lower catalyst concentration offers time for the segregation of TEOS molecules.

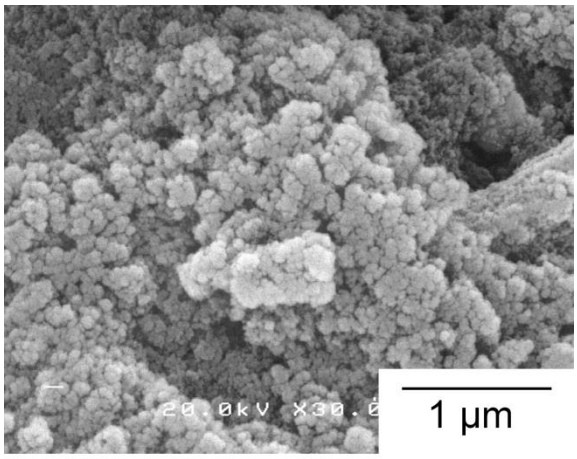

Figure 4. SEM image of silica synthesized in tetradecane.

The sol-gel synthesis of silica was performed in tetradecane to examine the effects of spatial confinements by the amorphous region of PP on the structure of synthesized silica. For the sake of fair comparison, the sol-gel reaction was conducted under conditions similar to those for PPSN3: 0.3 mol/L of TEOS in tetradecane was reacted at 80 °C for 24 h in the presence of the same HCl amount. The morphology of silica formed in tetradecane (Fig. 4) was significantly different from that formed in PP, where silica particles around 100 nm formed severe secondary agglomeration. Consequently,

it seemed plausible that the growth of primary particles as well as the secondary agglomeration was greatly suppressed in PP due to the confinement in the amorphous region. It is also notable that the dimension of silica formed in PP (except for some larger aggregates at lower contents) was nearly identical to the amorphous thickness (ca. 10 nm).

The results of tensile tests are summarized in Table 1. The formation of silica nanoparticles increased both the Young's modulus and tensile strength compared with pristine PP, where the reinforcement degree was almost proportional to the silica content for the Young's modulus and convergently increased for the tensile strength (PPSN1-3). At the silica content of 2.4 wt% (PPSN3), the reinforcement reached 21% in the Young's modulus and 11% in the tensile strength. The linear dependences of the reinforcement on the silica content was unexpected, since PPSN1,2 with the lower silica contents exhibited the presence of relatively large nanoparticles around 20-30 nm. This result suggests that the mechanical properties of the nanocomposites were mainly affected by the nanoparticles below 10 nm, while the contribution from the large nanoparticles was negligible. The Young's modulus was also improved by prolonging the reaction time (PPSN3-5) even though the silica content and morphology were hardly dependent on the reaction time. It was considered that longer reaction time led to a higher condensation degree of silica, resulting in the formation of silica with higher rigidity. However, when the reaction time was prolonged from 24 to 72 h, the mechanical properties were rather decreased due to oxidative degradation of PP (not shown in Table 1). PPSN6 (catalyzed by NH_3) exhibited higher reinforcement with respect to its low silica content, whose origin is discussed below.

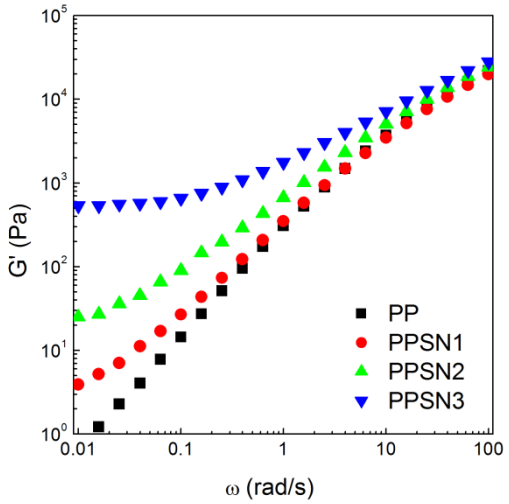

Figure 5. Viscoelastic properties of PP/silica with different silica contents.

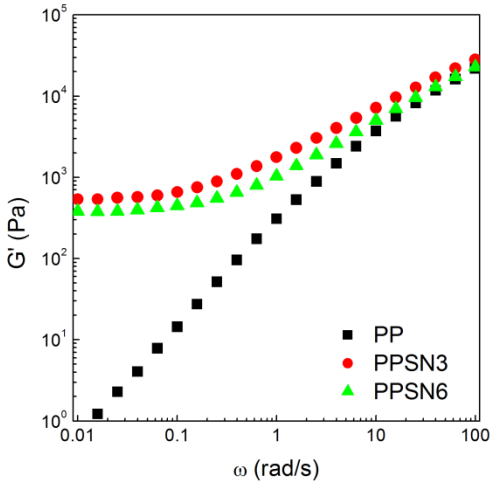

Figure 6. Viscoelastic properties of PP/silica prepared with HCl or NH_3.

The linear viscoelastic behaviors of the molten PP and PP/silica nanocomposites were investigated (Figs. 5 and 6). The results for PPSN4,5 (prepared at shorter reaction time) are omitted, since these samples posed time-dependent alternation of the moduli plausibly due to the progress of the condensation in the rheometer. All the

nanocomposites had much higher storage moduli (*G*') at lower frequencies than the pristine PP. As long as the samples were made by the same catalyst (HCl, PPSN1-3), the degree of the reinforcement in low-frequency *G*' values was related to the silica content, similar to the tensile behaviors in the solid state (Table 1). The percolation threshold was apparently located between 1.6 and 2.4 wt%, beyond which the terminal flow at lower frequencies was replaced by the solid-like behavior. The observed percolation threshold was as low as those obtained for well-dispersed and exfoliated clay with high aspect ratios [50-52] and that observed for PP/carbon nanotube nanocomposites [53-56]. This fact clearly indicates that the sol-gel method combined with $scCO_2$ can create a percolation network quite efficiently. The usage of a NH3 catalyst was found to significantly enhance the percolation (Fig. 6): PPSN6 possessed the *G*' value at the low-frequency plateau comparable to that of PPSN3 in spite of the much lower silica content (1.1 wt%), again consistent with the results of the tensile test in Table 1. The observed consistencies between the reinforcement in tensile tests (solid) and in rheological measurements (molten) strongly suggest that inorganic network structures themselves are mainly responsible for the reinforcement in the solid state.

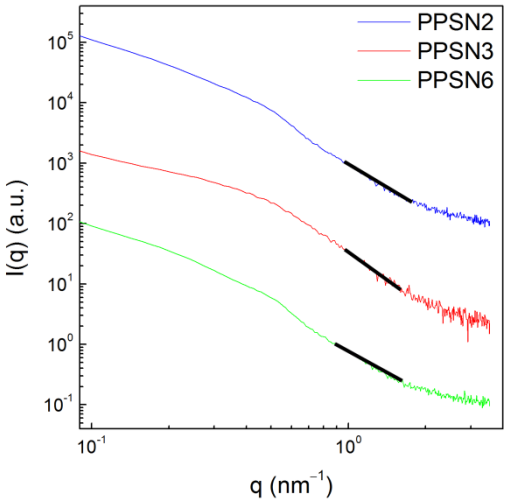

Figure 7. SAXS profiles of PPSN2, PPSN3 and PPSN6.

SAXS was measured to examine the effects of silica structures on the mechanical properties of the nanocomposites. The data for selected samples are shown in Fig. 7. In general, the SAX pattern of nanocomposites is dominated by scattering from nanoparticles, where $I(q)$ reflects their structural characteristics. The radius of gyration (R_g) is acquired through a Gunier plot for $qR_g < 2$ [57] while the gradient of a linear region in the q range $> 1/R_g$ corresponds to the mass fractal dimension of nanoparticles, i.e. D_m. The Gunier analysis for PPSN2,3,6 respectively led to the R_g values of 5.4, 4.1, and 5.2 nm, supporting our conclusion that the major portion of synthesized nanoparticles was < 10 nm-sized (seen as small dots in Fig. 3) rather than clearly visible particles with the dimension around 20-30 nm. The mass fractal dimension, D_m, determined from a SAXS profile, indicates the morphology of the particles. Particles with $D_m = 3$ possess a compact spherical structure, while lower D_m indicates more open or anisotropic structures. The D_m values are summarized in Table

1. The silica nanoparticles prepared in the presence of HCl (PPSN1-5) had the D_m values around 2.8 regardless of the silica content and the reaction time, which indicates the formation of similar silica structures. This is likely why the mechanical reinforcement was simply proportional to the silica content. The sample catalyzed by NH3 (PPSN6) showed a much lower D_m value, 2.32. It is generally known that base-catalyzed sol-gel reactions form compact and large particles due to enhanced condensation as compared with acid-catalyzed reactions [58]. In this regard, the observed low D_m value for PPSN6 was believed to arise from anisotropic morphology of silica nanoparticles formed under the two-dimensional spatial restriction, rather than fractal-like morphology.

As a second series, nanocomposites (PPSN7-9) were prepared by using different precursors, where the basic conditions for the impregnation and the sol-gel reaction were set to those for PPSN3. Table 2 summarizes various characteristics of samples prepared from different precursors. As the precursor became bulkier from TMOS to TBOS, the weight of the impregnated precursor monotonically increased. However, the molar content of the impregnated precursor was almost constant, leading to similar silica contents around 2.4-2.6 wt%.

Table 2. Properties of PP/silica nanocomposites prepared from different tetraalkoxysilane precursors

Sample	Silica content (wt%)	Tensile strength (MPa)	Young's modulus (MPa)	log$G'_{plateau}$	D_m
PP	-	28.1±0.6	574±28	-	-
PPSN7 (TMOS)	2.5	29.5±1.0	615±42	2.1	2.92
PPSN3 (TEOS)	2.4	31.2±1.7	695±48	2.7	2.81
PPSN8 (TPOS)	2.6	31.6±0.5	724±15	3.5	2.38
PPSN9 (TBOS)	2.4	30.3±1.4	647±59	2.6	2.57

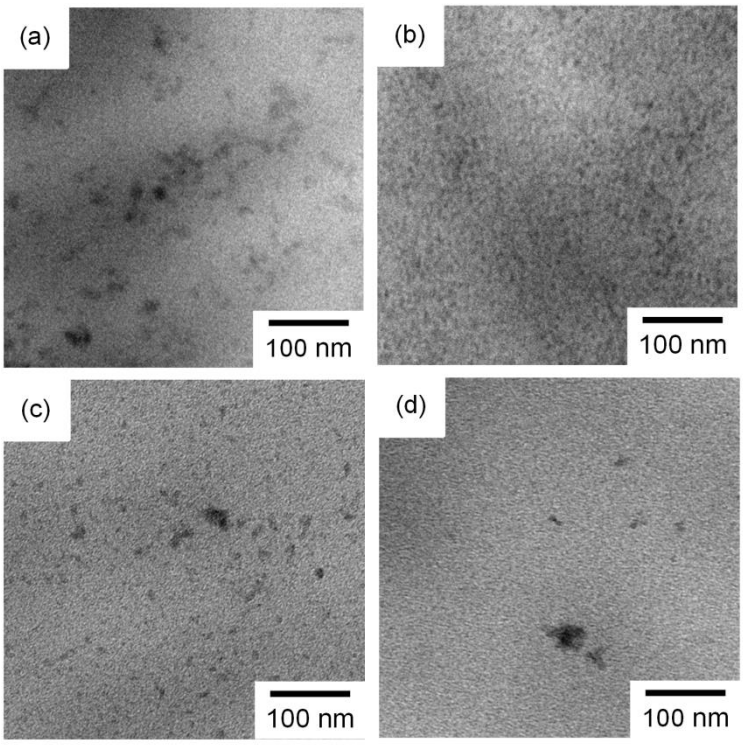

Figure 8. TEM images of (a) PPSN7, (b) PPSN3, (c) PPSN8 and (d) PPSN9.

The dispersion and size of synthesized silica were observed by TEM (Fig. 8). Synthesized silica particles basically had a nano-dimension and were homogeneously dispersed in PP matrix except for a minor fraction of larger nanoparticles. The frequency of these larger nanoparticles was relatively higher for TMOS. This is probably attributed to the highest diffusivity of TMOS, i.e. the highest probability of segregation during the sol-gel reaction. As shown in Table 2, the order of the reinforcement in tensile tests is TPOS > TEOS > TBOS > TMOS. The highest reinforcement was obtained for TPOS: 26% increase in the Young's modulus and 12% increase in the tensile strength as compared with pristine PP.

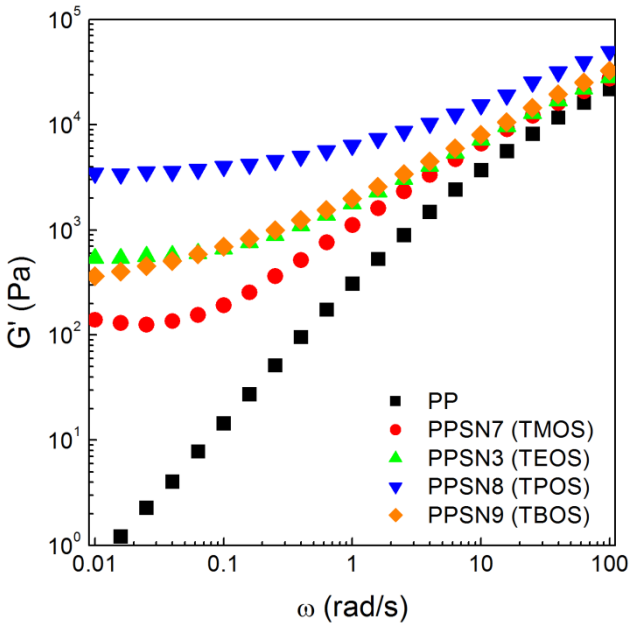

Figure 9. Viscoelastic properties of PP/silica prepared from different tetraalkoxysilane precursors.

The disappearance of the terminal flow was observed for all the samples (Fig. 9, PPSN3,7-9), and the order of the G' values at 0.01 rad/s again followed the degrees of

the reinforcement in the solid state (Table 2). Thus, in the sol-gel-based synthesis of nanocomposites, inorganic network structures are critically important for their solid and melt behaviors.

To identify the origin of the observed reinforcement, the silica structures were examined by SAXS. The D_m value decreased from TMOS to TPOS by increasing the molar mass of the precursor while it rebounded for TBOS (Table 2). The obtained trend can be again explained by the competition between the segregation and the sol-gel reaction [59]. The increase in the alkoxy size generally reduces the diffusivity and reactivity of tetraalkoxysilane. It was thought that the influences of decelerated diffusion were predominant from TMOS and TPOS, while the reduction in the reactivity overcame the reduction in the diffusivity for TBOS. As a consequence, TPOS probably gave the best balance to achieve the lowest dimension. In the first series of the nanocomposites (PPSN1-6), it was concluded that the mechanical reinforcement is correlated with the dimension of silica nanoparticles. Since the silica contents were similar among PPSN3,7-9, it is now possible for us to quantitatively verify the conclusion.

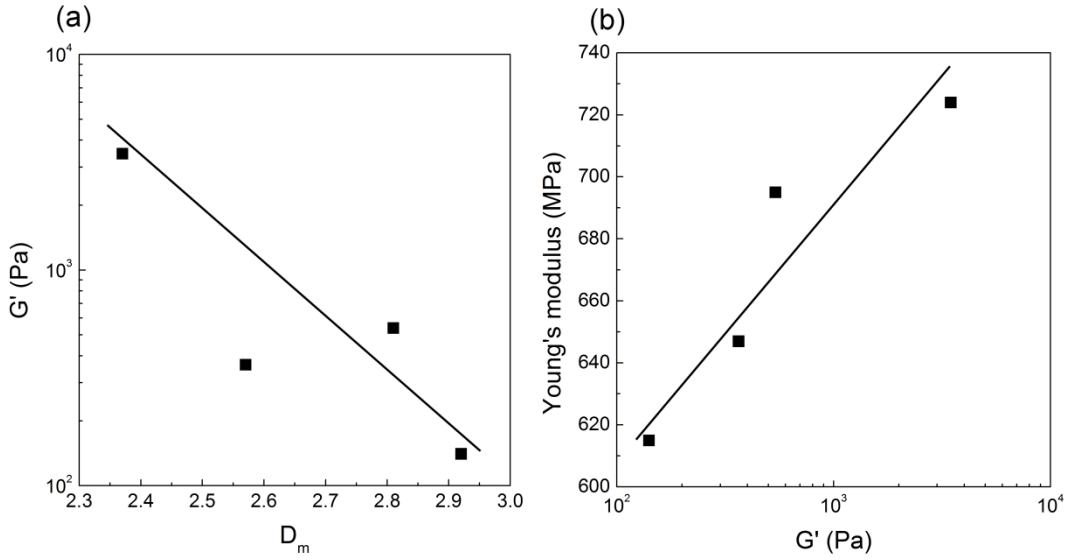

Figure 10. Relationships (a) between D_m and G' and (b) between G' and Young's modulus.

The relevant correlations plotted in Fig. 10 clearly evidenced that the formation of silica nanoparticles with more anisotropic structures (lower D_m) led to higher reinforcement in the molten state (higher G'), and that the reinforcement in the solid state (Young's modulus) directly reflected the reinforcement in the molten state.

2.4. Conclusion

In order to establish structure-property relationships between the morphology of inorganic nanoparticles and physical properties of nanocomposites for semi-crystalline polymer, a series of nanocomposites were prepared by the impregnation of silicon alkoxide in the amorphous region of polypropylene (PP) with the aid of supercritical carbon dioxide followed by the sol-gel reaction. Silica synthesized in the confined

amorphous space of PP was highly dispersed nanoparticles, whose sizes below 10 nm were much smaller than silica prepared in an unconfined condition. The mass fractal dimension of synthesized silica was dependent on the kinds of catalysts and precursors for the sol-gel reaction. Especially, TPOS led to the formation of the silica with the lowest mass fractal dimension, which was explained by the optimum balance between the diffusivity and sol-gel reactivity of the precursor in PP.

The physical properties of PP nanocomposites having silica with different fractal dimensions were examined in terms of tensile properties in solid and linear viscoelastic properties in melt. The sol-gel approach facilitated quite efficient formation of an inorganic percolation network structure in PP, where the percolation threshold became as low as those of nanocomposites containing high-aspect-ratio filler. Furthermore, it was found that the degree of the mechanical reinforcement obtained by the introduction of silica nanoparticles was mainly dominated by the mass fractal dimension of the silica particles at a given filler content and silica with a lower mass fractal dimension led to higher reinforcement for the resultant nanocomposites.

Thus we have successfully employed a novel approach for the synthesis of nano-sized inorganic particles using the semi-crystalline structures of PP as a template for the confined sol-gel reaction and successfully clarified structure-property relationships for nanocomposites of semi-crystalline polymer.

Reference

[1] Chabert E, Bornert M, Bourgeat-Lami E, Cavaillé JY, Dendievel R, Gauthier C, Putaux JL, Zaoui A. Mat Sci Eng A 2004;381:320.

[2] Moll JF, Akcora P, Rungta A, Gong S, Colby RH, Benicewicz BC, Kumar SK. Macromolecules 2011;44:7473.

[3] Akcora P, Kumar SK, Moll J, Lewis S, Schadler LS, Li Y, Benicewicz BC, Sandy A, Narayanan S, Ilavsky J, Thiyagarajan P, Colby RH, Douglas, JF. Macromolecules 2010;43:1003.

[4] Jouault N, Vallat P, Dalmas F, Said S, Jestin J, Boué F. Macromolecules 2009;42:2031.

[5] Foygel M, Morris RD, Anez D, French S, Sobolev VL. Phys Rev B 2005;71:104201.

[6] Bonnet P, Sireude D, Garnier B, Chauvet O. Appl Phys Lett 2007;91:201910.

[7] Moniruzzaman M, Winey KI. Macromolecules 2006;39:5194.

[8] Gojny FH, Wichmann MHG, Fiedler B, Kinloch IA, Bauhofer W, Windle AH, Schulte K. Polymer 2006;47:2036.

[9] Lu C, Mai YW. Phys Rev Lett 2005;95:088303.

[10] Li J, Kim JK. Compos Sci Technol 2007;67:2114.

[11] Li J, Ma PC, Chow WS, To CK, Tang BZ, Kim JK. Adv Funct Mater 2007;17:3207.

[12] Barnes HA. Rheology Reviews 2003. British Society of Rheology; 2003. p. 1-36.

[13] Otsubo Y. Langmuir 1990;6:114.

[14] Zhu Z, Thompson T, Wang SQ, von Meerwall ED, Halasa A. Macromolecules 2005;38:8816.

[15] Zhang Q, Archer LA. Langmuir 2002;18:10435.

[16] Cheah K, Forsyth M, Simon GP. J Polym Sci Part B: Polym Phys 2000;38:3106.

[17] Gubbels F, Jérôme R, Teyssié P, Vanlathem E, Deltour R, Calderone A, Parenté V, Brédas JL. Macromolecules 1994;27:1972.

[18] Gubbels F, Blacher S, Vanlathem E, Jérôme R, Deltour R, Brouers F, Teyssié P. Macromolecules 1995;28:1559.

[19] Kim YS, Wright JB, Grunlan JC. Polymer 2008;49:570.

[20] Wang Y, Anderson C. Macromolecules 1999;32:6172.

[21] Yu C, Kim YS, Kim D, Grunlan JC. Nano Lett 2008;8:4428.

[22] Regev O, ElKati PNB, Loos J, Koning CE. Adv Mater 2004;16:248.

[23] Ray SS, Okamoto K, Okamoto M. Macromolecules 2003;36:2355.

[24] Shen L, Lin Y, Du Q, Zhong W. Compos Sci Technol 2006;66:2242.

[25] Wang S, Chen L, Tong Y, J Polym Sci Part A: Polym Chem 2006;44:686.

[26] Tjong SC. Mater Sci Eng R Rep 2006;53:73.

[27] Jancar J, Douglas JF, Starr FW, Kumar SK, Cassagnau P, Lesser AJ, Sternstein SS, Buehler MJ. Polymer 2010;51:3321.

[28] Hasegawa N, Kawasumi M, Kato M, Usuki A, Okada A. J Appl Polym Sci 1998;67:87.

[29] Hasegawa N, Okamoto H, Kato M, Usuki A. J Appl Polym Sci 2000;78:1918.

[30] Pavlidou E, Bikiaris D, Vassiliou A, Chiotelli M, Karayannidis G. J Phys 2005;10:190.

[31] Wu CL, Zhang MQ, Rong MZ, Friedrich K. Compos Sci Technol 2002;62:1327.

[32] Cai LF, Huang XB, Rong MZ, Ruan WH, Zhang MQ. Polymer 2006;47:7043.

[33] Zhou HJ, Rong MZ, Zhang MQ, Ruan WH, Friedrich K. Polym Eng Sci 2007;47:499.

[34] Umemori M, Taniike T, Terano M. Polym Bull 2012;68:1093.

[35] Nam PH, Maiti P, Okamoto M, Kotaka T, Hasegawa N, Usuki A. Polymer 2001;42:9633.

[36] Kalaitzidou K, Fukushima H, Askeland P, Drzal LT. J Mater Sci 2008;43:2895.

[37] Nitta K, Asuka K, Liu B, Terano M. Polymer 2006;47:6457.

[38] Assouline E, Lustiger A, Barber AH, Cooper CA, Klein E, Wachtel E, Wagner HD. J Polym Sci Part B: Polym Phys 2003;41:520.

[39] Ma J, Zhang S, Qi Z, Li G, Hu Y, J Appl Polym Sci 2002;83:1978.

[40] Fukuyama Y, Kawai T, Kuroda S, Toyonaga M, Taniike T, Terano M. J Therm Anal Calorim 2013;113:1511.

[41] Khan J, Harton SE, Akcora P, Benicewicz BC, Kumar SK. Macromolecules 2009;42:5741.

[42] Sun D, Zhang R, Liu Z, Huang Y, Wang Y, He J, Han B, Yang G. Macromolecules 2005;38:5617.

[43] Miao Z, Xu D, Ouyang J, Guo G, Zhao X, Tang Y. Nano Lett 2002;2:717.

[44] Kovtyukhova NI, Mallouk TE, Mayer TS. Adv Mater 2003;15:780.

[45] Gaponenko NV. Synthetic met 2001;124:125.

[46] Lours T, Zarzycki, J, Craievich A, Stantos DID, Aegerter M. J Non-Cryst Solids 1988;100:207.

[47] Breiner JM, Mark JE. Polymer 1998;39:5483.

[48] Rubio F, Rubio J, Oteo JL. Spectrosc Lett 1998;31:199.

[49] Innocenzi P. J Non-Cryst Solids 2003;316:309.

[50] Kim DH, Fasulo PD, Rodgers WR, Paul DR. Polymer 2007;48:5308.

[51] Li J, Zhou C, Wang G, Zhao D. J Appl Polym Sci 2003;89:3609.

[52] Wang K, Liang S, Deng J, Yang H, Zhang Q, Fu Q, Dong X, Wang D, Han CC. Polymer 2006;47:7131.

[53] Seo MK, Park SJ. Chem Phys Lett 2004:395;44.

[54] Prashantha K, Soulestin J, Lacrampe MF, Krawczak P, Dupin G, Claes M. Compos Sci Technol 2009;69:1756.

[55] Wu D, Sun Y, Wu L, Zhang M. J Appl Polym Sci 2008;108:1506.

[56] Menzer K, Krause B, Boldt R, Kretzschmar B, Weidisch R, Pötschke P. Compos Sci Technol 2011;71:1936.

[57] Lairez D, Pauthe E, Pelta J. Biophys J 2003;84:3904.

[58] Mackenzie JD, Ulrich DR. Ultrastructure Processing of Advanced Ceramics. John Wiley & Sons; 1988. p. 355.

[59] Rodrigues DE, Risch BG, Wilkes GL. Chem Mater 1997;9:2709.

Chapter 3.

Morphological Control of Silica in Polypropylene Using Confined Amorphous Space as Template

3.1. Introduction

Nano-sized inorganic oxide has been proposed as promising materials for wide applications including supported materials for catalyst [1,2], reinforcing agents [3,4] and electronic device such as lithium ion battery , transistor , solar cell and so on [5-7]. Characteristic of nanoparticles largely depends both on the size and on the shape in terms of appearance of quantum size effects and dramatic increase of the specific surface area. Nanostructure of inorganic particles plays a key role on the performance and the application.

Nano-sized inorganic oxide have been prepared using typical synthetic methods like solvothermal synthesis [8,9], sol-gel technique [10-20], freeze drying [21], ultrasound irradiation [22,23], laser pyrolysis techniques [24,25], microwave plasma synthesis [26] thermal evaporation [27] and so on. Especially, solvothermal or sol-gel technique combined with template method is regarded as a promising method not only to prepare uniform nano-sized metal oxide but also to control the morphology. Addition of structure directing agents represented by surfactant [8,9,12-14] and block copolymer [15,16] is a good example of such combined template synthesis. Structure directing agents act as a template in solution through the self-assembly, forming typical morphologies. In addition, using mesoporous alumina membrane as a template directly produces nanowire particles [17-20]. Thus, using template for nanoparticle synthesis is useful to design nano-sized structure of particles.

Sol-gel synthesis of nanoparticle in polymer is frequently employed for high performance polymer-based nanocomposites. The sol-gel synthesis combined with solution mixing [29-31], impregnation [32-35] or melt mixing approaches [36-39] leads to in-situ formation of nanoparticle with homogeneous dispersion in polymer.

Nano-sized particles raise both large interfacial area between polymer and filler and short filler-filler distance compared to micro-sized particle, leading to drastic reinforcement and addition of new functionalities. The properties of polymer-based nanocomposites are mainly determined by dispersion and shape of nanoparticles. Preparation of polymer-based nanocomposites through sol-gel method has great advantage to achieve homogeneous dispersion of nanoparticles in polymer. However, the morphological control of particle in polymer was not in spite of importance of particle shape on the resultant properties. Because spherical particles are generally synthesized through sol-gel reaction in polymer, the development of new template method to prepare nanoparticles with high aspect ratio is important for performant polymer-based nanocomposites.

We focused on inherent structure of polymer, in other words, higher order structure of semicrystalline polymer like polypropylene (PP) as a template. The most suitable approach for the purpose is to prepare PP-based nanocomposites, which consists of impregnation of metal alkoxide in a PP film with the aid of supercritical CO_2 ($scCO_2$), followed by sol-gel synthesis of silica [40,41]. The advantage of this method is formation of silica in defined higher order structure. Since $scCO_2$ can disperse metal alkoxide into the swollen amorphous region without dissolving the crystal part, silica is synthesized in confined amorphous nano-space, which acts as a template. It is possible to precisely design structure of nanoparticles using higher order structure which template is easily controlled by crystallization conditions.

The purposes of this study are (i) to control the morphology of silica by utilizing the higher order structure of PP and (ii) to examine the relationship between the morphology of synthesized silica and viscoelastic properties because morphological

differences of silica is sensitively reflected in viscoelastic measurements. The higher order structure was controlled by crystallization conditions such as quenching and crystallization temperature. Silica nanoparticles were homogeneously synthesized in PP amorphous region. It was found that the shape of silica was successfully controlled by confined amorphous space because the mass fractal dimension of silica varied from between 3 (spherical) and 2 (sheet) according to amorphous thickness. It was found that the reinforcement in molten state is dramatically affected not only by the shape of silica but also by the dispersion.

3.2. Experimental

3.2.1. Materials

Isotactic PP (melt flow rate: 5.0 g/10min, mmmm: 95 mol%, donated by Japan Polypropylene Co., Ltd.). Tetra-n-propoxysilane (TPOS) was used as a silica precursor.

3.2.2. Sample preparation

PP pellet was hot pressed at 230 °C under 20 MPa for 5 min, and then stepwisely quenched at 100-140 °C for 360 min and at 0 °C for 2 min to obtain a film with the dimension of 30 x 40 x 0.1 mm^3. The quenching procedure was also performed at 0 °C after hot pressing PP, and then it was annealed at 100-120 °C for 360 min before quenching at 0 °C again. Impregnation of a PP film with TPOS using $scCO_2$ was carried out in 50 ml high pressure stainless steel reactor for 3 h at 80 °C under 165 kg/cm^2. After removing CO_2 gas, the PP film was immediately transferred into glass

vessel and was treated in the presence of HCl vapor for 24 h at 80 °C to convert TPOS into silica. The crystal growth was suppressed by temperature below 100 °C during the impregnation and sol-gel reaction.

3.2.3. Characterization

PP matrix was burned out at 600 °C with the heating rate of 10 °C/min using thermogravimetry (TG, Mettler Toledo, TG50). Silica content was calculated from inorganic residue amount after incinerating organic component.

Wide angle X-ray measurements (WAXD, Rigaku, Rint2000) were performed in a reflection mode at room temperature with CuKα radiation operating at 40 kV and 30 mA with the step of 0.02 ° from 10 ° to 30 ° to evaluate crystallinity of PP. Long period of PP and morphology of silica were evaluated by Small angle X-ray scattering (SAXS, Rigaku, Smartlab). The measurements were performed in the transmission mode using CuKα radiation at 40 kV and 30 mA with the step angle of 0.02 ° from 0.06 ° to 5 °. Spherulite structures of PP were observed by optical microscope equipped with two polarizing plates.

The dispersion and morphology of silica synthesized in PP were observed by a transmission electron microscope (TEM, Hitachi, H-7650). Samples were sliced with the thickness of 100 nm by an ultramicrotome with a Leica ULTRACUT FCS to prepare TEM specimens. Oscillatory shear measurements in the linear region were carried out by a cone-and-plate rheometer (TA, AR2000ex) at 200 °C with a frequency range from 100 to 0.01 rad/s under N_2 atmosphere.

3.3. Results and Discussion

3.3.1. Higher order structure of PP

Higher order structure of PP plays a key role on the mechanical properties. Higher order structure was determined by primary structure of PP and crystallization conditions. In this study it tried to be controlled by crystallization conditions such as quenching and annealing temperature. The results of the higher order structure prepared with different crystallization condition were shown in Table 1.

Table 1. Higher order structures of PP

	X_c (wt%)[a]	X_{vol} (vol%)[b]	q (nm^{-1})[c]	l_0 (nm)[d]	l_c (nm)[d]	l_a (nm)[d]
PP-100	54	52	0.42	15.0	7.7	7.2
PP-120	60	58	0.36	17.6	10.2	7.5
PP-130	59	56	0.34	18.4	10.4	8.0
PP-140	59	56	0.30	21.0	11.9	9.2
PP-0-100	49	47	0.46	13.6	6.3	7.2
PP-0-120	49	46	0.37	17.0	7.8	9.2

[a] Determined by WAXD

[b] $X_{vol} = \dfrac{\frac{X_c}{\rho_c}}{\frac{X_c}{\rho_c} + \frac{100 - X_c}{\rho_a}}$ (ρ_c = 0.95 g/cm^3, ρ_a = 0.85 g/cm^3 [15])

[c] Determined by SAXS

[d] l_0 (long period) = $2\pi/q$, l_c (lamellar thickness) = $X_{vol}/100 \times l_0$,

l_a (amorphous thickness) = $(100 - X_{vol})/100 \times l_0$

While random PP was used as previous in previous chapter, γ crystal is formed by elevated crystallization temperature, which results in complicated interpretation on higher order structure. Therefore, PP homopolymer, which leads to only α crystal under general crystallization condition, was used as a matrix (Figure 1). Crystallinity analyzed from WAXD pattern was from 48 to 60 wt%.

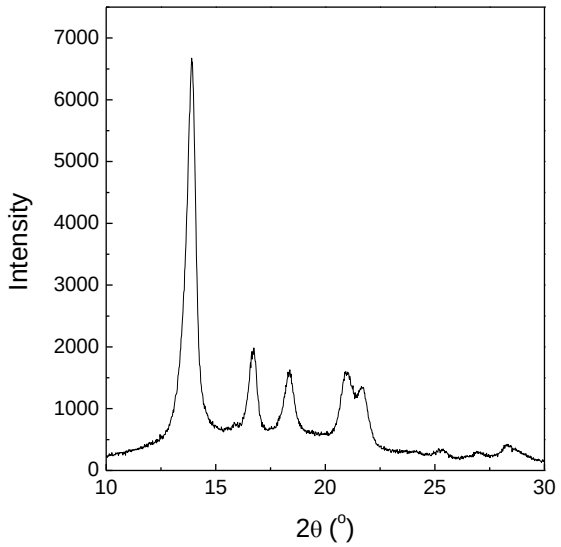

Figure 1. WAXD patterns of PP-100.

The long period was evaluated from SAXS (Figure 2). The peak is shifted to low q value with increasing crystallization temperature, indicating formation of larger long period. Consequently, thick lamellae were formed with increasing crystallization temperature. Lamellar thickness is shown using supercooling temperature ($\Delta T = T_m^0 - T_c$) as follows

$$l_c = \frac{a}{\Delta T} + b,$$

where a and b are constant [42]. Considering chain sliding diffusion, it is adaptable to form thick lamellar by severe thermal treatment [43].

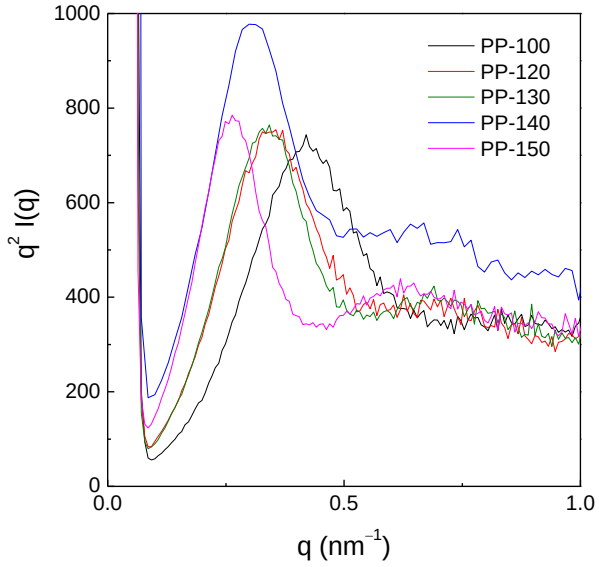

Figure 2 SAXS Lorentz-corrected plots of PP prepared with different crystallization temperature.

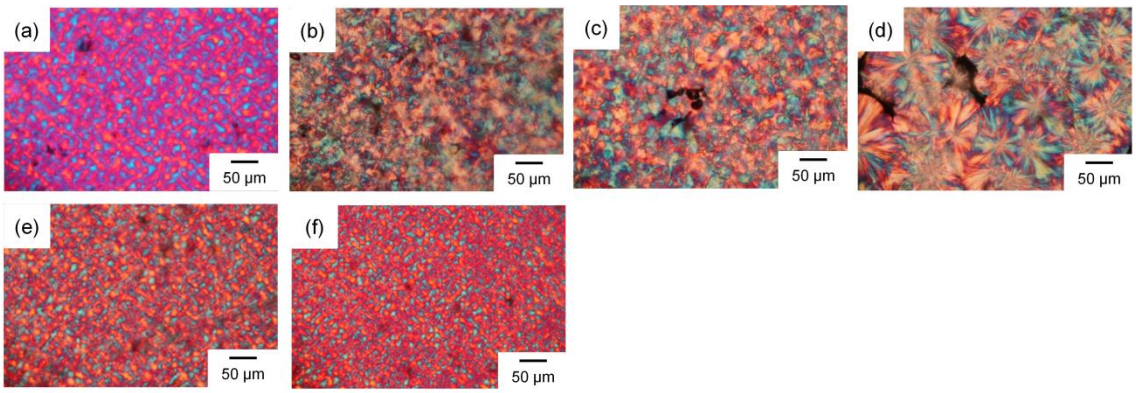

Figure 3. POM images of (a) PP-100, (b) PP-120, (c) PP-130, (d) PP-140, (e) PP-0-100 and (f) PP-0-120.

Polarized optical microscope (POM) observation was performed to evaluate the spherulite size (Figure 3). The spherulite size increased with quenching temperature.

Spherulite size is mainly determined by an amount of nuclei, which is associated with nucleation rate. It is known that nucleation rate (I) depends on degree of supercooling (ΔT), Nishi et al. showed that the relationship was defined as

$I = I_0 \exp(-C/\Delta T^2)$,

where I_0 and C are constants [44]. It was considered that high quenching temperature led to slow nucleation rate, resulting in the formation of large spherulite. Spherulite was also observed in samples quenched at 0 °C because quenching procedure was performed by inserting melt PP between two steel plates, leading to not mesophase but α crystal by slow cooling rate [45]. The spherulite size was hardly affected by annealing temperature after quenching at 0 °C probably because I is determined by supercooling temperature. The higher order structure such as crystallinity, lamellar thickness, amorphous thickness and spherulite size is successfully controlled by quenching and crystallization temperature.

3.3.2. Properties of resultant nanocomposites

Silica was synthesized in PP films prepared with different crystallization conditions though the impregnation of TPOS with the aid of $scCO_2$ and subsequent sol-gel reaction. All properties of resultant nanocomposites were summarized in Table 2. These parameters were compared with higher order structure of PP to examine the effects of it on the morphology of synthesized silica.

Table 2. Properties of PP/silica nanocomposites

	Silica content (wt%)[a]	D_m[b]	R_g[c]	LogG' (Pa)[d]
PP-100/silica	2.1	2.1	3.3	2.3
PP-120/silica	1.8	2.4	4.4	1.8
PP-130/silica	1.9	2.6	5.0	1.9
PP-140/silica	1.9	2.8	6.9	2.5
PP-0-100/silica	2.2	2.2	3.2	2.4
PP-0-120/silica	2.2	2.8	4.4	2.0

[a] Determined by TGA

[b] Mass fractal dimension. Determined by SAXS

[c] Radius of gyration. Determined by SAXS

[d] The value at the frequency of 0.01 rad/s in dynamic oscillatory shear measurements

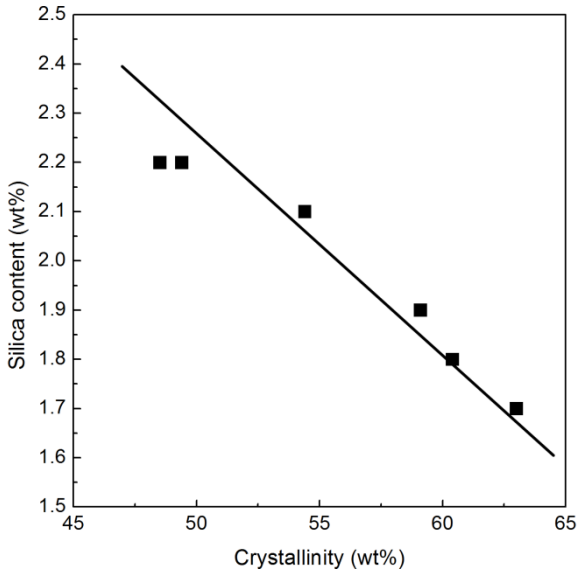

Figure 4. Relationship between crystallinity of PP and silica content.

Firstly, silica content was plotted against crystallinity of PP (X_c) (Figure 4). Silica content linearly decreased with the X_c, and the relationship was shown as below equation,

Silica content = $-0.034\ X_c + 3.9$

Since TPOS was only impregnated in amorphous region of PP, silica content depended on the area of amorphous region. However, silica is synthesized in PP with 100 wt% of crystallinity according to equation, indicating that the relation is not linear and the efficiency of swelling amorphous region using $scCO_2$ might depend on crystallinity.

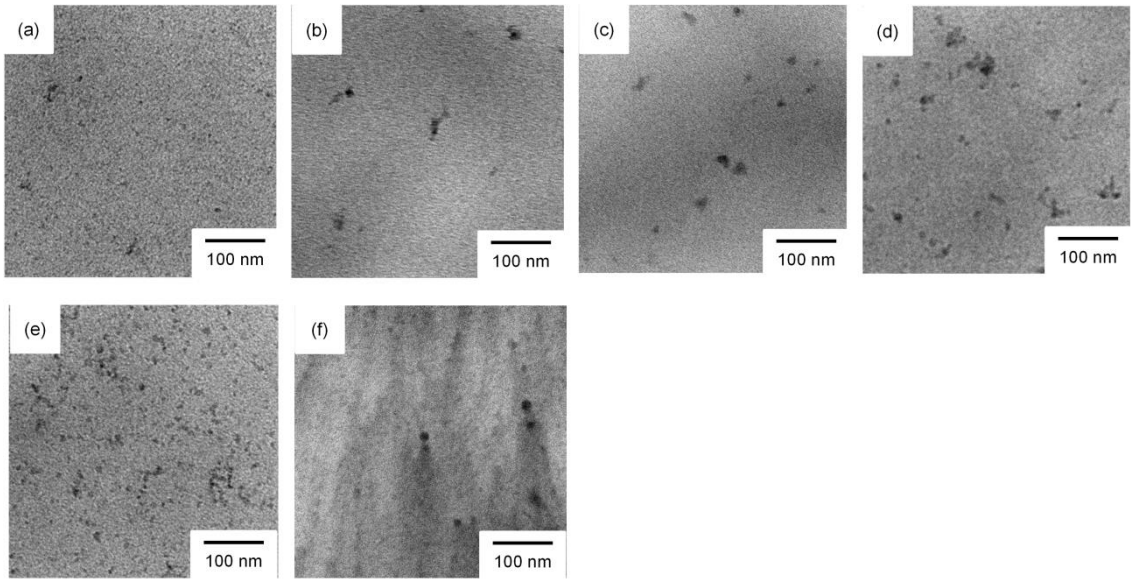

Figure 5. TEM images of (a) PP-100/silica, (b) PP-120/silica, (c) PP-130/silica, (d) PP-140/silica, (e) PP-0-100/silica and (f) PP-0-120/silica.

The dispersion and morphology of formed silica were observed by TEM (Figure 5). The morphology of silica in PP had highly dispersed nanoparticles around 10 nm in all of the PP/silica. The size of silica was comparative to PP amorphous thickness and

this tendency is also observed in gyration of radius (R_g) evaluated from Guinier plot in SAXS profiles for $qR_g < 2$ [46]. This is probably because the confinement in amorphous region of PP. Since formation of silica was confined by the amorphous region, the size of formed silica was well correlated to amorphous thickness.

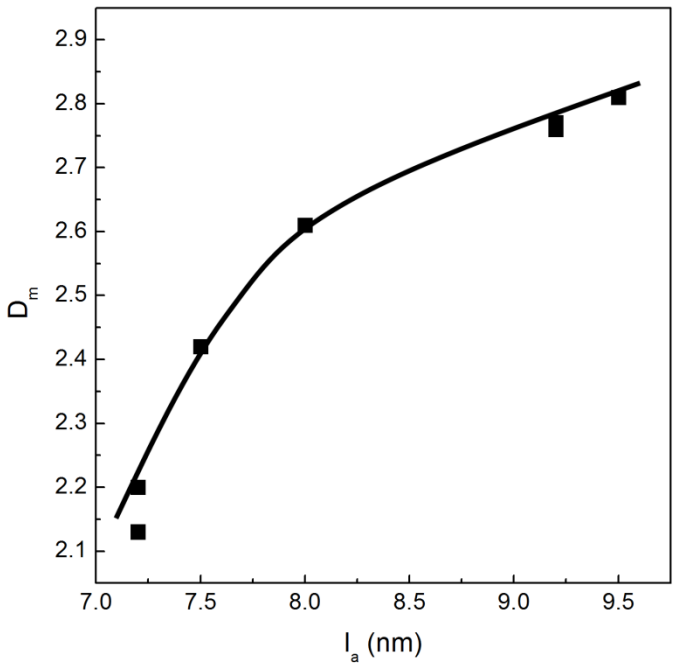

Figure 6. Relationship between amorphous thickness of PP and mass fractal dimension of silica.

The shape of formed silica was investigated by SAXS measurements. The main scattering of PP/silica nanocomposites measured by SAXS is generally attributed from silica, where $I(q)$ reflects their morphological characteristics. The mass fractal dimension (D_m, $1 < D_m < 3$) determined by SAXS profile from slope in the range of $qR_g > 1$ reflects the shape of silica [47,48]. For example, silica with $D_m = 3$, 2 or 1 possess spherical, sheet-type or rod-type structure, respectively, i.e. lower D_m value expresses

the structure with anisotropy. The D_m value of silica synthesized in PP decreased from 3 to 2 with amorphous thickness (l_a), indicating morphological change from spherical to sheet-type morphology (Figure 6). As mentioned in observation of silica using electron microscope, the synthesis of silica in PP was confined by the higher order structure of PP while spherical silica is formed by usual sol-gel reaction (Figure 4). The confinement should be stronger as amorphous thickness decreases, in short, the small l_a led to severe restriction of growth direction of silica, resulting in the formation of anisotropic silica. It was found that the morphological control of silica was successfully achieved by the higher order structure as a template.

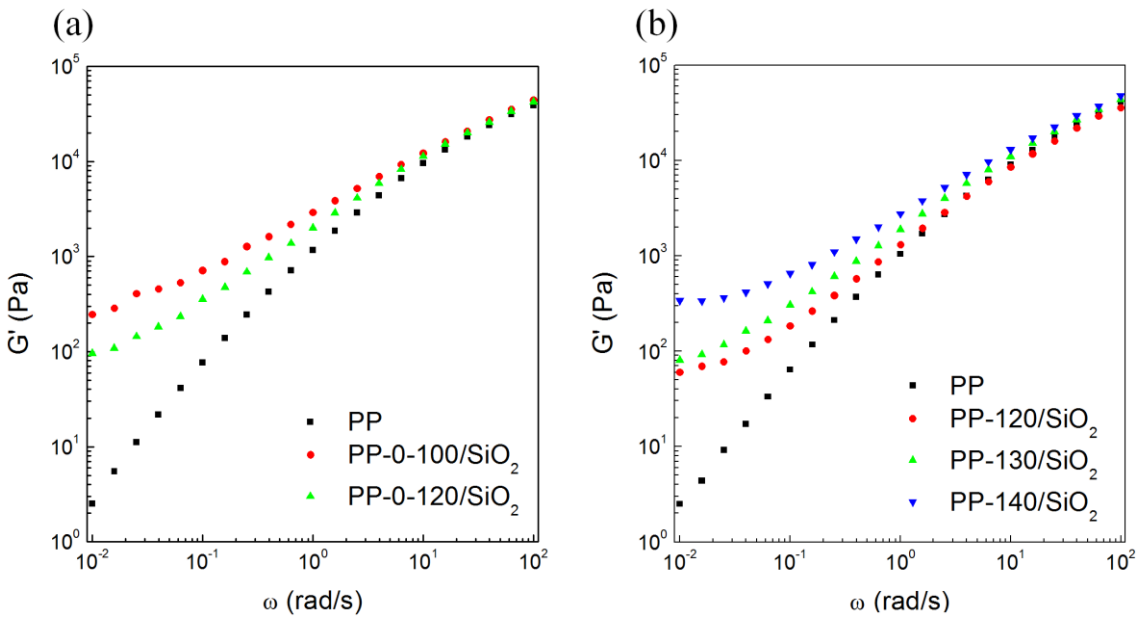

Figure 7. Viscoelastic properties of PP/silica with (a) 2.2 wt% and (b) 1.9 wt%.

Linear viscoelastic measurements were carried out to investigate the effects of silica morphology in PP on the network formation. In this series, viscoelastic properties were separately discussed using samples with similar silica content because the measurements are dramatically influenced by silica content. Figure 7 (a) shows the

viscoelastic properties of PP/silica (PP-0-100/silica, PP-0-120/silica) with same silica content (2.2 wt%) and different D_m value (PP-0-100/silica: 2.20, PP-0-120/silica: 2.77). All PP/silica had much higher storage modulus (G') at low-frequency area than neat PP. With respect to the morphology of silica, low D_m value i.e. anisotropic silica led to high reinforcement in low-frequency G'. This results well corresponds to the fact, which the formation of network is dominated by the aspect ratio of filler [49,50]. Figure 7 (b) shows viscoelastic properties of PP/silica (PP-120/silica, PP-130/silica and PP-140/silica) with similar silica content (1.9 wt%) and different D_m value (PP-120/silica: 2.42, PP-130/silica: 2.61, PP-140/silica: 2.76). In contrast to previous results, the G' at low frequency area was positively correlated with D_m value. The appearance of plateau at low frequency area, which indicates the formation of the network structure, was observed for PP-140 with only 1.9 wt% of silica. The threshold is as low as that incorporating filler with high aspect ratio like clay or carbon nanotube [51-56]. A network formation is mainly affected by the dispersion and shape of silica. The dispersion of silica should be different from others. Kalaitzidou et al. indicated the percolation threshold is affected by size of spherulite [57]. Therefore, the boundary area between spherulites plays key role on percolation threshold. Since low area of spherulite boundary was provided with large spherulite size, the localized dispersion of silica was obtained on large spherulite. Consequently, the network structure was successfully constructed by the localized dispersion in spite of forming spherical silica.

3.4. Conclusions

In order to control the morphology of silica in PP, silica was synthesized through sol-gel reaction with the aid of supercritical CO_2 in PP with different higher order structures. The higher order structure of PP was controlled by the conditions of quenching and annealing temperature. The formed silica was controlled by amorphous thickness, which led to the confinement of silica synthesis. The viscoelastic properties were found to be affected by the shape and dispersion of silica.

Thus we have successfully employed a novel approach for the control of silica structure using the amorphous strucutre of PP as a template for the confined sol-gel reaction.

References

[1] Kageyama K, Tamazawa J, Aida T. Science 1999;285:2113.

[2] Millera CJ, O'Hare D. Chem Commun 2004;15:1710.

[3] Jordan J, Jacob KI, Tannenbaum R, Sharaf MA, Jasiuk I. Mater Sci Eng A 2005;A393:1.

[4] Khaled SM, Sui R, Charpentier Rizkalla AS. Langmuir 2007;23:3988.

[5] Tsai MC, Chang JC, Sheu HS, Chiu HT, Lee CY. Chem Mater 2009;21:499.

[6] Nguyen P, Ng HT, Yamada T, Smith MK, Li J, Han J, Meyyappan M. Nano Lett 2004;4651.

[7] Keis K, Magnusson E, Lindström H, Lindquist SE, Hagfeldt A. Sol Energ Mater Sol Cells 2002;73:51.

[8] Yan A, Liu X, Qiu G, Wu Hongyi, Yi R, Zhang N, Xu J. J Alloys Compd 2008;458:487.

[9] Kim CS, Moon BK, Park JH, Choi BC. J Cryst Growth 2003;257:309.

[10] Matsuda A, Matoda T, Kogure T, Tadanaga K, Minami T, Tatsumisago M. Chem Mater 2005;17:749.

[11] Teoh GL, Liew KY, Mahmood WAK. J Sol-Gel Sci Technol 2007;44:177.

[12] Niesz K, Yang P, Somorjai GA, Chem Commun 2005;15:1986.

[13] Zhang L, Zhu Y, He Y, Li W, Sun H. Appl Catal B 2003;40:287.

[14] Wang Y, Yang W, Shi W. Ind Eng Chem Res 2011;50:11982.

[15] Yang P, Zhao D, Chmelka BF, Stucky GD. Chem Mater 1998;10:2033.

[16] Zhao D, Melosh YN, Feng J, Chmelka BF, Stucky GD. Adv Mater 1998;10:1380.

[17] Chae WS, Lee SW, Kim YR. Chem Mater 2005;17:3072.

[18] Limmer SJ, Seraji S, Wu Y, Chou TP, Nguyen C, Cao G. Adv Funct Mater

2002;12:59.

[19] Lakshimi BB, Patrissi CJ, Martin CR. Chem Mater 1997;9:2544.

[20] Wang X, Wang X, Huang W, Sebastian PJ, Gamboa S. J Power Sources 2005;140:211.

[21] Abdelwahed W, Degobert G, Stainmesse S, Fessi H. Adv Drug Deliv Rev 2006;58:1688.

[22] Kim KH, Kim KB. Ultrason Sonochem 2008;15:1019.

[23] Pol VG, Palchik O, Gedanken A, Felner I. J Phys Chem B 2002;106:9737.

[24] Alexandrescu R, Dumitrache F, Morjan I, Sandu I, Savoiu M, Voicu, Fleaca C, Piticescu R. Nanotechnology 2004;15:537.

[25] Morjan I, Alexandrescu R, Dumitrache F, Birjega R, Fleaca C, Soare I, Luculescu CR, Filoti G, Kuncer V, Vekas L, Popa NC, Prodan G, Ciupina V. J Nanosci Nanotechnol 2010;10:1223.

[26] Kim JF, Hong YC, Uhm HS. Surf Coat Tech 2007;201:5114.

[27] Dai ZR, Pan ZW, Wang ZL. J Phys Chem B 2002;106:902.

[28] Dai ZR, Pan ZW, Wang ZL. Adv Funct Mater 2003;13:9.

[29] Hsu YG, Tu LC, Lin KH. J Polym Res 2001;8:37.

[30] Tang H, Wan Z, Pan M, Jiang AP. Electrochem Commun 2007;9:2003.

[31] Bounour-Legaré V, Angelloz C, Blanc P, Cassagnau P, Michel A. Polymer 2004;45:1485.

[32] Mark JE, Ning YP, Jiang CY, Tang MY, Roth WC. Polymer 1985;26:2069.

[33] Chaichua B, Prasassarakich P, Poompradub S. J Sol-Gel Sci Technol 2009;52;219.

[34] Yuan QW, Mark JE. Macromol Chem Phys 1999;200:206.

[35] Tangpasuthadol V, Intasiri A, Nunticanich D, Niyompanich N, Kiatkamjournwong

S. J Appl Polym Sci 2008;109:424.

[36] Mizutani Y, Nago S J Appl Polym Sci 1999;72:1489.

[37] Dou Q, Zhu X, Peter K, Demco DE, Möller M, Melian C, J Sol-Gel Sci Technol 2008;48:51.

[38] Bahloul W, Legare VB, David L, Cassagnau P. J Polym Sci Part B Polym Phys 2010;48:1213.

[39] Kaneko K, Yadav N, Takeuchi K, Maira B, Terano M, Taniike T. Compos Sci Tech 2014;102:120.

[40] Sun D, Zhang R, Liu Z, Huang Y, Wang Y, He J, Han B, Yang G. Macromolecules 2005;38:5617.

[41] Takeuchi K, Terano M, Taniike T. Polymer 2014:55;1940.

[42] Gedde UW. Polymer physics. London: Kluwer; 1999.

[43] Hikosaka M. Polymer 1990;31:458.

[44] Nishi M, Hikosaka M, Ghosh SK, Toda A, Yamada K. Polym J 1999;31:749.

[45] Coccorullo I, Pantani R, Titomanlio G. Polymer 2003;44:307.

[46] Lairez D, Pauthe E, Pelta J. Biophys J 2003;84:3904.

[47] Lours T, Zarzycki, J, Craievich A, Stantos DID, Aegerter M. J Non-Cryst Solids 1988;100:207.

[48] Breiner JM, Mark JE. Polymer 1998;39:5483.

[49]Li J, Ma PC, Chow WS, To CK, Tang BZ Kim JK. Adv Func Mater 2007;17:3207.

[50] Lu C, Mai YW. Phys Rev Lett 2005;95: 088303.

[51] Li J, Zhou C, Wang G, Zhao D. J Appl Polym Sci 2003;89:3609.

[52] Wang K, Liang S, Deng J, Yang H, Zhang Q, Fu Q, Dong X, Wang D, Han CC. Polymer 2006;47:7131.

[53] Seo MK, Park SJ. Chem Phys Lett 2004:395;44.

[54] Prashantha K, Soulestin J, Lacrampe MF, Krawczak P, Dupin G, Claes M. Compos Sci Technol 2009;69:1756.

[55] Wu D, Sun Y, Wu L, Zhang M. J Appl Polym Sci 2008;108:1506.

[56] Menzer K, Krause B, Boldt R, Kretzschmar B, Weidisch R, Pötschke P. Compos Sci Technol 2011;71:1936.

[57] Kalaitzidou K, Fukushima H, Askeland P, Drzal LT. J Mater Sci 2008;43:2895.

Chapter 4.

Development of Bio-Inspired Polypropylene-Based Materials through Sol-Gel Reaction in Laminated Biaxially Oriented Polypropylene

4.1. Introduction

Designing materials, which exhibit exceptional mechanical properties, is challenging goal on polymer-based nanocomposites. The properties of polymer nanocomposites are mainly affected by the dispersion of filler particles as well as the interaction between polymer and filler. Especially, several researchers have focused on controlling the orientation of filler with high aspect ratio. For example, Okamoto et al. reported the construction of particular clay orientation, what is called "house of cards like structure" in maleic anhydride grafted polypropylene and the vertical orientation led to higher reinforcement [1]. Nanocomposite gel, which possesses ductile and strong properties, is also reinforced by similar mechanism [2,3]. Whereas the design of filler orientation in polymer is important to develop high performance materials, it is necessary to obtain new design direction for further reinforcement.

Hierarchical control of filler is a key to achieve drastic reinforcement on polymer-based nanocomposites. Natural materials like tooth, bone, nacre have hierarchical structures, which induce far excellent mechanical properties in contrast to artificial mixture of their component [4,5]. In particular, nacre is a good example of such high performance natural materials. Nacre, which is composed by brittle $CaCO_3$ with a few percent addition of biopolymer exhibits a toughness about 3000 times higher than $CaCO_3$ (Figure 1) [6], and the resulting properties are originated from architecture of nacre constructing the densely packed brick structure of layered $CaCO_3$ crystal [7,8]. The formation of compact brick structures leads to the several mechanisms including crack deflection at the platelet/matrix interface [9], viscoelastic energy dissipation in the polymer matrix [10], interfacial strain hardening [11] and so on, resulting in strong and ductile hybrid materials. Therefore, it is important to precisely control the dispersion

of filler from macro to nano-scale by mimicking the structure of nacre.

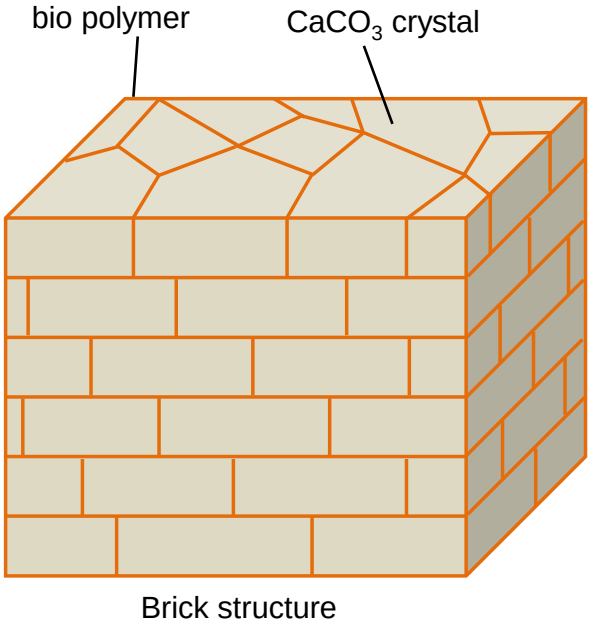

Figure 1. Image of hierarchical structure of nacre.

Recently, many studies have been conducted to produce high performance materials by mimicking structure of nacre. Posiadlo employed layer-by-layer approach using two kinds of solution including polyvinylalcohol and nanoclay, respectively (Figure 2) [12]. They prepared high oriented structure of clay particles in polyvinylalcohol and achieved dramatic reinforcement. Bonderer et al. also prepared the structure through repetition of the casting of solution containing Al_2O_3 plate and subsequent spin coating of polymer solution [13]. Since these bottom up designs such as spin coating [13], layer by layer [12,14,15] and casting [16,17] enable precise control of filler orientation, the brick structures mimicking nacre were successfully prepared and the mechanical properties of resultant composites were dramatically improved. Another approach was reported by Randall, who controlled the orientation of Al_2O_3 particles using magnetic field after homogeneously dispersing particles in polyurethane though solvent mixing

[18]. As mentioned in above, bottom-up assembly process using solvent is frequently employed to artificially design a nacre-like brick structure.

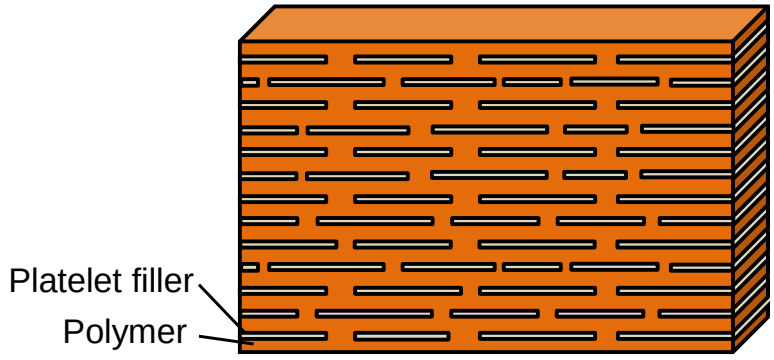

Figure 2. Images of nanocomposites prepared through solution methods by mimicking the structure of nacre.

Polypropylene (PP) has been widely used as from commodity to special products due to its various excellent properties such as low production cost, good processability, low environmental load, balanced mechanical properties and so on. It is considered that construction of a nacre-like brick structure in PP have a great potential to achieve expansion of the versatility. While bottom up assembly process using solvent is approach to prepare a nacre-like brick structures, non-polar nature of polypropylene (PP) makes it impossible to employ the method due to poor solubility in general solvent. Bonderer et al. attempted to prepare a brick structure by gel-cast using decaline as a solvent, but low volatility of decaline led to incomplete orientation and formation of cavitation, resulting in poor reinforcement [19]. PP-based nanocomposites also suffer from poor compatibility between polymer and filler, forming three dimensional aggregates of filler in PP. To prepare a nacre-like structure in PP is important not only for the drastic reinforcement but also for developing versatile method to employ every polymer.

In order to form a nacre-like brick structure in PP, the PP nanocomposites were prepared in laminated biaxially oriented polypropylene (BOPP) film through impregnation of silicon alkoxide with the aid of supercritical CO_2 ($scCO_2$), followed by sol-gel reaction. Since the silicon alkoxide is only impregnated in PP amorphous region without dissolving crystal part of PP using $scCO_2$, silica morphologies enables to control using PP amorphous region as a template [20,21]. BOPP, which is produced through elongation process under melting temperature, has various properties such as high modulus, strength, transparency and so on. The typical properties are originated from the morphology of BOPP, which the lamellar and amorphous part are strongly oriented perpendicular to film thickness. In this study, thin BOPP was firstly hot pressed to produce laminated BOPP film, then silica is synthesized using the impregnation and subsequent sol-gel reaction. It is expected that silica is synthesized not only in restricted PP amorphous part but also adhesive layer between BOPP films, leading to formation of a nacre-like brick structure (Figure 3).

The purpose of this study is to achieve drastic reinforcement of PP by forming a nacre-like brick structure in BOPP through impregnation of silicon alkoxide with the aid of $scCO_2$ and subsequent sol-gel reaction.

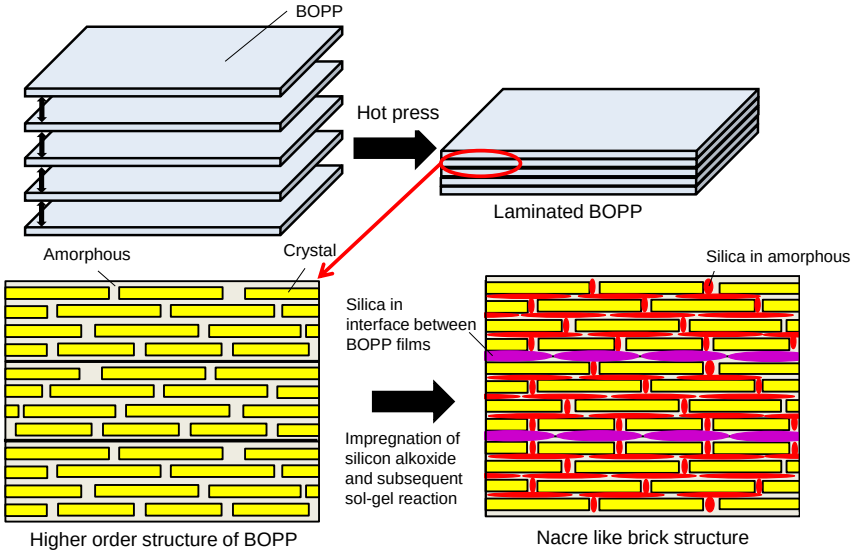

Figure 3. Synthetic images

The silica was synthesized not only in amorphous region but also in interface between BOPP films. The maximum reinforcement reached and 25% for tensile strength and 32% for Young's modulus compared to BOPP and 1010% for tensile strength and 260% for Young's modulus compared to unoriented PP.

4.2. Experimental

4.2.1. Materials

Biaxially oriented polypropylene (BOPP) films with the thickness of 2.5, 10, 22 μm were employed as matrices. Tetra-*n*-propoxysilane (TPOS) was used as a silica precursor.

4.2.2. Sample preparation

Overlapped thin BOPP films were adhered by hot-press at 150-167 °C for 1 h under

20 MPa to produce film with the thickness of 100 μm (Scheme 1). BOPP/silica samples were prepared by two steps: (1) impregnation of TPOS in the BOPP amorphous region and adherend between BOPP using $scCO_2$, and (2) subsequent sol-gel reaction of TPOS in the matrix. A adhered BOPP film and TPOS (0.3 mol/l) were placed in a 50 ml autoclave and then $scCO_2$ was introduced at 80 (120) °C for 3 h under 165 kg/cm^3. After that, the film containing TPOS was immediately transferred in a glass reactor, where the sol-gel reaction was performed for 24 h in the presence of HCl vapor at 80°C. The hot-press was also performed at 230°C under 20 MPa for 5 min, and then quenched at room temperature to prepare unoriented PP film.

4.4.3. Characterization

The silica content in BOPP/silica was evaluated from the weight of inorganic residue after incinerating organic components at 600°C using electric furnace. The used sample was hot pressed at 230°C under 20 MPa for 5 min to avoid the removal of sample from a holder, coused by the heat shurinkage of BOPP. Sample crystallinities were measured by wide-angle X-ray diffraction (WAXD, Rigaku, Rint2000). The measurements were performed in a reflection mode at room temperature with CuKα radiation operating at 40 kV and 30 mA with the step of 0.02° from 10° to 30°. The dispersion and particle morphology of silica synthesized in film were observed by a transmission electron microscope (TEM, Hitachi, H-7650). TEM specimens with the thickness of 50 nm were prepared by an ultramicrotome with a Leica ULTRACUT FCS. Tensile tests (Abecks Inc., DAT-100) were carried out at a crosshead speed of 1 mm/min at room temperature using a dumbbell-shaped specimen. The Young's modulus and tensile strength were determined as average values in five measurements. The samples

were elongated to either MD (machine direction) or TD (transverse direction).

4.3. Results and Discussion

Firstly, effects of hot-pressing temperature on mechanical properties of laminated BOPP films were examined by tensile tests. The results of tensile tests were shown in Table 1 and Figure 4.

Table 1. Results of tensile test

	Tensile strength (MPa)	Young's modulus (MPa)	Elongation at break (%)
BOPP-130	94	967	108
BOPP-150	98	979	129
BOPP-160	104	963	149
BOPP-165	106	979	170
BOPP-167	108	987	196

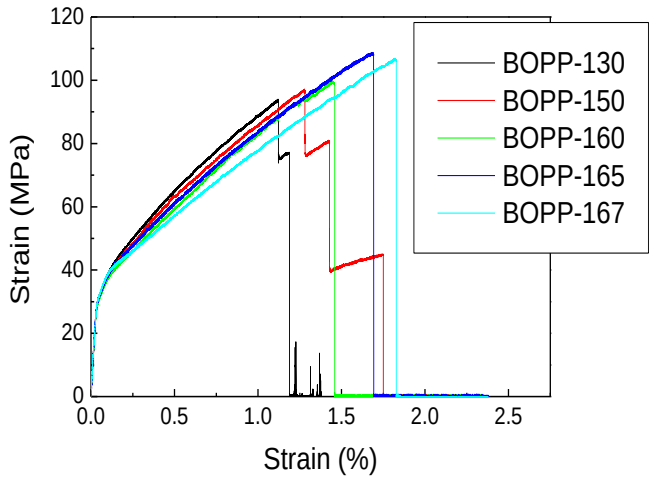

Figure 4. Stress-strain curves of BOPP

The elongation and tensile strength were improved by increasing hot press temperature. However, the slope above 0.1 of elongation was reduced from Figure 4, so high tensile strength was attributed from extended elongation. These results were related to relaxation of molecular orientation and strong adhesion between BOPP films, which results in better elongation. Table 2 shows silica content of BOPP/silica. The silica content of BOPP-150/silica is the highest in these samples. In the previous chapter, it was found that silica content largely depends on the crystallinity. Therefore, the results listed in Table 2 were added into the figure written about the relationship between the crystallinity and the silica content.

Table 2. Silica content of BOPP/silica

Sample	Silica content (wt%)	Crystallinity (wt%)[a]
BOPP-150/SiO_2	2.0	81
BOPP-160/SiO_2	1.3	83
BOPP-165/SiO_2	1.4	83
BOPP-167/SiO_2	1.3	83

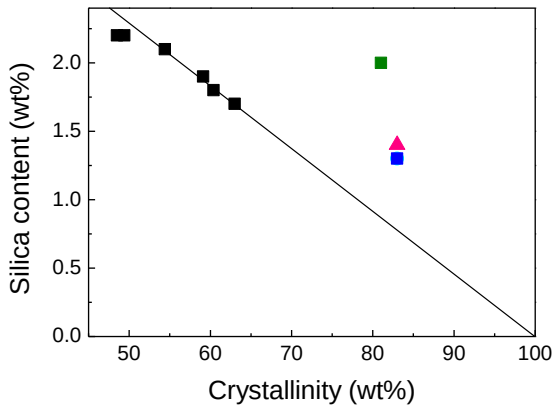

Figure 5. Relationship between the crystallinity and the silica content.

The silica content of composites prepared in this time is higher than linear line. Upper parts from line indicate the silica content in interface between BOPP films. The separated silica content was summarized in Table 3.

Table 3. Silica content of BOPP/silica located in amorphous region of BOPP and interface between BOPP films

Sample	Silica content (wt%)	Crystallinity (wt%)[a]	Silica content in amorphous (wt%)	Silica content in interface between BOPP films (wt%)
BOPP-150/Silica	2.0	81	0.9	1.1
BOPP-160/Silica	1.3	83	0.8	0.5
BOPP-165/Silica	1.4	83	0.8	0.6
BOPP-167/Silica	1.3	83	0.8	0.5

The silica content of BOPP-150/silica located in interface between BOPP films is highest, indicating that silica is largely synthesized there due to weak interface connection between BOPP films. The hot press temperature was consequently determined at 150 °C and the BOPP/Silica was hot-pressed at 160°C for 1 h under 20 MPa after synthesis of silica to enhance the adhesion between thin BOPP films. TEM observation was performed to examine the dispersion and morphology of formed silica.

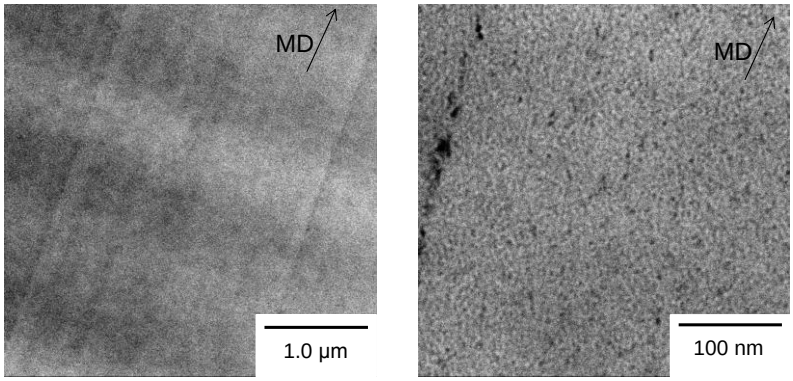

Figure 6. TEM images of BOPP/Silica

Lines of silica were observed with respect to each period of 2.5 μm, which corresponds to initial BOPP film thickness, resulting in the formation of silica in interface between initial BOPP films. The size of silica formed in amorphous region was below 10 nm. Seeing from TEM pictures, different size of silica was observed in the amorphous region and interface between BOPP films, inducing the difficulty to measure SAXS. Considering the previous results showing the relationship the amorphous thickness and shape of silica, disc type silica was formed in amorphous region because of enough confinement to produce low dimensional silica. The results of tensile tests were summarized in Table 4.

Table 4. Results of tensile test

Sample	Tensile strength (MPa)	Young's modulus (MPa)	Elongation at break (%)	Silica content (wt%)
BOPP-MD	108	910	210	-
BOPP/Silica-MD	111	1040	197	2.0
BOPP-TD	177	1181	86	-
BOPP/Silica-TD	193	1376	72	2.0

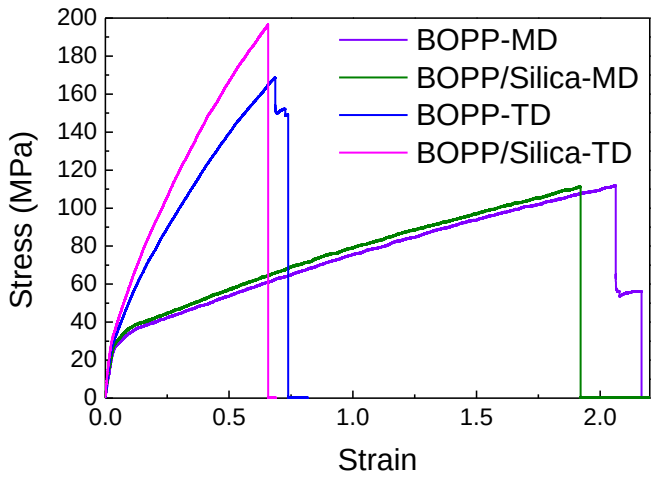

Figure 7. Strain-stress curves of BOPP and BOPP/Silica.

The mechanical properties of BOPP elongated to TD was higher than that to MD. It was thought that the molecular chain and crystals in BOPP are preferentially oriented to TD while the draw ratio is unknown. The addition of silica led to high reinforcement in the case of TD. The precise reason is unclear, but the orientation of synthesized

silica to TD might be caused by strong orientation of crystals to TD, resulting in high reinforcement.

Effects of initial BOPP film thickness on mechanical properties and synthesized structures were examined (Table 5)

Table 5. Results of tensile test

	Tensile strength (MPa) [a]	Young's modulus (MPa)	Elongation at break (%)	Silica content (wt%)	Crystallinity (wt%)
BOPP(2.5)-MD	108	910	210	-	
BOPP(2.5)/Silica-MD	111	1040	197	2.0	
BOPP(2.5)-TD	177	1181	86	-	82
BOPP(2.5)/Silica-TD	193	1376	72	2.0	
BOPP(10)-MD	92	718	220	-	
BOPP(10)/Silica-MD	95	796	207	1.4	
BOPP(10)-TD	166	1219	69	-	85
BOPP(10)/Silica-TD	179	1380	65	1.4	
BOPP(22)-MD	102	832	229	-	
BOPP(22)/Silica-MD	102	946	211	1.1	
BOPP(22)-TD	186	1323	63	-	87
BOPP(22)/Silica-TD	191	1494	61	1.1	

Silica content was decreased with film thickness of initial BOPP film probably because amorphous area and adhesive area between BOPP films to incorporate silicon alkoxide decreased. Because of large error range, the tendency elongated into MD direction was not observed. Therefore, the results of mechanical properties elongated to TD were discussed in this session due to overcoming the change from effort range. The effects of initial BOPP film thickness on mechanical properties were hardly observed regardless of increasing crystallinity with the film thickness. It might relate to the level of orientation and the orientation degree of BOPP-22 is perhaps low. While the mechanical properties of BOPP-2.5 and BOPP-10 were improved by the addition of silica, the reinforcement was not obtained by the synthesis of silica in BOPP-22 (Figure 8). Three scenarios were considered as the reason: 1) reduction of silica content, 2) increase of crystallinity and 3) change of synthesized silica structure such as size and shape. Especially, 3) is key factor to determine the properties of resulting composites. While the small-angle X-ray scattering were powerful tool to examine the size and dimension of synthesized silica, it was not available because of problems previously mentioned. Therefore, the structure of synthesized silica was observed using TEM (Figure 9).

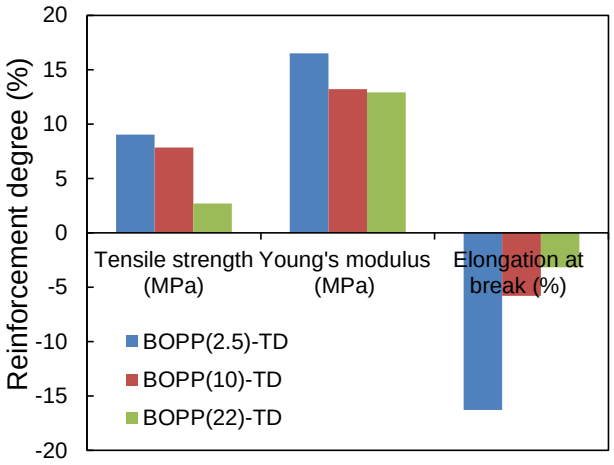

Figure 8. Reinforcement degree of BOPP/Silica with different initial BOPP film thickness.

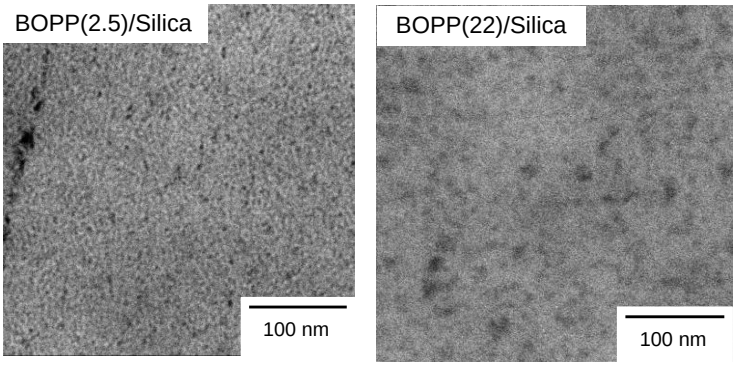

Figure 9. TEM images of BOPP(2.5)/Silica and BOPP(22)/Silica.

Formed SiO_2 mainly had the morphology of highly dispersed nanoparticles. The size of SiO_2 synthesized in BOPP-2.5 (6 nm) was smaller than that in BOPP-22 (>10 nm). From the previous study, it was found that the size and dimension of synthesized silica were affected by the amorphous thickness, and thinner amorphous thickness led to smaller and lower-dimensional silica particles. Therefore, it was considered that the

formation of large and sphere-like silica diminished the mechanical reinforcement. The images of formed structure was shown in Figure 10. It was considered that the structure of BOPP(2.5)/Silica was similar with nacre compared to BOPP(22)/Silica, resulting in high reinforcement.

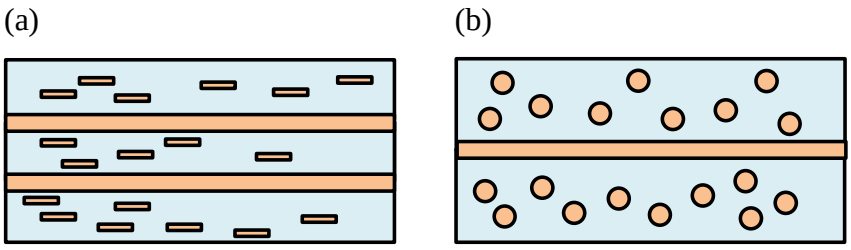

Figure 10. Considerable illustration of formed silica structure in (a) BOPP(2.5) and (b) BOPP (22).

HCl and NH_3 were firstly employed as catalysts for sol-gel reaction to control the morphology of silica. The morphology and dispersion were observed by TEM (Figure 11).

(a)

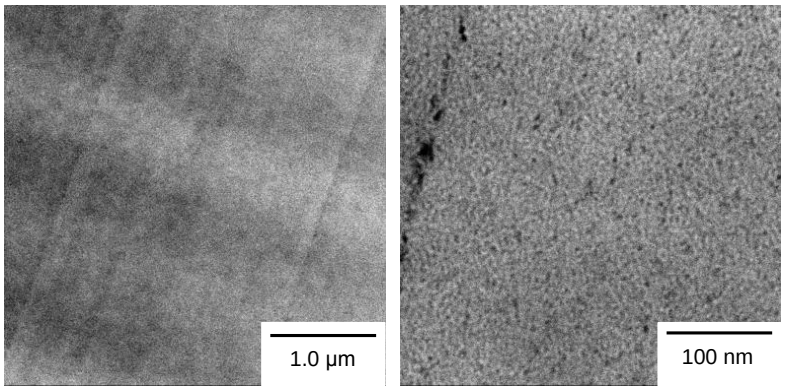

(b)

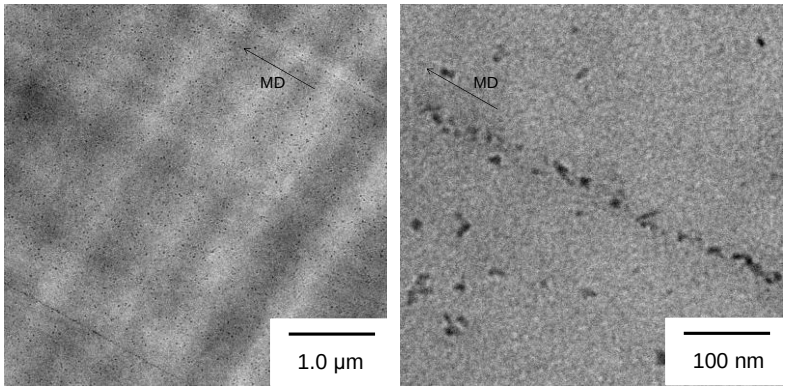

Figure 11. TEM images of BOPP/Silica prepared with (a) HCl or (b) NH_3.

Lines of silica were observed with respect to each period of 2.5 μm, which corresponds to initial BOPP film thickness, resulting in the formation of silica in interface between initial BOPP films. The morphology of synthesized silica had highly dispersed nanoparticle. The size of silica synthesized with NH_3 was larger than that with HCl.

In order to evaluate mechanical properties of BOPP/Silica prepared with different catalyst, tensile tests were carried out (Table 6, Figure 12).

Table 6. Results of tensile test of BOPP/Silica prepared with different catalyst

	Tensile strength (MPa) [a]	Young's modulus (MPa) [a]	Elongation at break (%) [a]	Silica content (wt%) [b]
BOPP-MD	108	910	210	-
BOPP/Silica (HCl)-MD	111	1040	197	2.0
BOPP/Silica (NH_3)-MD	119	1088	186	0.9
BOPP-TD	177	1181	86	-
BOPP/Silica (HCl)-TD	193	1376	72	2.0
BOPP/Silica (NH_3)-TD	188	1428	73	0.9

[a] Determined by tensile test

[b] Evaluated from the weight of inorganic residue after incinerating organic components

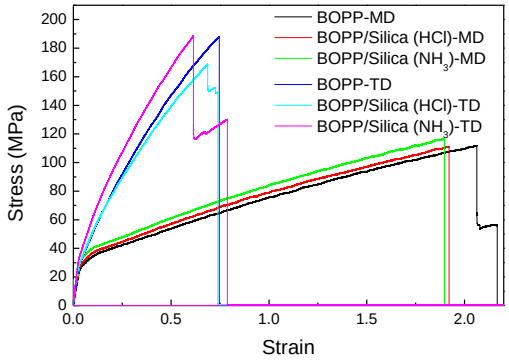

Figure 12. Stress-strain curves of BOPP/Silica prepared with different catalyst.

Silica content of BOPP/Silica prepared with NH_3 was lower than that with HCl. This is because impregnated TPOS was evaporated from BOPP film. It was indicated that silicon alkoxide was migrated to liquid phase at low concentration of catalyst vapor during sol-gel reaction in previous study. Less volatility of NH_3 led to low conversion of silicon alkoxide to silica in PP in contrast to the full conversion in HCl with more volatility, resulting in low silica content.

The mechanical reinforcement of PP/silica (NH_3) was relatively high in spite of low silica content. The sol-gel reaction catalyzed by base catalyst usually produces silica particle with high condensation and large size. On the other hand, the size of silica synthesized in the amorphous region was much smaller compared to that prepared through usual sol-gel reaction due to spatial confinement in the amorphous region. The confinement should be stronger by sol-gel conditions to prepare larger particle, leading to formation of anisotropic silica. It was considered that the high reinforcement was attributed from the formation of anisotropic silica with high condensation.

In order to increase the silica content, TPOS was impregnated at high temperature (120°C). The results of tensile tests are summarized in Table 7 and Figure 13. TEM images are also shown in Figure 14.

Table 7. Results of tensile tests of BOPP/Silica prepared through different impregnation temperature

	Tensile strength (MPa) [a]	Young's modulus (MPa) [a]	Elongation at break (%) [a]	Silica content (wt%) [b]	Crystallinity (wt%) [c]
PP [d]	22	601	>500	-	62
BOPP-MD	108	910	210	-	82
BOPP/Silica (imp.80)-MD	119	1088	186	0.9	82
BOPP/Silica (imp.120)-MD	127	1118	220	2.1	82
BOPP-TD	177	1181	86	-	82
BOPP/Silica (imp.80)-TD	188	1428	73	0.9	82
BOPP/Silica (imp.120)-TD	222	1564	73	2.1	82

[a] Determined by tensile test

[b] Evaluated from the weight of inorganic residue after incinerating organic components

[c] Determined by WAXD

[d] Prepared by hot press of BOPP

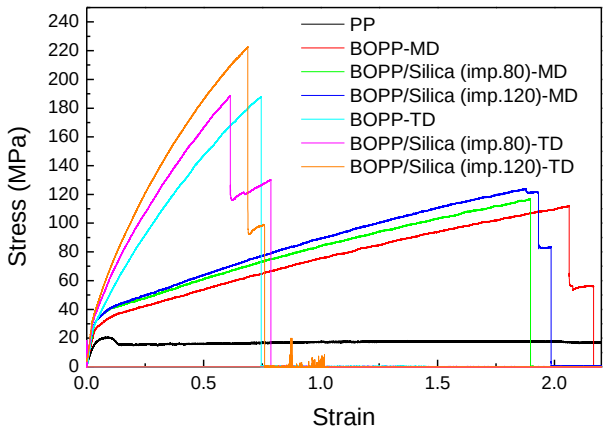

Figure 13. Stress-strain curves of BOPP/Silica with different silica content.

(a)

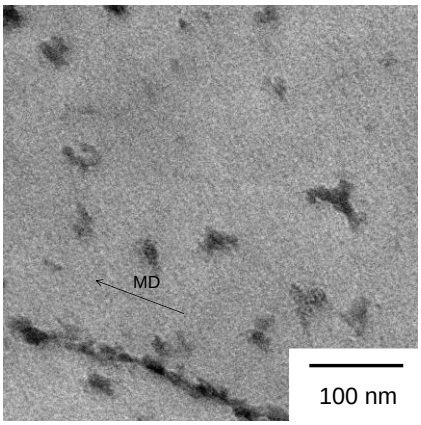

(b)

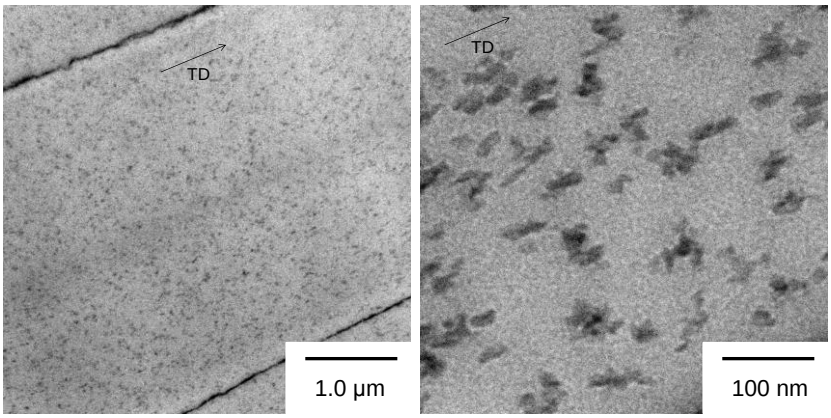

Figure 14. TEM images of (a) BOPP/silica (imp.120)-MD and (b) BOPP/silica (imp.120)-TD.

The silica content was successfully improved by increasing impregnation temperature. By increasing silica content, not only mechanical properties but also elongation at break was improved in contrast to previous experiments. It was considered that the reinforcement by the addition of silica overcame the deterioration by $scCO_2$. The deterioration by $scCO_2$ might depend on treatment time rather than temperature, or the retreatment leads to further expansion of amorphous part, which promoted chain session or relaxation of chain orientation. From TEM results, parallel oriented disc-type silica was observed in BOPP/silica (imp.120)-TD (Figure 14 (b)). The amount of disc-type in TD silica looked more than that in MD, which might attribute from the orientation of PP amorphous region. The maximum reinforcement reached and 25% for tensile strength and 32% for Young's modulus compared to BOPP and 1010% for tensile strength and 260% for Young's modulus compared to unoriented PP. The reinforcement degree from BOPP is relatively high in case of polymer with high stiffness and it was found that the combination of oriented lamellar and synthesized silica produces drastic reinforcement.

4.4. Conclusions

In order to mimic a hierarchical structure of nacre, silica was synthesized in amorphous region of BOPP and interface between laminated BOPP films through sol-gel reaction with the aid of BOPP films. The structure was optimized by laminated temperature, initial BOPP film thickness and employed catalyst. Silica was successfully synthesized in amorphous region of BOPP and interface between laminated BOPP films. The maximum reinforcement reached and 25% for tensile strength and

32% for Young’s modulus compared to BOPP and 1010% for tensile strength and 260% for Young’s modulus compared to unoriented PP.

Thus, it was found that combination of oriented lamellar and silica formed in amorphous region resulted in exceptional reinforcement.

References

[1] Okamoto M, Nam PH, Kotaka T, Hasegawa N, Usuki A. Nano Lett 2001:1;295.

[2] Haraguchi, K, Takehisa T. Adv Mater 2002;14:1120.

[3] Tanaka Y, Gong JP, Osada Y. Prog Mater Sci 2005;30:1.

[4] Heuer, A. Fink DJ, Laraia VJ, Arias JL, Calvert PD, Kendall K, Messing GL, Blackwell J, Rieke PC, Thompson DH, Wheeler AP, Veis A, Caplan AI.
Science 1992;255:1098.

[5] Espinosa HD, Rim JE, Barthelat F, Buehler MJ. Prog Mater Sci 2009;54:1059.

[6] Fratzl P, Gupta HS, Paschalis EP, Roschger P. J Mater Chem 2004;14:2115.

[7] Li X, Chang WC, Chao YJ, Wang R, Chang M. Nano Lett 2004;4:613.

[8] Rousseau, M, Lopez E, Stempflé P, Brendlé M, Franke L, Guette A, Naslain R, Bourrat X. Biomaterials 2005;26:6254.

[9] Fratzl P, Gupta HC, Fischer FD, Kolednik O. Adv Mater 2007;19:2657.

[10] Bouchbinder E, Brener EA. J Mech Phys Solid 2011;59:2279.

[11] Espinosa HD, Juster AL, Felix J. Latourte, Loh OY, Gregoire D, Zavattieri PD. Nature Commun 2011;2:173.

[12] Podsiadlo P, Kaushik AK, Arruda EM, Waas AM, Shim BS, Xu J, Nandivada H, Pumplin BG, Lahann J, Ramamoorthy A, Kotov NA. Science 2007;318:80.

[13] Bonderer LJ, Studart AR, Gauckler LJ. Science 2008;319:1069.

[14] Priolo MA, Gamboa D, Holder KM, Grunlan JC Nano Lett 2010;10:4970.

[15] Podsiadlo P, Michel M, Lee J, Verploegen E, Kam NWS, Ball V, Lee J, Qi Y, Hart AJ, Hammond PT, Kotov NA. Nano Lett 2008;8:1762.

[16] Munch E, Launey ME, Alsem DH, Saiz E, Tomsia AP, Ritchie RO. Science 2008;322:1516.

[17] Wang YC, Huang TK, Tung SH, Wu TM, Lin JJ. Sci Rep 2013;3:2621.

[18] Erb RM, Libanori R, Rothfuchs N, Studart AR. Science 2012;335:119.

[19] Bonderer LJ, Feldman K, Gauckler LJ. Compos Sci Techn 2010;70:1958.

[20] Sun D, Zhang R, Liu Z, Huang Y, Wang Y, He J, Han B, Yang G. Macromolecules 2005;38:5617.

[21] Takeuchi K, Terano M, Taniike T. Polymer 2014;55:1940.

Chapter 5.

General Conclusions

In this study, PP/silica nanocomposites were prepared through the impregnation of PP amorphous part with silicon alkoxide and subsequent sol-gel reaction. Since $scCO_2$ enables to disperse metal alkoxide in the amorphous region, the structural design was achieved utilizing the amorphous part. The silica was synthesized in confined amorphous region of PP and the establishment of relationship between the structure of formed silica and properties of resultant nanocomposites was tried by changing conditions of sol-gel reaction. Nano-silica was formed in PP amorphous part due to spatial confinement. Silica network structures were successfully constructed in PP at low silica loading. The relationship between the structure of formed silica network and properties of nanocomposites was established, where formation of low dimensional silica led to high reinforcement both in solid state and in molten state.

Silica was synthesized in PP with different higher structure in chapter 3. The size and shape of silica was controlled by amorphous region of PP also due to confinement by PP amorphous region. Sol-gel template synthesis using amorphous region of PP was newly proposed as new method to control morphology of silica synthesized through sol-gel method combined with template approach.

BOPP films were laminated, and then sol-gel reaction was performed after impregnation of BOPP with silicon alkoxide in chapter 5. The drastic reinforcement was obtained by incorporating silica not only into amorphous part of BOPP and interface between laminated thin BOPP films. The method results in new method to mimic nacre-like structure by top-down synthesis and versatile method employing every semi-crystalline polymer.

It was believed that obtained results contribute not only to academic but also to industrial field. Since the method led to effective network formation, it is expected

that various properties such as electro or thermal conductivity are added by incorporating other oxide materials such as tin or alumina oxide. In addition, the films after processing is possible to reinforce by incorporating filler using sol-gel method combined with the impregnation.

Finally, novel design of nano-silica network in polypropylene using sol-gel method with supercritical carbon dioxide was successfully achieved and the development is expected to expand both academic and industrial area.

Acknowledgement

I would like to express my sincere regards to Professor Minoru Terano for his continually guidance and warm encouragement.

I am deeply grateful to Associate Professor Toshiaki Taniike, JAIST for many helpful discussion and many supports.

I would like to thank Professor Masayuki Yamaguchi, JAIST for the assistance of my research and borrowing me various experimental machines.

Great acknowledgments are made to Professor Jaques Lacoste who provided valuable advices for my minor research and daily life in France.

I would like to thank to Dr. Ikki Katada, Mr. Kei Kaneko, Mr. Taira Tobita and other members of nanocomposite group in Terano laboratory. I highly appreciate their supports.

I am also grateful heartily to Masaki Umemori and Masahito Toyonaga, graduated student of Terano laboratory for his kind help in supporting the research.

Sincere thanks to all the members in Terano, Yamaguchi laboratories for their kind supports.

I highly appreciate our parents for their endless supports for my life.

Achievements

＜Original paper＞

1. "Critical Role of Interfacial Structures in Degradation and Stabilization of Polypropylene/SiO_2 Composites" by Toshiaki Taniike, Masaki Umemori, Hibiki Chiba, Kengo Takeuchi, Minoru Terano, Journal of Materials Life Society, 2012, 24, 102-106.

2. "Sol-gel synthesis of nano-sized silica in confined amorphous space of polypropylene: impact of nano-level structures of silica on physical properties of resultant nanocomposites" by Kengo Takeuchi, Minoru Terano, Toshiaki Taniike, Polymer, 2014, 55, 1940-1947.

3. "Versatile Strategy for Fabrication of Polypropylene Nanocomposites with Inorganic Network Structures based on Catalyzed in-situ Sol-Gel Reaction during Melt Mixing" by Kei Kaneko, Nitin Yadav, Kengo Takeuchi, Bulbul Maira, Minoru Terano, Toshiaki Taniike, Composites Science and Technology, 2014, 102, 120-125.

＜International conference＞

“Construction of Inorganic Network Structures in Polypropylene through Sol-gel Method”

8th International Colloquium on Heterogeneous Ziegler-Natta Catalysts, Kanazawa, Japan, Mar. 2011.

“Design of inorganic network structure in polypropylene through sol-gel Method with super-critical CO_2”

4th International Conference on Polyolefin Characterization, Houston, USA, Oct. 2012.

“Time-Dependent Property Change during In-Situ Preparation of Polypropylene Nanocomposites”

9th International Symposium on Weatherability 3rd International Workshop on Polymer Degradation and Stability, Tokyo, Japan, Mar. 2013.

“Sol-gel Synthesis of Silica Network Using Amorphous Region of Polypropylene”

International Symposium for Green-Innovation Polymers, Kanazawa, Japan, Mar. 2014.

“Formation of silica network structures using sol-gel reaction in polypropylene amorphous region as template”

5th International Conference on Polyolefin Characterization, Valencia, Spain, Sep. 2014.

＜Domestic conference＞

ゾル - ゲル法を用いたポリプロピレン中でのナノシリカの直接合成

第 61 回高分子学会年次大会、大阪、2011 年、5 月

ポリプロピレン中で in-situ 合成したシリカ粒子の形態と物性への影響

マテリアルライフ学会第 22 回研究発表会、東京、2011 年、7 月

超臨界二酸化炭素によるシリカ前駆体含浸法を用いたポリプロピレン／シリカナノコンポジットの調製

第 56 回高分子夏季大学、福井、2011 年、7 月

各種アルコキシシラン前駆体のゾル - ゲル反応によるポリプロピレン中でのナノシリカの in-situ 合成

高分子学会討論会、岡山、2011 年、9 月

ナノシリカの in-situ 合成によるポリプロピレン中でのフィラーネットワーク構造の構築

マテリアルライフ学会第 16 回春季研究発表会、東京、2012 年、2 月

ゾル - ゲル法を用いたポリプロピレン中での無機ネットワーク構造の制御

第 62 回高分子学会年次大会、横浜、2012 年、5 月

ポリプロピレン系ナノコンポジットの物性改良を目的とした無機ネットワーク構造の in-situ 構築

マテリアルライフ学会第 23 回研究発表会、群馬、7 月

ポリプロピレンの高次構造が in-situ 合成した無機ネットワーク構造に与える影響

第 61 回高分子学会討論会、名古屋、2012 年、9 月

ポリプロピレンの非晶部を鋳型として利用したシリカネットワーク設計

マテリアルライフ学会第 17 回春季研究発表会、東京、2013 年、3 月

ポリプロピレンの非晶部を利用したナノフィラーの構造制御と溶融物性に与え

る影響

第 63 回高分子学会年次大会、京都、2013、5 月

無水マレイン酸変性ポリプロピレンを共存させたゾル - ゲル法よるポリプロピレン／シリカナノコンポジットの直接合成

第 64 回高分子学会年次大会、名古屋、2014 年、5 月

ポリプロピレン中でゾル - ゲル法を用いたポリプロピレングラフトシリカの in-situ 合成

マテリアルライフ学会第 25 回研究発表会、東京、7 月

Degradation Behavior of Lacquers with Different Pigments

by

Kengo Takeuchi

Submitted to

School of Materials Science

Japan Advanced Institute of Science and Technology

Supervisor: Professor Jacques Lacoste

Professor of National Centre for the Evaluation of Photoprotection (CNEP),

Universite Blaise Pascal, 63 177 Aubiere Cedex, France

1. Introduction

Lacquer is one of the oldest coating materials. It has been used on wood to paint many kinds of traditional materials such as architecture, craft and so on, producing many famous cultural heritages in Japan. The raw materials of lacquer are consisted of an oil-in-water emulsion containing urushiol (Figure 1) sapped from lacquer tree [1,2]. The emulsion pasted on crafts is converted into stiff, lustrous and beautiful coating since urushiol was crosslinked under air moisture during drying in the presence of enzyme and laccase as catalyst. However, crosslinked lacquer chain is susceptible to be cleaved by light because the light is absorbed by the double bond contained in the lacquer chain, resulting in the degradation of lacquer. Since the degradation induces serious problem such as loss of gloss and/or formation of cracks, various studies were performed to examine the mechanism of the lacquer degradation [3-5]. In addition, stabilization of lacquer is essential to improve the resistance against light.

One the other hand, lacquer is used by introducing pigments such as carbon, titanium oxide and so on. Especially, carbon materials act not only as a pigment to give them black but also as a stabilizer because it enables to absorb light. In other words, it has possibility to improve light stability by only incorporating carbon-type pigments. In this study, pine smoke, which is traditionally employed and industrial smoke were chosen as pigments and other coating materials were used to compare effects of the addition of the pigments on the degradation.

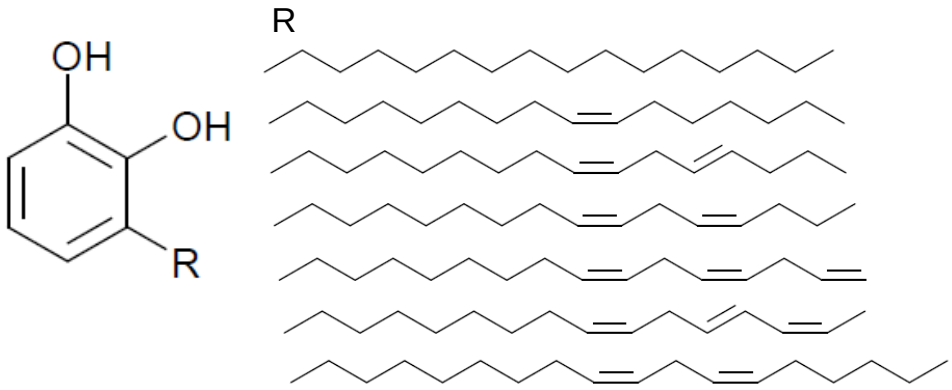

Figure 1. Chemical structure of lacquer

2. Experimental

Materials

Lacquer, glue, casein and acrylic emulsion resin kindly donated by Institute of Technology were employed as coating materials. These materials were painted on woods. Pine smoke and industrial smoke were also contained in lacquer as pigments. Lacquer with pine smoke, lacquer with industrial smoke, natural lacquer, glue, casein and acrylic emulsion resin were named as sample A, sample B, sample C, sample D, sample E and sample F, respectively. The colors of lacquers are black and other materials are brown (Figure 2).

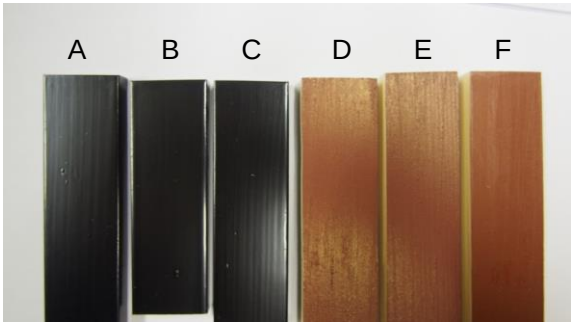

Figure 2. Picture of materials

Sample exposures

The samples were exposed by light (SEPAP 12/24, ATLAS) at 60°C. The wavelength of exposure light is above 290 nm.

Instruments

The degradation was detected by attenuated total reflection infrared spectroscopy (ATR-IR, MAGNA-IR 860, Nicolet) with 32 scans equipped with Ge crystal and photoacoustic infrared spectroscopy (PAS-IR, Nicolet 6700 FT-IR, Thermo SCIENTIFIC) with 124 scans. The gloss of

surface was measured by gloss meter (PICOGLOSS 560MC, ERICHSEN). UV-vis spectrometry (Lambda 650 S, Parkin elmer) were used to evaluate color difference. The value of color difference was calculated from below equation.

$$\Delta E^*_{ab} = \left[(\Delta L^*)^2 + (\Delta a^*)^2 + (\Delta b^*)^2 \right]^{\frac{1}{2}}$$

The surface was observed by optical microscope. The chemiluminescence analyzer (CLA, CLA-FS3, Tohoku Electronic Industrial Co.,Ltd.) was employed to evaluate the oxidation state of lacquers. The measurements were performed at different temperature under nitrogen to examine the activation energy.

3. Results and discussion

3.1. Degradation of sample A, B and C

ATR-IR spectra of sample A, B and C are shown in Figure 3.

(a)

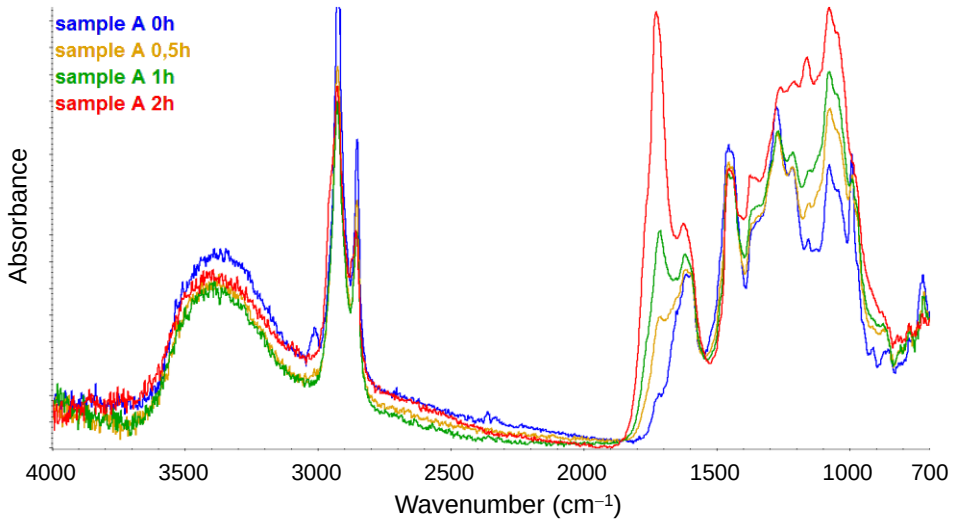

(b)

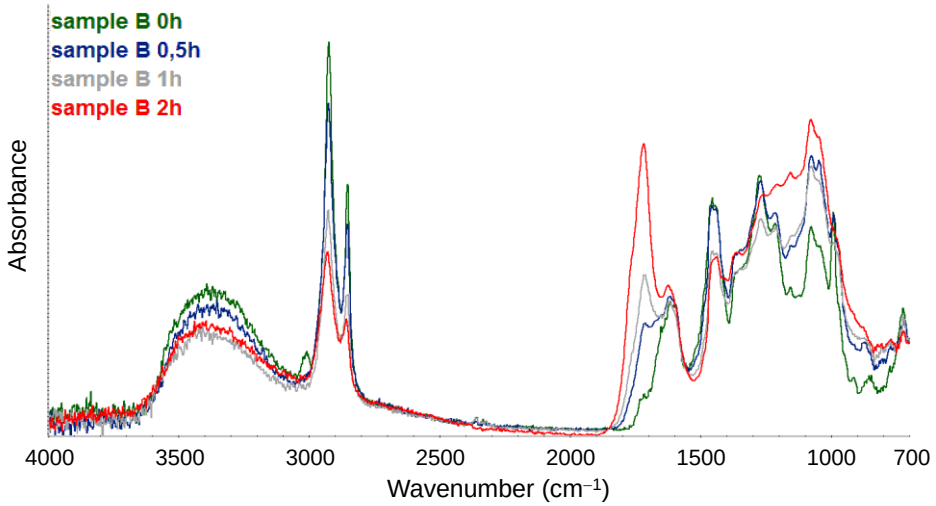

(c)

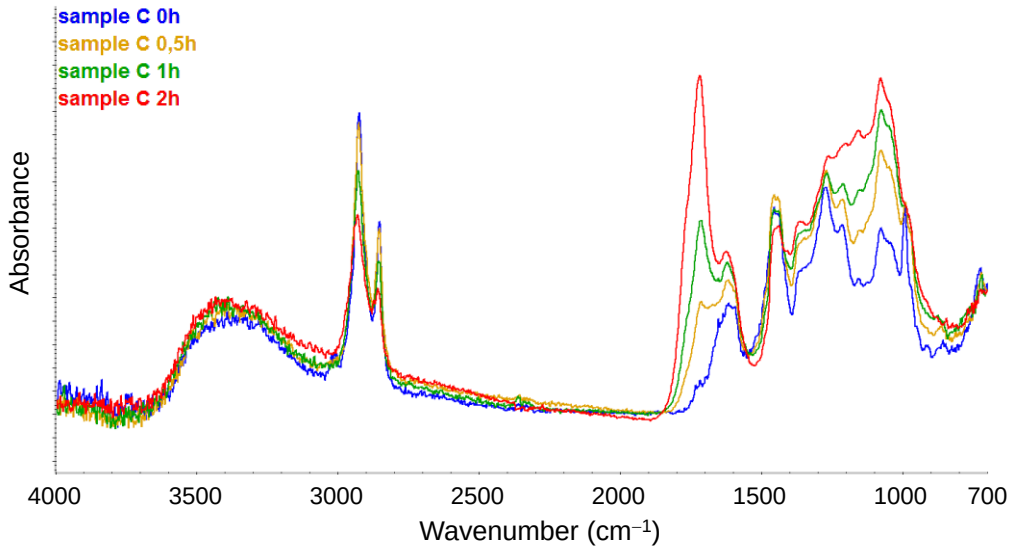

Figure 3. ATR-IR spectra of (a) sample A, (b) sample B and (c) sample C.

The intensity around 1710 cm^{-1} was increased with exposure time and new peak appeared. The peak is assigned to carboxyl or ketone groups caused by the degradation of the lacquer. These lacquers are quite susceptible to be damaged by light exposure because the intensity increased rapidly for only a few hours. The peak intensity was normalized by using a peak around 2900 cm^{-1} attributed from CH_2 to compare oxidation degree among lacquers with or without carbon (Figure 4 (a)). The comparison were also performed using a peak around 3400 cm^{-1}, coming from OH groups because OH groups are induced by the degradation (Figure 4 (b)).

(a)

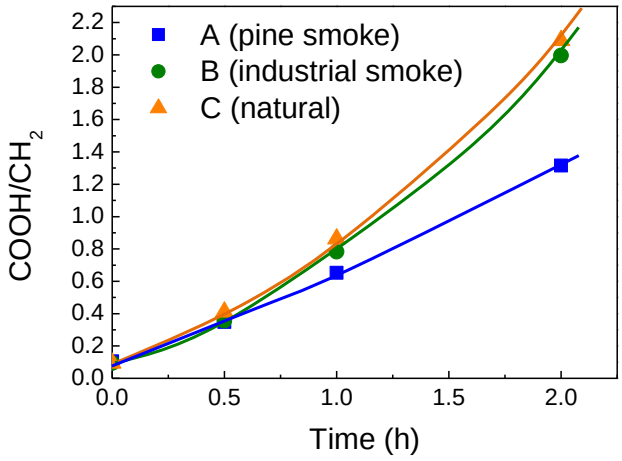

(b)

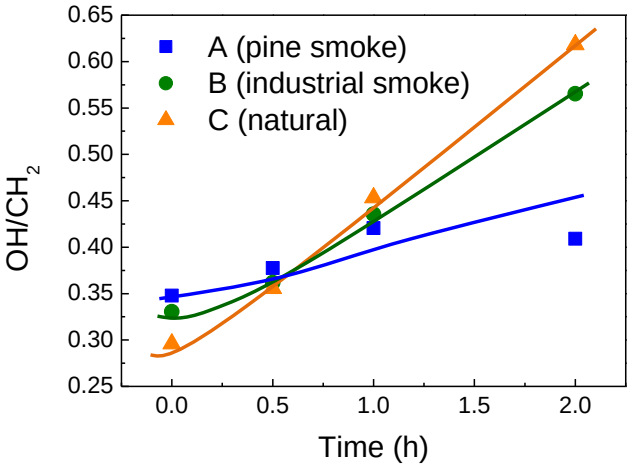

Figure 4. Relationship between exposure time and intensity of (a) COOH or (b) OH.

The intensity ratio was increased with exposure time and the order of the degradation speed was C > B > A. It is found the addition of carbon is effective to stabilize lacquer materials and pine smoke shows highest stability. However, it is thought that the improvement is insufficient to use it long period, so it is essential to add not only pigments but also stabilizers.

Gloss was measured to examine surface properties.

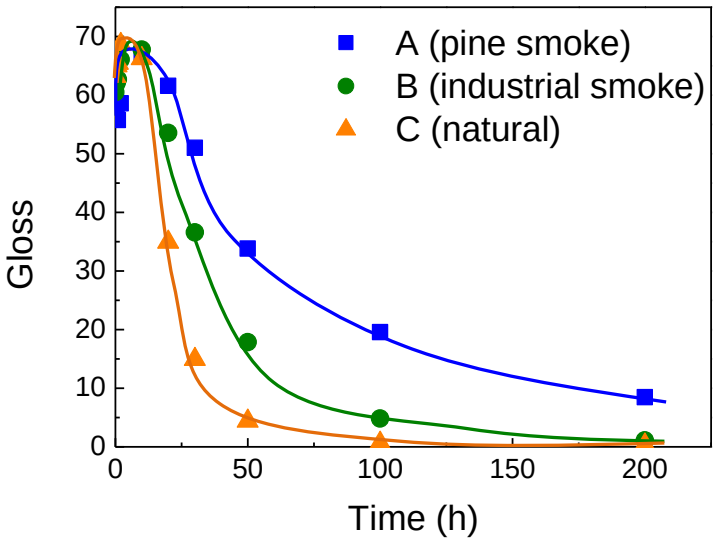

Figure 5. Gloss measurements.

The gloss was increased by initial exposure, and then dramatically decreased by long exposure. The order of the tendency was corresponded to that of surface degradation. Though the gloss of sample C was almost lost by exposing for only 50 h, the retardation of gloss loss was induced by the addition of carbon and it is found that pine smoke is the most effective additives to keep the gloss.

Color differences were measured by UV-vis measurements.

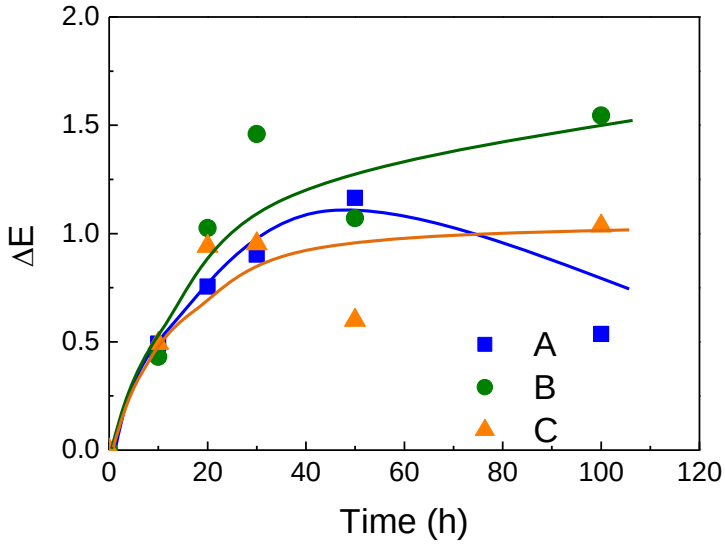

Figure 6. Color differences

Though large differences were observed on gloss loss, the gloss value did not change dramatically and the obvious tendency was not obtained. It is probably originated from the color of lacquer. The color of lacquer is black, so it is thought that color does not change dramatically in spite of proceeding the degradation.

Optical microscope was employed to observe surface of lacquers.

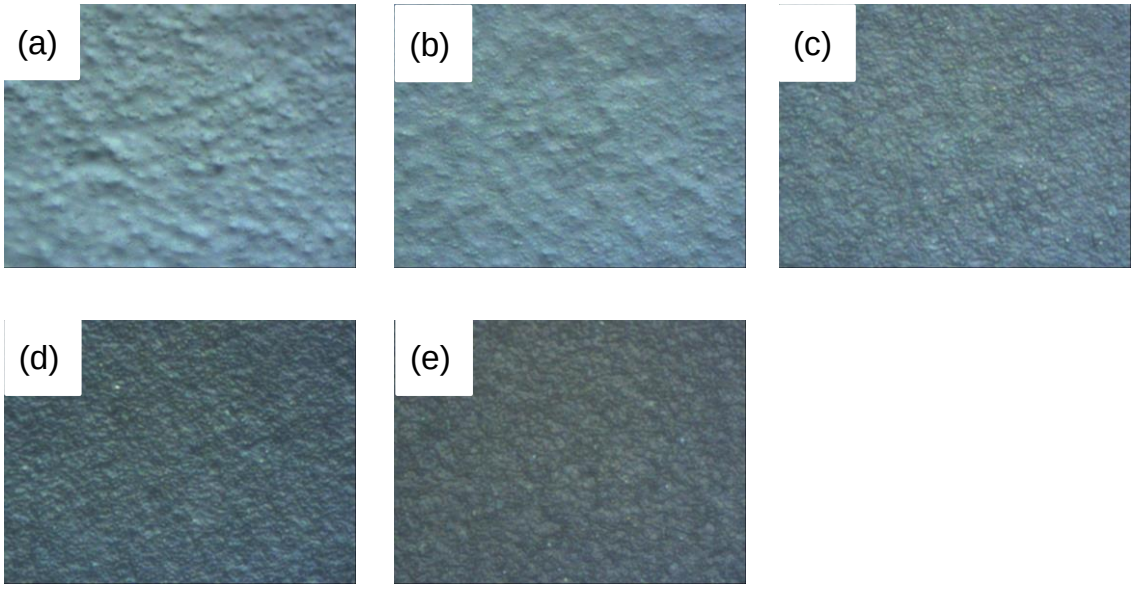

Figure 7. Optical microscope images of sample A exposed for (a) 0 h, (b) 10 h, (c) 20 h, (d) 30 h and (e) 50 h.

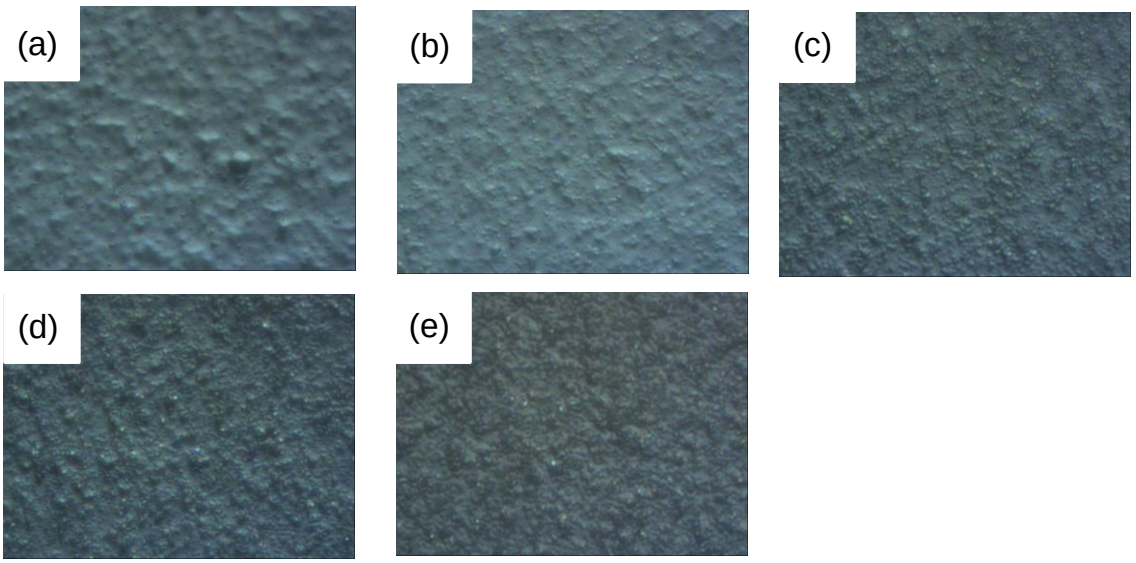

Figure 8. Optical microscope images of sample B exposed for (a) 0 h, (b) 10 h, (c) 20 h, (d) 30 h and (e) 50 h.

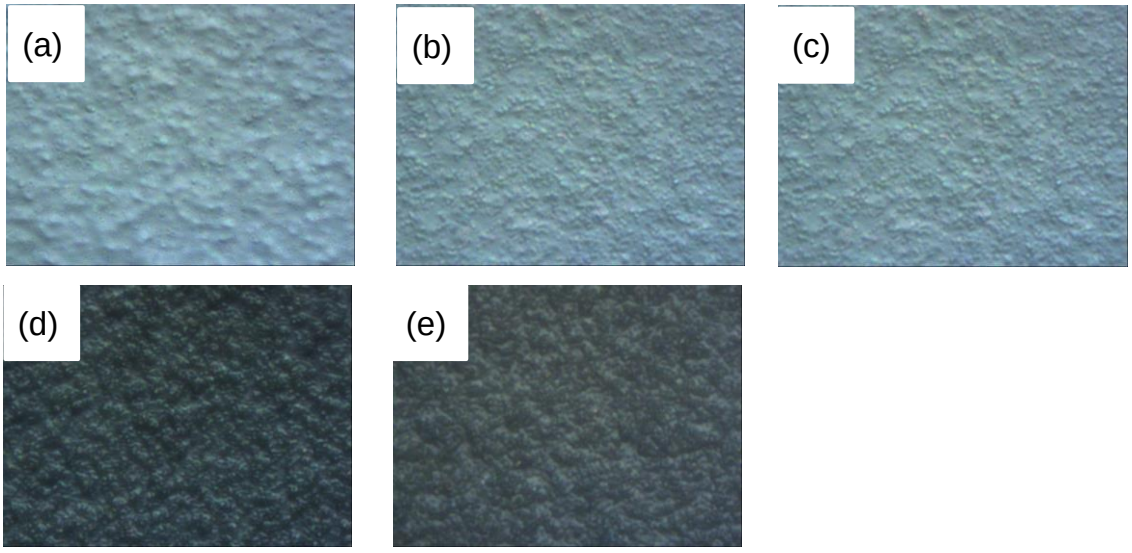

Figure 9. Optical microscope images of sample C exposed for (a) 0 h, (b) 10 h, (c) 20 h, (d) 30 h and (e) 50 h.

Cracks are usually formed after stating oxidation, resulting in degradation of surface properties. However, any cracks were not observed in spite of increasing aging time in these lacquer samples. It is suggested that the mechanism of surface degradation is different from that of usual degradation

while cracks might be observed using scanning electric microscope. Initially, the chain of lacquer is cleaved by light exposure, forming low molecular weight materials. The low molecules caused by chain session are evaporated from surface and new layer appears. The degradation is proceeded by repeating the procedure. Therefore, it is thought that cracks is not observed due to volatilization of oxidative materials.

3.1. Degradation of sample D, E and F

IR measurements were performed to examine the degradation of sample D, sample E and sample F. Concerning these samples, PAS-IR measurements were carried out because ATR-IR measurements were not adequate due to bad roughness. Figure 10 shows expanded IR spectra.

(a)

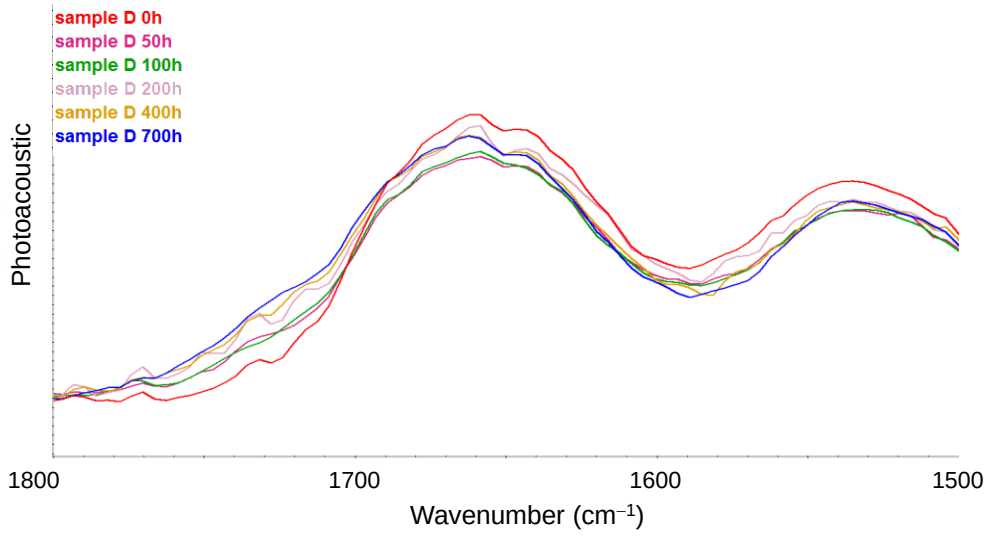

(b)

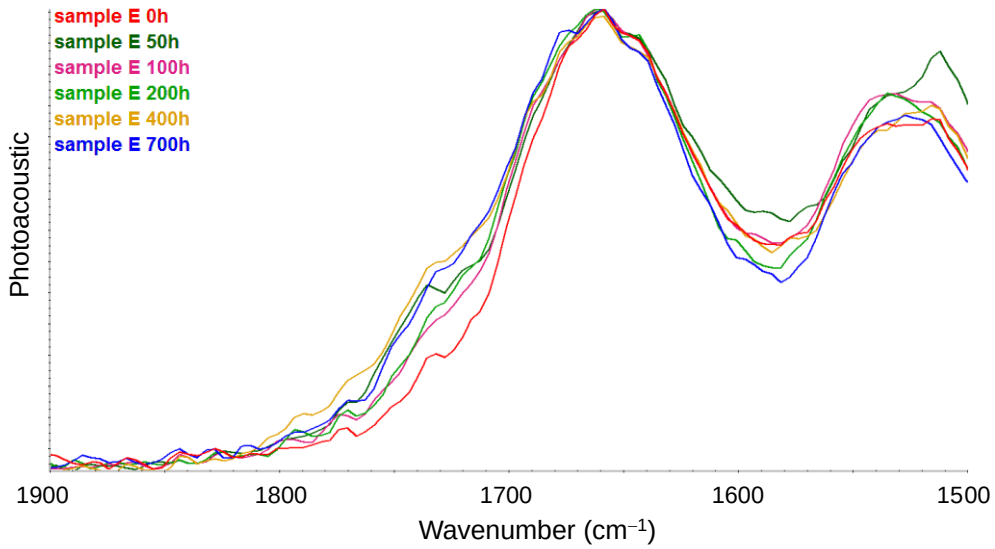

(c)

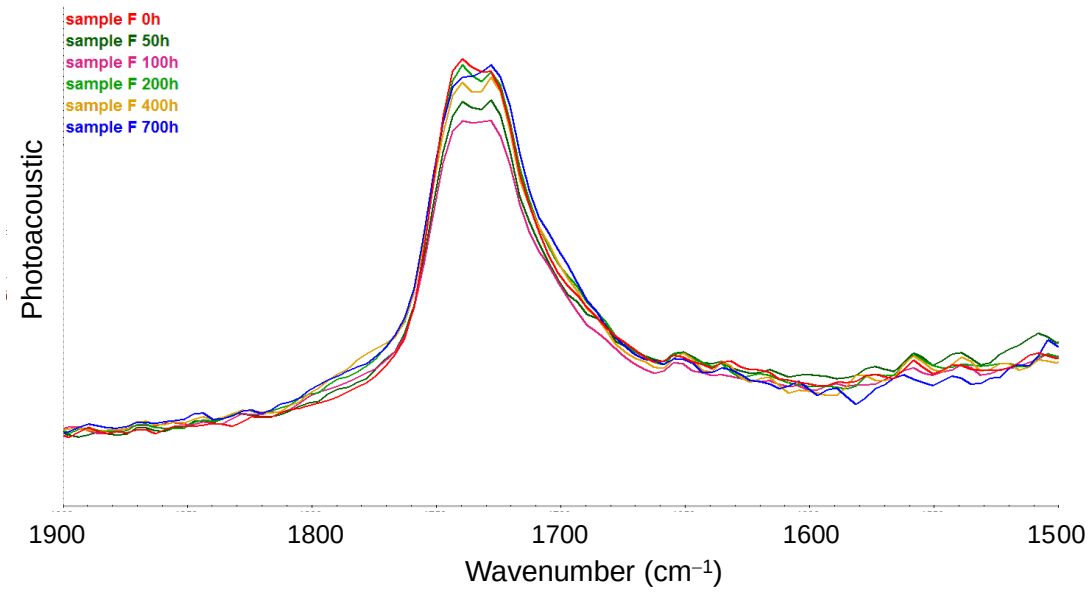

Figure 10. PAS-IR spectra of (a) sample D, (b) sample E and (c) sample F.

It is difficult to compare the oxidation state between lacquers and other samples due to the difference of depth resolution between ATR and PAS. Therefore PAS-IR measurements of lacquers were also performed. The degradation started to be progressed by exposure for 2 h along lacquers, but the degradation speed of sample D and sample E was very slow. According to spectrum of sample F, the degradation was unclear because of overlap of peaks, but the degradation was gradually proceeded due to increase of intensity around 1780 cm^{-1}. It is found that these materials are much more stable than lacquers.

The properties of surface were affected by degradation. Therefore, gloss was measured to examine surface properties of these samples.

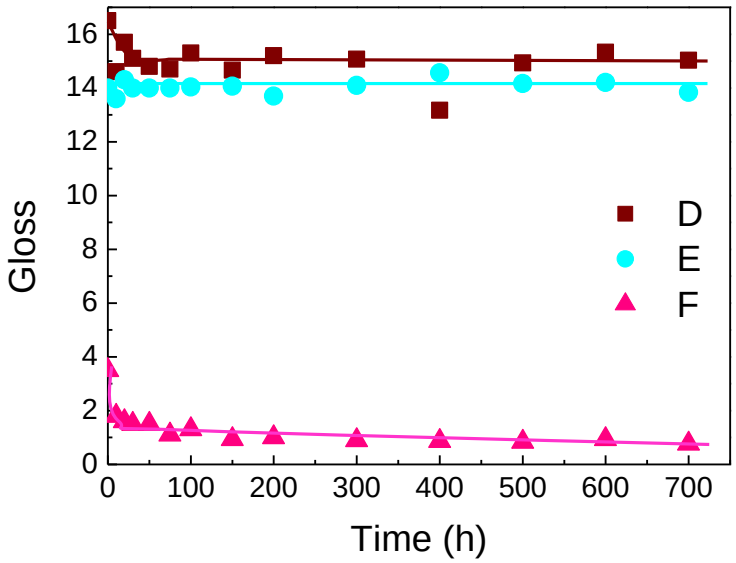

Figure 11. Gloss measurements.

The gloss value was almost constant about sample D and sample E even exposure time was prolonged. The gloss of sample B was lost by initial exposure and became constant. Then, color differences were measured by UV-vis measurements to also examine the surface properties.

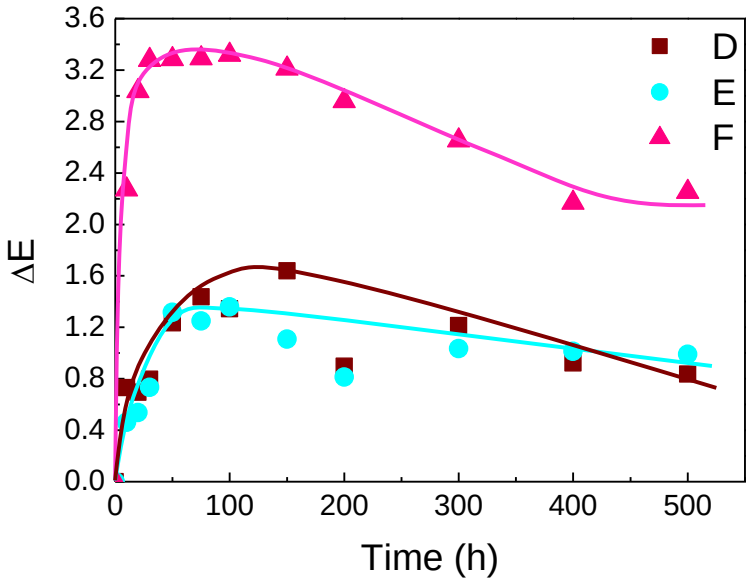

Figure 12. Gloss measurements.

The color difference of sample F was increased with short exposure. This result is well correlated with that of gloss measurements. Therefore the surface properties might be lost by short exposure. The color differences of sample D and sample F were not changed dramatically by exposure.

Optical microscope was employed to observe surface of these samples.

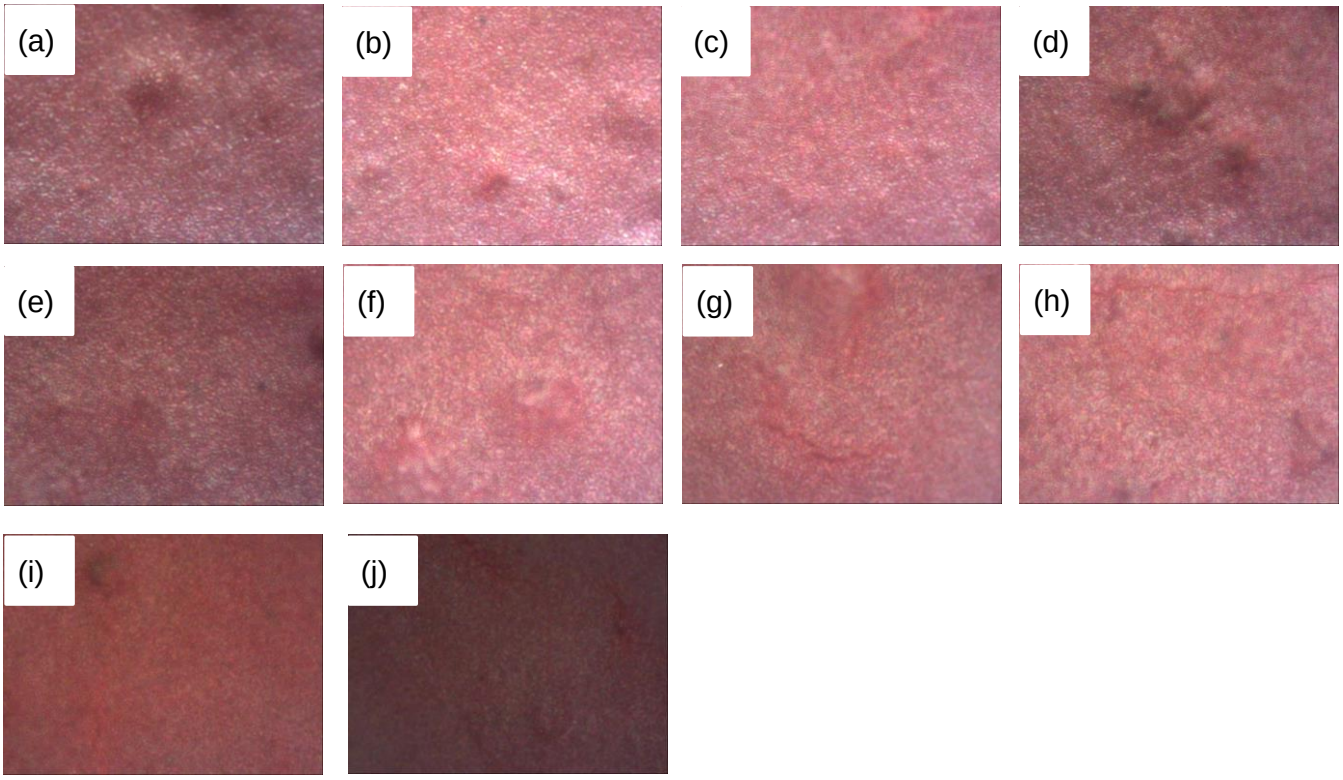

Figure 13. Optical microscope images of sample D exposed for (a) 0 h, (b) 10 h, (c) 20 h, (d) 30 h, (e) 50 h, (f) 100 h, (g) 150 h, (h) 200 h, (i) 300 h, and (j) 500 h.

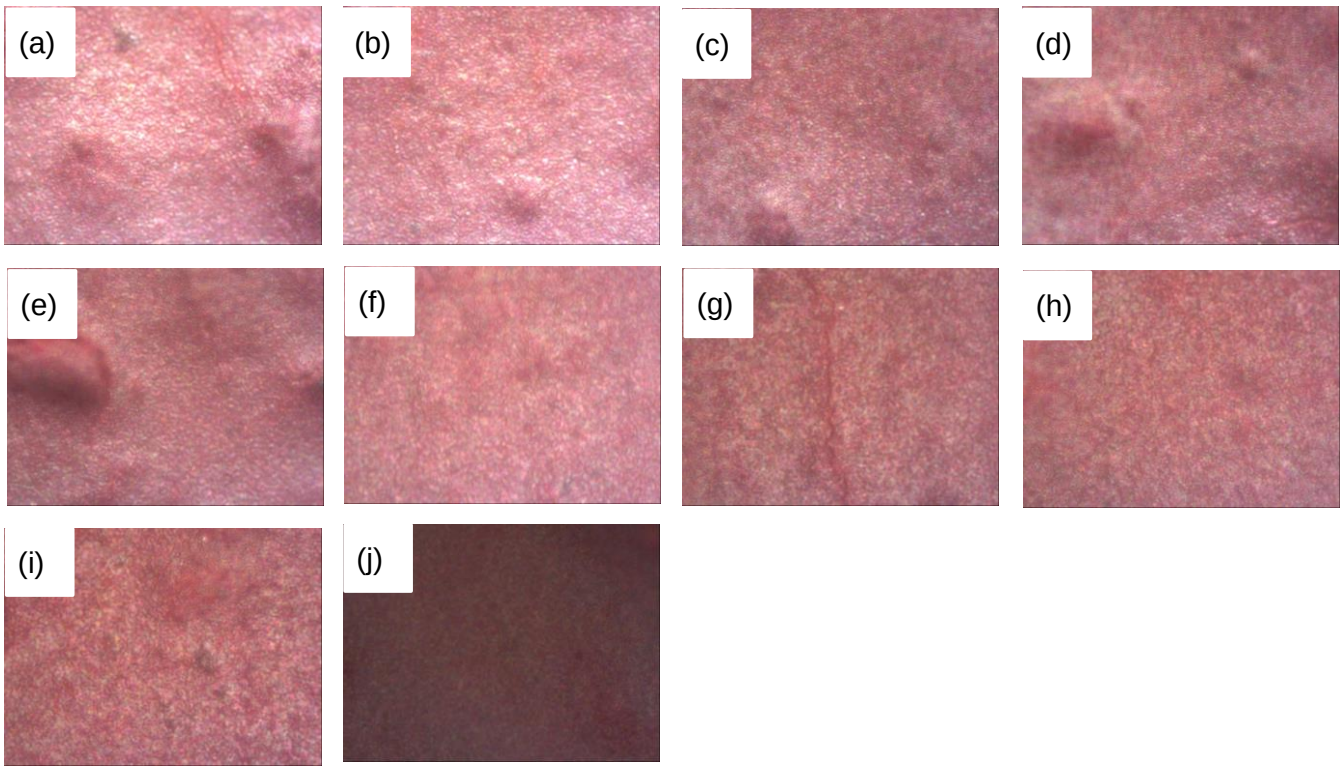

Figure 14. Optical microscope images of sample E exposed for (a) 0 h, (b) 10 h, (c) 20 h, (d) 30 h, (e) 50 h, (f) 100 h, (g) 150 h, (h) 200 h, (i) 300 h, and (j) 500 h.

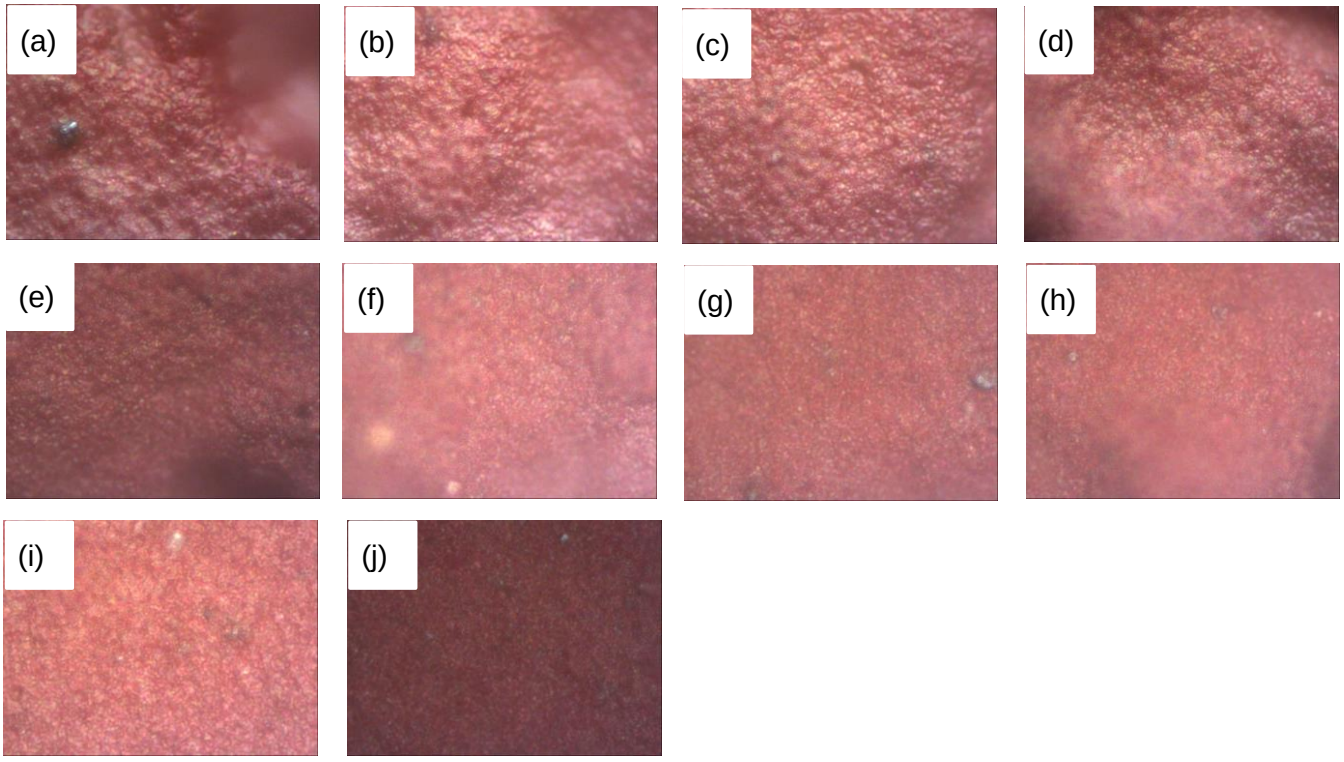

Figure 15. Optical microscope images of sample F exposed for (a) 0 h, (b) 10 h, (c) 20 h, (d) 30 h,

(e) 50 h, (f) 100 h, (g) 150 h, (h) 200 h, (i) 300 h, and (j) 500 h.

These samples were too rough to adjust focus of picture completely. The surface structure was not change by the progress of degradation. It is suggested that the mechanism of surface degradation is corresponded to that of lacquers.

3.3. Chemiluminescence analysis

CLA is a powerful tool to early detect a degradation of materials. There are two methods to evaluate the degradation. One is to measure oxidation induction time under oxygen. The other is to access CL maximum intensity under nitrogen. Concerning latter experiment, the oxidation degree is expressed by CL intensity and the measurements enable to perform with different temperature, making it possible to calculate activation energy. In this time, CLA measurements were carried out under nitrogen with different temperature using sample B. CL curves are shown in Figure 16.

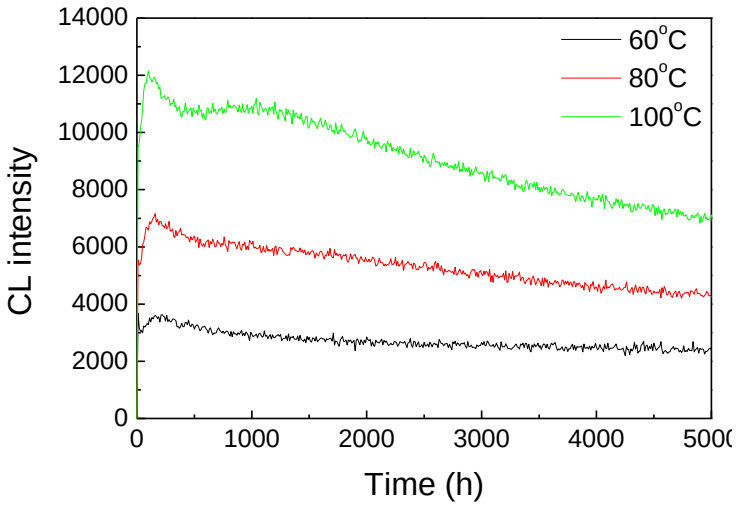

Figure 16. CL curves measured by different temperature.

The initial peak is attributed from a decomposition of hydroperoxide contained in sample, then

peak intensity decreases because the decomposition was completed and hydroperoxide was lost. The sample intensity was increased with measurement temperature. These maximum intensities of CL peaks measured by different temperature were used to apply Arrhenius equation.

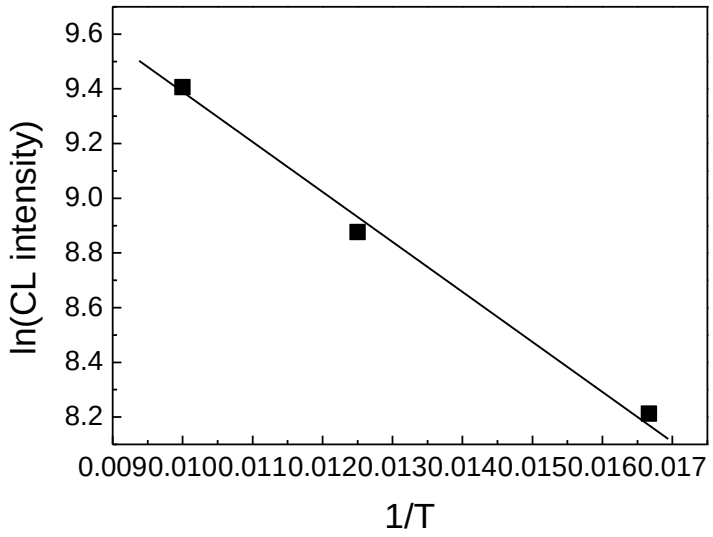

Figure 17. Arrehenius plot of sample B

The linear relationship was obtained by applying Arrehenius equation and this linearity enables to calculate activation energy from the slop. The value of energy was 1.46 kJ/mol. It was found that CL measurements are powerful tool to evaluate the activation energy.

4. Conclusion

These lacquers were likely to degrade by light and the surface properties were dramatically influenced by the degradation. Addition of pine smoke was the most effective ways to stabilize the lacquers. The mechanism of surface degradation was expected that new layer was created by the degradation due to volatilization of oxidative materials. Other brown materials were much stable than lacquers. It was found that CL is a powerful tool to measure the activation energy.

5. Reference

[1] A. Burmester *Archaeometry* **1983**, *25*, 45.

[2] J. Kumanotani, K. Inoue, M. Achiwa, L. W. Chen *Polym. Sci. Technol.* **1986**, *33*, 163.

[3] N. Niimura, T. Miyokoshi *Talanta* **2006**, *70*, 146.

[4] K. Nakagoshi, K. Yoshizumi *Mater. Sci. Appl.* **2011**, *2*, 1507.

[5] N. Niimura Int. *J. Polymer Anal. Char.* **2012**, *17*, 540.

Acknowledgements

I would like to express my sincere regards to Professor Jacques Lacoste for giving me the opportunity to work in CNEP. This work has never achieved without his kind guidance and support.

I am deeply grateful to Prof. Jacques Lemaire and Dr. Dominique Fromageot for their constant help to progress my experiment. I would like to also appreciate Dr. Nicolas Pichon teaching me various experimental technique and giving me kind advice. I am greatly thankful to all CNEP members to support my work and life in CNEP.

I would like to appreciate Prof. Tetsuo Hojo donating all materials.

Finally, I would like to thank to Prof. Minoru Terano and Prof. Toshiaki Taniike.

Kengo Takeuchi

Terano Laboratory,

School of Materials Science,

Japan Advanced Insititute of Technology